PERFORMANCE ANALYSIS OF COEXISTENCE BASED INTEGRATED COMMUNICATION AND SENSING SYSTEMS

A

Ph.D. Thesis submitted

by

Aparna Mishra

Department of Electronics and Electrical Engineering
Indian Institute of Technology Guwahati
Guwahati - 781039, Assam, India
January 2025

To my parents,

Late Mr. Umesh Mishra & Mrs. Mridula Mishra.

Certificate

This is to certify that the thesis entitled "**Performance Analysis of Coexistence Based Integrated Communication and Sensing Systems**", submitted by **Aparna Mishra** (206102006), a research scholar in the *Department of Electronics and Electrical Engineering, Indian Institute of Technology Guwahati*, for the award of the degree of **Doctor of Philosophy**, is a record of an original research work carried out by her under my supervision and guidance. The thesis has fulfilled all requirements as per the regulations of the institute and in my opinion has reached the standard needed for submission. The results embodied in this thesis have not been submitted to any other University or Institute for the award of any degree or diploma.

Date:

Place: Guwahati

Ribhu

Dept. of Electronics and Electrical Engg.,

Indian Institute of Technology Guwahati,

Guwahati - 781 039, Assam, India.

Acknowledgements

First and foremost, I feel it as a great privilege in expressing my deepest and most sincere gratitude to my supervisor Dr.Ribhu for their excellent guidance throughout my study. His kindness, dedication, hard work and attention to detail have been a great inspiration to me. My heartfelt thanks to him for the unlimited support and patience shown to me. I sincerely thank him for the pain he undertook in scrutinizing every work I presented to them and offering critical comments for improvisations.

I want to give my deepest gratitude to my doctoral committee members Dr. Prithwijit Guha, Dr. Mahima Arrawatia, and Prof. Ashish Anand for sparing their precious time out of their busy schedule to evaluate my progress and enrich this work with their invaluable suggestions and feedbacks. I feel very much fortunate to have had the opportunity of having the guidance of Prof M.R. Bhavani Shankar. I am deeply thankful to Prof. Gaurav Trivedi for his motivation and immense support throughout this incredible journey.

I would also like to thank the Head of the Department and other faculty members for their kind help in carrying out this work. I am also grateful to all the members of the research and technical staff of the department.

I feel truly delighted and blessed to have the friends like Ashish and Himani. The evening conversations and endless laughter with them are among the cherish-able memories for life time. I would also like to thank my lab-mates, Gangesh bhaiya, Vikash bhaiya and Tanmay bhaiya for fostering a warm and familial atmosphere at our lab.

Finally, I am thankful to my family for their unconditional love and support in this exceptional journey. I am grateful to my elder brother, Akshay Mishra and my husband, Brij Nandan Tripathi for their emotional support and for being my pillars of strength.

(Aparna Mishra)

Abstract

Intelligent transportation systems (ITSs) have emerged as a promising technology to address two major challenges in the road transportation system; road accidents and traffic congestion. ITS require smart vehicles to provide both radar and communication capabilities. This in turn requires a large bandwidth for the effective deployment of both. However, the bandwidth and space constraint at vehicular terminals poses a major challenge for the effective deployment of ITS.

The advancements in wireless communication technology have led to the development of integrated communication and sensing (ICS) systems. These type of systems are designed to share either spectrum or hardware, or both, and thereby reduce the overall cost of the system. It has been argued that these systems can be broadly classified into three categories, viz.; radar communication co-existence, where both the radar and communication sub-systems operate independently; radar communication co-operation, where they coordinate to reduce mutual interference; and radar communication co-design, where they share common hardware and process their signals to mitigate mutual interference.

Both the co-operation and co-design based ICS systems aim to improve the performance of the radar and communication functionalities, however, they are incompatible with legacy systems. Therefore, in this thesis we investigate co-existence based ICS systems.

In coexistence based ICS systems, we consider that both the radar and communication sub-systems do not share any information, and treat each other as interference sources. Therefore, we investigate the overall system performance and that of each

sub-system in the presence of interference generated by the other sub-system.

The first problem we address in this thesis entails the analysis of a single cell massive multi input multi output (mMIMO) communication system in coexistence with a mono static multi input multi output (MIMO) radar. Here, considering that the presence of radar is known at communication base station (BS), we analyse the performance of the ICS system under three communication subframes viz. the channel estimation subframe, the uplink and the downlink transmission subframes. During the first subframe, the BS performs uplink channel estimation in the presence of radar generated interference and we derive the corresponding mean square error (MSE) expression. Further, during the second subframe, using these estimates, the BS performs minimum mean square error (MMSE) combining and we obtain the expression for uplink achievable rate via deterministic equivalent (DE) analysis. Following this, in the downlink communication sub-frame, the BS performs null space projection to eliminate the communication interference at the radar subsystem. We derive the expression for Crammer Rao Bound (CRB) on the radar's angle of arrival (AOA) estimation error in both the uplink and downlink communication subframes and utilize the notion of radar rate to measure the performance of radar and communication system on the same scale and obtain rate regions for both uplink and downlink communication sub-frame.

Following this, we analyse the performance of a cell free massive multi input multi output (CF-mMIMO) communication system in coexistence with a multistatic tracking radar. CF-mMIMO is a key enabling technology for the air interface of next generation wireless communication systems due to its attributes, including uniform coverage, high power scaling and energy efficiency. Here, we analyse the performance of both the radar and communication subsystems in the uplink communication frames. The radar subsystem performs two stage target tracking at each sensing instant using the extended Kalman filter (EKF) algorithm. During the uplink channel estimation subframe, the BS estimates the uplink communication

channels in the presence of radar generated interference, and we derive an expression for uplink achievable rate using these estimates. Through numerical simulations, we observe that a multi-static tracking radar can coexist with a CF-mMIMO system without any significant loss. We further extend this model to a stochastic geometry framework to consider a more realistic wireless environment and analyze the performance of both the subsystems.

Finally, we examine an intelligent reflecting surface (IRS) enabled communication system and a MIMO radar in coexistence with each other in millimeter wave (mmWave) spectrum. We derive the best case and the worst case CRBs on the AOA estimate at the radar sub-system in the presence of communication interference, and obtain an expression of uplink achievable communication rate in the presence of radar generated interference. Through extensive simulations, we observe that IRS improves the performance of communication subsystem while the effect of IRS on the radar performance can be ignored and concluded that IRSs barely degrade the performance of the radar subsystem and at the same time improve communication system performance, enabling coexistence.

Contents

List of Figures

List of Tables

List of Acronyms

2D	Two Dimensional
AoA	Angle of Arrival
AP	Access Point
AWGN	Additive White Gaussian Noise
BS	Base Station
CF-mMIMO	Cell-Free massive Multiple Input Multiple Output
CRB	Crammer Rao Bound
CSI	Channel State Information
DARPA	Defence Advance Research Agency
DE	deterministic equivalent
DoF	Degrees of Freedom
DFRC	Dual Functional Radar Communication
EKF	Extended Kalman filter
FC	Fusion Centre
ICS	Integrated Communication and Sensing
i.i.d.	independent and identically distributed
IRS	Intelligent Reflecting Surface
ITS	Intelligent Transportataion Systems
LoS	Line of Sight
LTE	Long Term Evolution
MIMO	Multiple Input Multiple Output
mMIMO	massive Multiple Input Multiple Output

MMSE	Minimum Mean Square Error
MSE	Mean Square Error
mmWave	millimeter wave
NSP	Null Space Projection
OFDM	Orthogonal frequency division modulation
PU	Primary User
PPP	Poisson Point Process
RZF	Regularized Zero Forcing
SINR	Signal to Interfereence plus Noise Ratio
SU	Secondary User
TDD	Time Division Duplex
ZMCSCG	Zero Mean Circularly Symmetric Complex Gaussian

List of Symbols

Lowercase boldface letters denote vectors

Uppercase boldface letters denote matrices

$\mathbf{A}^T$	Transpose of the matrix $\mathbf{A}$
$\mathbf{A}^H$	Hermitian (conjugate transpose) of the matrix $\mathbf{A}$
$\mathbf{A}^{-1}$	Inverse of the matrix $\mathbf{A}$
$\mathcal{CN}(\boldsymbol{\mu}, \boldsymbol{\Sigma})$	Circularly symmetric complex Gaussian (CSCG) random vector with mean vector $\boldsymbol{\mu}$ and covariance matrix $\boldsymbol{\Sigma}$
$card(\mathcal{A})$	The cardinality of set $\mathcal{A}$
diag($\mathbf{a}$)	Diagonalization of a vector $\mathbf{a}$
$det(.)$	The determinant of a matrix
$E[.]$	The Expectation Operator
f_D	The Doppler frequency shift
f_c	The carrier frequency
$\mathbf{I}_K$	The K × K Identity matrix
K	Number of UEs
L	The number of radar sensors
M_t	The number of radar transmit antennas
M_a	The number of AP or BS antenna elements

N_0	variance of AWGN
N	Number of APs
Pr{.}	Probability of the argument
P	The number of IRS elements
$\mathbf{Q}_P$	The IRS reflection coefficient matrix
R	Achievable rate ib bits/sec/Hz
$\Re(.)$	real part of the complex number
$\mathbf{R}$	covariance matrix of a vector
Tr($\mathbf{A}$)	Trace of the matrix $\mathbf{A}$
vec($\mathbf{A}$)	The vectorization of matrix $\mathbf{A}$
$\delta[.]$	The Kronecker Delta function
$\psi[n]$	Uplink pilot signal
γ	SINR
β	Large scale fading coefficient of wireless channel
$\|.\|$	absolute value of scalar arguments
$\xrightarrow[M\to\infty]{a.s.}$	Almost sure convergence when $M \to \infty$
$(.)^*$	Complex conjugate of a complex number
$\otimes$	The Kronecker product
$\odot$	The Hadamard product
$\|\|.\|\|$	The Euclidean norm of a vector
$\epsilon_{u,k}$	The uplink transmit power by the kth user
$\epsilon_{p,k}$	The uplink pilot power by the kth user
$\epsilon_{d,k}$	The downlink signal power corresponding to the kth user

List of Publications

Published

1. Aparna Mishra, and Ribhu Chopra, ”MIMO radars and massive MIMO communication systems can coexist.” IEEE Transactions on Vehicular Technology (2023).
2. Aparna Mishra, Ribhu Chopra and Bhavani Shankar M. R., ”On the Coexistence of Multi-Static Tracking Radars with Cell Free Massive MIMO,” 2024 National Conference on Communications (NCC), Chennai, India, 2024, pp. 1-6, Feb. 2024.

Submitted

1. Aparna Mishra, Ribhu Chopra and Bhavani Shankar M. R., “Communication IRSs Can Enable radar Communication Coexistence,” to the IEEE Communication Letters, submitted Jan. 2025.

Under Preparation

1. Aparna Mishra, Ribhu Chopra and Bhavani Shankar M. R., “Multi-Static Tracking Radars can Coexist with Cell Free Massive MIMO”.

1

Introduction

Contents

1.1 Motivation

The consistent increase in population, along with the increased urbanization and vehicular densities has led to the dual problems of road accidents and vehicular congestion worldwide. It is to be noted that road accidents are one of the major causes of death across the globe. In the context of India, for example, a report by the research wing of ministry of road transport and highways states that 449,002 vehicular accidents were reported in the year 2019. These accidents have been reported to lead to 151,113 deaths and 451,361 injuries [1]. It has also been found that as much as 80% of these accidents are caused due to human error [2], and preventive assistance may help avoid these errors and consequently the accidents. The other major issued faced by transportation systems is that of traffic congestion. In this context, it is observed that this problem can be avoided by appropriate routing and congestion detection which require accurate congestion detection and the knowledge of vehicular locations.

Consequently, the idea of intelligent vehicle assisted driving, known as 'Intelligent Transportation Systems' [3] has recently attracted much research focus due to its potential capability to solve these dual problems. These systems entail the use of information and communication technologies to collect, process and disseminate information related to the surroundings of a vehicle to assist the driver, as well as other vehicles [3]. However, the performance of these ITSs has been observed to be contingent on two factors, viz. the vehicles being able to gather reliable data about their surroundings, and being able to take intelligent decisions based on these data. Out of these, the latter has received much research attention in the form of artificial intelligence and machine learning. Regarding the former, we note that a vehicle can collect information about its surroundings from two sources, viz. directly sensing the range and velocities of nearby objects, and by exchanging the information thus collected with nearby vehicles. We observe that the first source of information, i.e. direct sensing requires the vehicle to act as a radar. On the other hand, the second source of information, i.e. exchange of information between vehicles envisions vehicles as communication terminals. Hence, an effective deployment of ITS requires smart vehicles to be equipped with both radar and communication

functionalities.

It is to be noted that both radar and Communication functionalities require a large bandwidth and specialized hardware. In case of radars, a large bandwidth provides finer range resolution and improves sensing capability; while in case of communication systems it provides high data rate and the ability to simultaneously support multiple users. Additionally, separate, and well separated antenna arrays will also be required for efficient implementation of both radar and communication systems. However, these requirements also pose challenges for successful implementation of the aforementioned functionalities in vehicles, mainly due to the following reasons.

(i) The unavailability of physical space on a vehicle.

(ii) The scarcity of available spectrum.

It is also important to note that the frequency spectrum above 1MHz and below 100 GHZ is utilized for various applications including communication, radio and television broadcasting, radar sensing, ground traffic control, remote sensing and military and defence operations. A large portion the sub 6-GHz spectrum has been assigned to radar services remains under utilized due to the pulsating behaviour of the radars, and their confinement to military areas [4]. Consequently, there has been growing interest in the integrated sensing and communications systems [5], both specific to the idea of smart vehicles, and in general. The similarity in bandwidth, antenna structure, and system components coupled with the recent technological advancements have made the joint design of radar and communication systems possible. It has also been argued that joint design of radar and communication systems can result in improved performance for both the systems. For example, radars may assist communication systems in proper beam alignment and in sensing the surroundings for channel modelling. Similarly, communication systems may assist radars by allowing for the aggregation of the data collected and processed by multiples sensing nodes.

In 2013, the US defence advance research agency (DARPA) launched a program named "Shared Spectrum Access for radar and Communications (SSPARC)" for technological advancement of spectrum sharing techniques between radar and communication systems [6]. In

2015, this project was extended to utilize the sub-6 GHz radar spectrum for military as well as civilian communication systems. The solutions for ICS system developed under this project and other allied efforts can be broadly classified into three design philosophies, viz. coexistence, cooperation and co-design [7]. We discuss these in the sequel.

(i) **Co-existence**: In co-existence based ICS systems, the radar and communication subsystems share the same spectrum without sharing any information related to interference mitigation, that is, they do not cooperate with each other, and treat each other as sources of interference.

(ii) **Co-operation**: In cooperation based ICS systems, the radar and communications subsystems share the spectrum and assist each other by providing information related to interference mitigation without altering their respective functionalities.

(iii) **Co-design**: In co-designed ICS systems, the performance of both the systems is jointly optimization in the design of an integrated system. This integrated system can perform radar and communication system operations simultaneously, and is by known different names, e.g., radar-Communications (RadCom), ICS, dual functional radar communication (DFRC) system etc. [8]. These systems may utilize the same hardware and waveform for both the communication and the sensing functionalities.

Out of these approaches for the realization of ICS system, the joint design approach has recently attracted much research interest [8–12]. These works mainly focus on designing waveforms suited to both sensing and communications [9–11], and partitioning of large antenna arrays for dual function operation [12].

However, following the DFRC approach requires a complete redesign and replacement of existing communication and radar systems [13]. This poses serious challenges for legacy systems that have not been designed with ICS in mind. Therefore, in this thesis, we have investigated the compatibility of ICS systems with existing and upcoming wireless standards, and have focused on radar communications coexistence and not on co-design. We briefly discuss evolution of coexistence based ICS systems in the next section.

1.2 The Evolution of Coexistence based ICS Systems

The earliest efforts in ICS systems use the idea of opportunistic spectrum access to mitigate inter-system interference between the two subsystems. Under this approach, the secondary user (SU) or the cognitive user dynamically accesses the spectrum when it is not being accessed by the primary user (PU) operating in it [14]. The SU is permitted to transmit only when the PU is either inactive, or when the interference to the PU from the SUs signal remains within an acceptable limit. In this direction, the concept of cognitive radar is introduced in [14], and entails the use of intelligent signal processing and feedback from the receiver to the transmitter. It has also been postulated that cognitive radars require adaptability at both the transmitter, as well as the receiver, in contrast to adaptability just at the receiver side in traditional radars. The authors in [15] have investigated the components required for developing fully functional cognitive radars.

The authors in [16] have considered opportunistic spectrum sharing between a rotating radar and a cellular communications system, and have derived an upper bound on interference to noise ratio for system operation. This idea of spectrum sharing between rotating air traffic control-radars and cellular systems has been extended in [17], where the authors have utilized the path loss variations to prevent the communications signals from interfering with the rotating radar's main lobe. A detailed discussion on techniques and policies for gray space spectrum sharing are discussed in [18], where the co-existence of primary and secondary user transmissions has been proven quantitatively. An experimental study on the coexistence of Time Division Long-Term Evolution (TD-LTE) and radar in the 3.5 GHz band is performed in [19]. It is shown that LTE communication systems with low antenna height is not adversely affected by the radar signal while transmitting over adjacent frequencies.

However, it was observed that opportunistic spectrum access does not allow for simultaneous coexistence of radar and communication systems. To overcome this, the idea of null space projection (NSP) for radar communications coexistence was introduced in [20], where it was proposed to project the radar waveform onto the null space of the interference channel

between the radar and the communication system. It was shown that this approach can potentially eliminate the radar generated interference at the communication receiver. However, the implementation of this technique required the knowledge of the radar-communication interference channel at the radar transmitter. In general, NSP can be performed by the system having a larger number of degrees of freedom (DoF) and involves projecting its signal onto the null space of the system having the smaller number of DoF. That is, NSP can be performed either at the radar side or at the communication side, depending on the DoF of the two subsystems, but is contingent on interference channel state information (CSI). However, NSP based techniques face challenges if the two subsystems have approximately the same DoF, and the interference channel matrix does not have a null space.

In this direction, a null space expansion based strategy is proposed in [21] and it is observed that the radar performance can be improved at the cost of non-zero interference at the communication receivers. A more realistic extension of this work was discussed in [22], where an LTE cellular system with multiple BSs was considered in coexistence with a multiple input multiple output (MIMO) radar.

The authors in [23] consider a maritime MIMO radar with a time varying interference channel (attributed to the translatory or oscillatory motion of the ship, and modeled using matrix perturbation theory). The effect of this perturbed interference channel is then evaluted in terms of the likelihood estimate of target's angle of arrival. Following this, the loss in the radar's performance is quantified via Monte-Carlo simulations.

The authors in [24] consider the joint design of overlaid communications system and pulsed radars, in a coexistance based framework. This work introduces a novel metric for evaluting the performance of the communication system. This metric, called the compound rate is defined as a convex combination the rates achievable by the communications subsystem with and without the radar generated interference. Following this, the compound rate is optimized with constraints on the signal to interfereence plus noise ratio (SINR) of the radar subsystem, and power transmitted by both the subsystems.

The problem of interference mitigation between the two subsystems while optimizing the

overall system performance has also been discussed in the literature. The work [25] considers the coexistence of a MIMO radar with a MIMO communication system. In this paper, the authors obtain a lower bound on the communications SINR, and maximize this bound with constraints on the radar clutter and transmitted power. A similar approach has been followed in [26] where the covariance matrix of the communications signal, and the radar beamforming matrix are jointly optimized to enable the coexistence between a MIMO matrix completion radar and a MIMO communications system.

A linearly constrained minimum variance based optimization to design communication beamforming matrix at the BS is discussed in [27]. However, all these works consider the availability of perfect CSI at the radar or or at the communications BS, which is impractical. A radar specific optimization based technique is proposed in [28] to maximize the target detection probability at the radar, subject to constraints on the transmit BS power and per user SINR.

A coexistence based ICS system comprising a mMIMO based communications system and a MIMO radar is discussed in [13]. It is shown that the effect of radar generated interference disappears asymptotically as the number of antennas on the BS grows.

1.3 On the Performance Evaluation of ICS Systems

A significant challenge in the design and analysis of ICS systems is the characterization of their performance. This is because the operating principles and the objectives of the two underlying subsystems, viz. the radar and the communications subsystems are fundamentally different. That is, while radar systems extract the target information from the signal reflected by a non-cooperative target, the communication systems exchange information among cooperating transceivers. Therefore, while the performance of a radar system is measured in terms of the MSE in the AoA estimates, or the probability of detection of the targets, that of the communication systems is measured in terms of the achievable communication rate. However, the authors in [29] have used the normalized mean squared estimaton error in a radar system as a proxy for the interference-plus-noise to signal ratio, and defined the idea of radar rate. This is analogous to the communication rate and is a measure of information between the radar and the target,

that acts as an unwilling source of information. Following this, the authors have derived inner bounds on the performance of ICS system.

Similarly, the authors in [7] have introduced the ICS problem as a multiple access channel, and propound the idea *"all bits are equal but some bits are more equal"*. They complete their exploration of the ICS fulled dystopia by commenting on the information bounds under the coexistance, cooperation, and co-design regimes.

Another measure of radar capacity is introduced by Guerci et al. in [30] in terms of the number of range resolution cells that the radar can support. In this scheme, each resolution cell of the radar is considered as a constellation point, and the "Channel Capacity" of the radar is defined as the maximum information contained in the echo signal, that is shown to be equal to the number of resolvable targets.

1.4 Statement of Problems

In this thesis, we have broadly looked at the performance of three coexistence based ICS systems, viz. massive MIMO systems and MIMO radars; Cell Free massive MIMO systems and multi-static tracking radars; and AoA estimation and IRS enabled communications systems. We discuss the motivation for each of these problems in the sequel.

The idea of serving a large number of users over the same time frequency band using an even larger number of BS antennas has recently seen much active research interest [31], and has emerged as a front-runner among physical layer technologies for next generation wireless communication systems. However, massive MIMO systems have not been designed keeping ICS in mind. While there is a recent work showing that a coexisting radar has minimal effect on the functioning of a massive MIMO system [13], a complete analysis of the coexistence based ICS system as a whole is unavailable. Therefore, as a first problem, we have analyzed the performance of a coexistence based ICS system comprising a massive MIMO system with a MIMO radar sharing the same spectrum. With this work, we have established bounds on the performances of the two systems, and identified the trade offs involved in the joint implemen-

tation. [1]

For the second problem, we see that cell-Free mMIMO (CF-mMIMO), a decentralized version of massive MIMO [32] has recently seen much research interest. This is due to CF-mMIMO inheriting most of cellular massive MIMO's advantages while providing almost uniformly good quality of service to all the users due to its distributed nature. It has also been considered as a candidate for joint design based ICS systems [32]. We also note that the distributed cell free architecture is similar to a multi-static radar setup. Therefore, in the second set of problems, we have evaluated the performance of a coexistence based multi-static tracking radar and a CF-mMIMO system.[2]

Finally, we note that IRSs are being seen as an enabler for favorable radio signal propagating in next generation wireless communications systems [33]. These consist of a large number of passive reflector elements that ensure constructive combination of the transmitted signal at a given point in space. This makes the design and analysis of a coexistence based ICS system with an underlying IRS based communication system an interesting direction for research. As a direct consequence, we analyze an ICS system consisting of an IRS enabled communication subsystem and a AoA estimation radar as our final problem. We next describe our approaches to solving these problems along with the organization of this thesis.

1.5 Thesis Organization

The thesis is organized into six chapters whose contents are described in the sequel. The first chapter introduces ICS technology and provides a brief review of the state of the art in this field, and concludes by summarizing the contents of the rest of the thesis.

In the second chapter, we investigate the coexistence of a single cell massive MIMO communication system with a MIMO radar. We consider the case where the massive MIMO BS is aware of the radar's existence and treats it as a non-serviced user, but the radar is unaware of

[1]This work has been published as *A. Mishra and R. Chopra, "MIMO Radars and Massive MIMO Communication Systems Can Coexist," in IEEE Transactions on Vehicular Technology, vol. 73, no. 5, pp. 6486-6501, May 2024*

[2]Part of this work has been published as *A. Mishra, R. Chopra and B. S. M. R., "On the Coexistence of Multi-Static Tracking Radars with Cell Free Massive MIMO," 2024 National Conference on Communications (NCC), Chennai, India, 2024, pp. 1-6.*

the communication system's existence and treats the signals transmitted by both the BS and the communication users as noise. Using results from random matrix theory, we derive the rates achievable by the communication system and the radar. We then use these expressions to obtain the achievable rate regions for the proposed joint radar and communications system. We observe that the availability of a large number of degrees of freedom at the massive MIMO BS, results in minimal interference even without co-design. Finally we corroborate our findings via detailed numerical simulations and verify the validity of the results derived previously under different settings.

In the third chapter, we evaluate the performance of a coexistence based ICS system, combining a CF-mMIMO system with a multi-static sensing radar. The multi-static radar is assumed to consist of multiple sensors, all tracking a single target and connected to a fusion centre (FC). The radar subsystem is further assumed to employ a two level EKF that performs the tracking at both the individual sensors and at the FC. The communications subsystem is assumed to consist of the uplink of a CF-mMIMO system and its operation is divided into two sub-frames, viz. channel estimation and data transmission. We evaluate the system performance in terms of the achievable rates by the communication subsystem and the MSE tracking performance of the radar subsystem. Via extensive numerical simulations, we show that due to the increased diversity offered by distributed nature of both the subsystems, they are able to coexist.

In the fourth chapter, we revisit the problem considered in Chapter 3 under a stochastic geometry framework. More specifically, we extend the discussion from Chapter 3 by evaluating the communications and radar performances during in the full communications frame by considering both uplink and downlink and using tools from stochastic geometry to generalize the results in terms of the AP/ UE/ Sensor deployment. We evaluate the system performance in terms of the coverage probability of the the communication subsystem for both the uplink and the downlink sub-frames, and the MSE tracking performance of the radar subsystem. Finally, we evaluate the system performance via extensive numerical simulations.

In the fifth chapter, we study a coexistence based ICS system comprising a MIMO radar and an IRS aided communications subsystem operating simultaneously in the mmWave band.

We evaluate the effect of the availability of the information about the IRS on the radar system performance. We observe that the inclusion of the IRS in the proximity of the radar results in additional echos being heard by the radar receiver. We argue that these additional echos can either be incremental or detrimental to the radar performance based on the availability of the IRS related parameters at the radar. We obtain the quantitative effects of the availability of IRS information using the Crammer Rao Bound (CRB) on the AoA estimate as a proxy for radar performance. Finally, via detailed numerical experiments, we evaluate the overall system performance and prescribe appropriate operating points for the system.

Finally, we summarize the conclusions of the present work and outline the potential directions for future in the sixth chapter.

2

On the Coexistence of MIMO Radars and Massive MIMO

Contents

Over the last decade, the idea of using a large number of antennas in both radar and communications systems, dubbed mMIMO, has also gained much traction [34–37]. While the literature dealing with radar technologies has focused more on conventional MIMO radars [38], with limited focus on mMIMO [37]; mMIMO has been established as a front runner technology for next generation wireless communication systems. It has been argued that the presence of a large number of antennas in a mMIMO BS translates to the availability of a large number of degrees of freedom, that in turn leads to quasi-orthogonality among the channels to/from different users operating over the same time frequency resource. Another consequence of the large number of degrees of freedom, known as channel hardening [36] results in the effective gains seen by different users concentrating close to a deterministic constant, simplifying downlink data processing at the users. Therefore, contingent on the availability of accurate CSI at the BS, mMIMO systems offer increased spectral and energy efficiencies even with the use of simple linear signal processing at the BS. mMIMO systems have been shown to be resilient to jamming [13] and other forms of in-band interference making them ideal candidates for sharing spectrum with radars. These features, coupled with the fact that a BS with a large antenna array can easily form a null to minimize interference to a co-existent radar subsystem make mMIMO communication systems ideal candidates for coexistence based ICS systems. Consequently, in this chapter we study the performance of a ICS system where a MIMO radar co-exists with mMIMO communication system.

The idea of mMIMO enabled ICS has recently been explored in the literature [13, 39, 40]. Out of these only [13] discusses a coexistence based ICS system. However, the underlying analysis is limited to studying the effect of radar generated interference on the uplink of a mMIMO system. In contrast, in this chapter, we analyse the problem from perspectives of both the communication system and the radar, using the achievable rate regions as a performance metric over an entire communication frame (i.e. both uplink and downlink). Also, instead of the use-and-then-forget bounds [36] used in [13] for evaluating the performance of mMIMO systems, we use DE analysis [41], that results in better approximations of achievable SINRs for MMSE type receivers.

2.1 Chapter Contributions

In this chapter, we have used rate regions to characterize the performance of a coexistence based ICS system comprising a single cell mMIMO communication system and a static MIMO radar over a full communication frame. Our specific contributions are enumerated as follows:

(i) We first determine the channel estimation performance of the mMIMO system with uplink training in the presence of radar generated interference, and obtain expressions for consequent channel estimation MSE. Similarly, we obtain the MSE of the angle of arrival estimate at the radar in the presence of the interference generated by the communication system. These expressions are then used to characterize a trade-off between the pilot powers employed by the users and the radar transmit power.

(ii) Following this, using DE analysis, we obtain expressions for uplink achievable rates using MMSE combining at the BS in the presence of radar generated interference. We then derive the CRB on the AoA estimate at the radar, in the presence of interference caused due to uplink transmission by the users, and use it to form an upper bound on the radar rate.

(iii) We then derive the DEs for the downlink SINR at the users, assuming regularized zero forcing (RZF) beamforming at the BS, in the presence of radar generated interference. We assume that the RZF beamforming at the BS also forms a null in the direction of the available estimate of the radar channel, and use this information to calculate the CRB on the AoA estimation performance and the corresponding radar rates.

(iv) Via extensive numerical simulations we validate our derived results, and plot the achievable rate regions for our ICS system for various use cases. We find that the availability of a large number of degrees of freedom at the BS results in minimal interference to both the constituents of the ICS systems, resulting in a significantly convex rate regions

We can thus conclude that coexistence based design of ICS systems is possible in the mMIMO regime, thus allowing for the addition of sensing capabilities to legacy systems, without the need for an extensive redesign. We next describe the system model considered in this

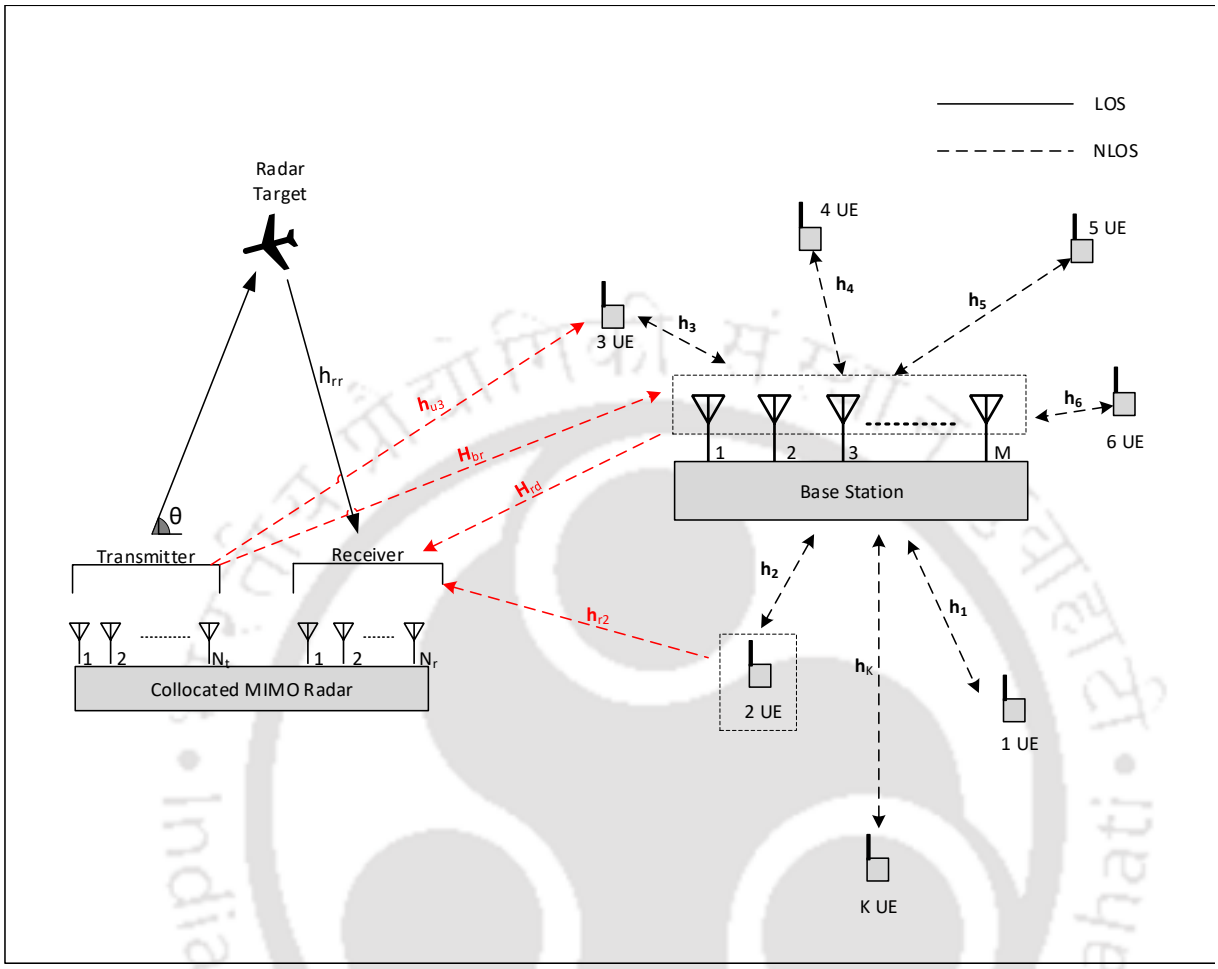

Fig. 2.1: The System Model

chapter.

2.2 System Model

We consider an ICS system comprising a single cell mMIMO subsystem coexisting with an in-cell MIMO radar as shown in Fig. 2.1. The two subsystems are assumed to transmit over the same time frequency resources with a full bandwidth overlap, but are assumed to have only non line of sight (NLoS), rich scattering interference channels. We next describe the system and signal models for the two subsystems individually.

2.2.1 The Radar Subsystem

We consider a mono-static pulsed MIMO radar equipped with collocated transmit and receiver antenna arrays, as shown in Fig. 2.1. The radar subsystem consists of M_t transmit anten-

nas and M_r receive antennas. Since the radar is mono-static, the transmit and receive antenna arrays can safely be assumed to be synchronized, allowing for coherent processing of transmit and receive signals. We assume that a single target is present in the LoS of the radar, at an angle θ, such that the array response vectors of the transmit and receive arrays are respectively given by $\mathbf{a}_t^T(\theta)$ and $\mathbf{a}_r^T(\theta)$. Note that the transmit and receive array responses are purely functions of the azimuth angle, θ, and not of the angle of elevation. Making the radar sensing problem, two dimensional (2D). We can also perform a similar analysis with a three dimensional radar sensing model accounting for both the azimuth and the elevation. We also let h_{rr} denote the reflection coefficient of the said target that accumulates the effects of propagation attenuation, phase shifts, and the radar cross section of the target. Now, let $\mathbf{s}[n] \in \mathbb{C}^{M_t \times 1}$ be the signal transmitted by the radar at the nth instant, such that $E[\mathbf{s}[n]\mathbf{s}^H[n]] = \mathbf{R}_{ss} = \sigma_r^2 \mathbf{I}_{M_t}$, with $\mathbf{I}_K$ representing the order K identity matrix. Then, the signal received by the radar, denoted by $\mathbf{z}[n] \in \mathbb{C}^{M_r \times 1}$, in the absence of any communication interference and in multipath free propagation [42], can be expressed as,

$$\mathbf{z}[n] = h_{rr}\mathbf{A}(\theta)\mathbf{s}[n] + \sqrt{N_0}\mathbf{w}_r[n], \tag{2.1}$$

where $\mathbf{w}_r[n]$ denotes the temporally and spatially white, zero mean circularly symmetric complex Gaussian (ZMCSCG) additive noise, and $\mathbf{A}(\theta) = \mathbf{a}_r(\theta)\mathbf{a}_t^T(\theta)$. We also assume that the target is moving slowly with respect to the radar, and we can ignore the Doppler shift within a pulse [43].

2.2.2 The Communications Subsystem

We consider a single cell mMIMO communication system operating in the time division duplex (TDD) mode comprising a BS equipped with M_a antenna elements serving K single antenna user equipments (users). We assume the channels between the BS and the users to be correlated with frequency flat rich scattering. We let $\sqrt{\beta_k}\mathbf{h}_k \in \mathbb{C}^{M_a \times 1}$ denote the channel vector between the BS and the kth user with β_k and $\mathbf{h}_k \sim \mathcal{CN}(\mathbf{0}, \mathbf{\Sigma}_k)$ representing the large scale and small scale fading coefficients, respectively, where $\mathbf{\Sigma}_k \in \mathbb{C}^{M_a \times M_a}$ is the covariance matrix of $\mathbf{h}_k$.

The communication frame is divided into three sub-frames, viz. channel estimation, uplink

data transmission, and downlink data transmission. In the first sub-frame, spanning K channel uses, the users transmit orthogonal pilot signals that are received by the BS and are used to form MMSE estimates of the BS to user channels. Following this, during the second sub-frame, spanning τ_u channel uses, the users transmit uplink data, and the BS uses the available channel estimates to effectively decode this data via MMSE combining [44]. Finally, during the downlink data transmission sub-frame spanning τ_d channel uses, the BS, under the assumption of channel reciprocity [45, 46], uses the available channel estimates to appropriately beamform and transmit data to the users. We next describe the signal models for these sub-frames.

(i) **Channel Estimation**

Let the kth user transmit a pilot signal $\psi_k[n]$ for $n \in [1, K]$, with an energy $\epsilon_{p,k}$ such that $\sum_{n=1}^{K} \psi_k[n]\psi_l^*[n] = \delta[k-l]$, with $\delta[n-k]$ representing the Kronecker delta function. Then, the signal vector received by the BS at the nth instant without accounting for radar generated interference can be expressed as

$$\mathbf{y}[n] = \sum_{k=1}^{K} \sqrt{\beta_k \epsilon_{p,k}} \mathbf{h}_k \psi_k[n] + \sqrt{N_0}\mathbf{w}_b[n], \tag{2.2}$$

with $\mathbf{w}_b[n]$ representing the temporally and spatially white ZMCSCG additive noise with unit variance.

(ii) **Uplink Transmission**

Letting the kth user transmit the data symbol $x_k[n]$ ($E[x_k[n]x_l^*[m]] = \delta[n-m]\delta[k-l]$) at the nth instant with an energy $\epsilon_{u,k}$, we can write the signal received at the BS in the absence of any radar generated interference as,

$$\mathbf{y}[n] = \sum_{k=1}^{K} \sqrt{\beta_k \epsilon_{u,k}} \mathbf{h}_k x_k[n] + \sqrt{N_0}\mathbf{w}_b[n]. \tag{2.3}$$

(iii) **Downlink Transmission**

Letting $\mathbf{Q} \in \mathbb{C}^{M_a \times K}$ denote the precoding matrix at the BS, $\epsilon_{d,s,k}$ the downlink symbol energy for the kth user such that the corresponding symbol sent to the kth user at the nth instant is $p_k[n]$, we can write the downlink signal received at the kth user at the nth instant

as

$$r_k[n] = \mathbf{h}_k^T \mathbf{Q} \text{diag}(\sqrt{\boldsymbol{\epsilon}_{d,s}}) \mathbf{p}[n] + \sqrt{N_0} w_k[n], \tag{2.4}$$

where $\mathbf{p}[n] = [p_1[n], p_2[n], \ldots, p_K[n]]^T$, and $\boldsymbol{\epsilon}_{d,s} = [\epsilon_{d,s,1}, \ldots, \epsilon_{d,s,K}]^T$, and $w_k[n]$ is the ZMCSCG noise with unit variance at the kth user.

2.2.3 Interference Channel Models

As stated earlier, the MIMO radar and mMIMO communication sub-systems do not have line of sight interference channels. Since both the BS and Radar are fixed, the interference channels between them, denoted by $\mathbf{G}_{rb} \in \mathbb{C}^{M_a \times M_t}$ and $\mathbf{G}_{br} \in \mathbb{C}^{M_r \times M_a}$, respectively, for the radar transmit and receive arrays are also assumed to be time invariant. Now, in accordance with the rich scattering assumption, the entries of $\mathbf{G}_{rb}$ and $\mathbf{G}_{br}$ are assumed to be independent and identically distributed (i.i.d.) ZMCSCG with a variance $\eta_I = \min(d_{br}^{-\alpha}, 1)$ with d_{br} being the distance between the BS and the radar. Also, their MMSE estimates, respectively, given by $\hat{\mathbf{G}}_{rb}$ and $\hat{\mathbf{G}}_{br}$ are assumed to be available at the BS such that,

$$\mathbf{G}_{rb} = \hat{\mathbf{G}}_{rb} + \tilde{\mathbf{G}}_{rb}, \quad \mathbf{G}_{br} = \hat{\mathbf{G}}_{br} + \tilde{\mathbf{G}}_{br}, \tag{2.5}$$

where $\tilde{\mathbf{G}}_{rb}$ and $\tilde{\mathbf{G}}_{br}$ are estimation errors orthogonal to $\hat{\mathbf{G}}_{rb}$ and $\hat{\mathbf{G}}_{br}$, respectively, and their entries have a variance η_e. In case the BS is unable to estimate the interference channels, then $\hat{\mathbf{G}}_{rb}$ and $\hat{\mathbf{G}}_{br}$ are set to zero and $\eta_e = \eta_I$. During the training and uplink data transmission phases, the BS uses $\hat{\mathbf{G}}_{rb}$ to form nulls in the directions containing the radar interfering signals to minimize their effects on channel estimation and uplink performances. Similarly, during the downlink transmission, the BS forms nulls in the direction of $\hat{\mathbf{G}}_{br}$ to minimize the interference to the radar.

Similarly, the interference channel between the radar transmit array and the kth user is represented by $\mathbf{g}_{rk} \in \mathbb{C}^{M_t \times 1}$, $k \in \{1, 2, \ldots, K\}$, and the interference channel between the kth user and the radar receive array is represented by $\mathbf{g}_{kr} \in \mathbb{C}^{M_r \times 1}$, $k \in \{1, 2, \ldots, K\}$. Both $\mathbf{g}_{rk}$ and $\mathbf{g}_{kr}$ are assumed to consist of i.i.d. ZMCSCG entries having a variance η_{rk} that is equal to the large scale fading coefficient between the radar and the kth user. It is important to note that the radar

can be aware of the BSs signals as well, and optimize its performance while minimizing the interference to the communication subsystem. However, in this chapter, our aim is to demonstrate co-existence between radar and communication systems with minimal changes in either of the two subsystems. Therefore, we have considered the radar to be unaware of the communication system's presence, and hence unaware of the underlying interference channel coefficients.

2.3 The Channel Estimation Sub-frame

2.3.1 The Communication Subsystem

Considering the effect of radar generated interference, the signal received by BS antennas at the nth instant, denoted by, $\mathbf{y}[n] \in C^{M_a \times 1}$ can be expressed as,

$$\mathbf{y}[n] = \sum_{k=1}^{K} \sqrt{\beta_k \epsilon_{p,k}} \mathbf{h}_k \psi_k[n] + \mathbf{G}_{rb}^H \mathbf{s}[n] + \sqrt{N_0}\mathbf{w}[n], \tag{2.6}$$

Defining $\mathbf{y}_l \triangleq \sum_{n=1}^{K} \mathbf{y}[n]\psi_l^*[n]$, we obtain

$$\mathbf{y}_l = \sqrt{\beta_l \epsilon_{u,p,l}} \mathbf{h_l} + \sum_{n=1}^{K} \hat{\mathbf{G}}_{rb,}^H \mathbf{s}[n]\psi_l^*[n] + \sum_{n=1}^{K} \tilde{\mathbf{G}}_{rb}^H \mathbf{s}[n]\psi_l^*[n] + \sum_{n=1}^{K} \sqrt{N_0}\mathbf{w}[n]\psi_l^*[n]. \tag{2.7}$$

Now, the BS may or may not have the phase synchronization information for $\mathbf{s}[n]$. In the former case $\mathbf{y}_l'$ can be formed by subtracting $\sum_{n=1}^{K} \hat{\mathbf{G}}_{rb}^H \mathbf{s}[n]\psi_l^*[n]$ from $\mathbf{y}_l$ as

$$\mathbf{y}_l' = \sqrt{\beta_l \epsilon_{u,p,l}} \mathbf{h}_l + \sum_{n=1}^{K} \tilde{\mathbf{G}}_{rb}^H \mathbf{s}[n]\psi_l^*[n] + \sum_{n=1}^{K} \sqrt{N_0}\mathbf{w}[n]\psi_l^*[n]. \tag{2.8}$$

Clearly, in this case, the LMMSE estimate $\hat{\mathbf{h}}_l$ of $\mathbf{h}_l$ can be written as $\mathbf{A}_l'\mathbf{y}_l'$, with $\mathbf{A}_l' = E[\mathbf{h}_l\mathbf{y}_l'^H][E[\mathbf{y}_l'\mathbf{y}_l'^H]]^{-1}$, such that $E[\mathbf{h}_l\mathbf{y}_l^H] = E[\mathbf{h}_l\mathbf{y}_l'^H] = \sqrt{\beta_l \epsilon_{u,p,l}}\mathbf{\Sigma}_l$, and $E[\mathbf{y}_l'\mathbf{y}_l'^H] = \beta_l \epsilon_{u,p,l}\mathbf{\Sigma}_l + (M_t\eta_e\sigma_r^2 + N_0)\mathbf{I}_{M_a}$. Similarly, in case the synchronization information about $\mathbf{s}[n]$ is not available at the BS, $\hat{\mathbf{h}}_l = \mathbf{A}_l\mathbf{y}_l$, such that

$$\mathbf{A}_l = E[\mathbf{h}_l\mathbf{y}_l^H][E[\mathbf{y}_l\mathbf{y}_l^H]]^{-1} = \beta_l \epsilon_{u,p,l}\mathbf{\Sigma}_l[\beta_l \epsilon_{u,p,l}\mathbf{\Sigma}_l + \sigma_r^2\hat{\mathbf{G}}_{rb}\hat{\mathbf{G}}_{rb}^H + (M_t\eta_e\sigma_r^2 + N_0)\mathbf{I}_{M_a}]^{-1}. \tag{2.9}$$

Now, letting $\tilde{\mathbf{h}}_l$ represent the ZMCSCG estimation error orthogonal to $\hat{\mathbf{h}}_l$, it is easy to show that $\mathbf{h}_l$ can be represented as

$$\mathbf{h}_l = \hat{\mathbf{h}}_l + \tilde{\mathbf{h}}_l, \tag{2.10}$$

with $\hat{\mathbf{h}}_l$ and $\tilde{\mathbf{h}}_l$ having covariance matrices $\mathbf{B}_l$ and $\bar{\mathbf{B}}_l$ respectively. Here,

$$\mathbf{B}_l = \beta_l \epsilon_{p,l} \mathbf{\Sigma}_l [\beta_l \epsilon_{p,l} \mathbf{\Sigma}_l + (M_t \eta_e \sigma_r^2 + N_0) \mathbf{I}_{M_a}]^{-1} \mathbf{\Sigma}_l$$

and

$$\bar{\mathbf{B}}_l = \mathbf{\Sigma}_l - \beta_l \epsilon_{p,l} \mathbf{\Sigma}_l [\beta_l \epsilon_{p,l} \mathbf{\Sigma}_l + (M_t \eta_e \sigma_r^2 + N_0) \mathbf{I}_{M_a}]^{-1} \mathbf{\Sigma}_l,$$

when the radar signal synchronization information is known at the BS, and

$$\mathbf{B}'_l = \beta_l \epsilon_{u,p,l} \mathbf{\Sigma}_l [\beta_l \epsilon_{p,l} \mathbf{\Sigma}_l + \sigma_r^2 \hat{\mathbf{G}}_{rb} \hat{\mathbf{G}}_{rb}^H + (M_t \eta_e \sigma_r^2 + N_0) \mathbf{I}_{M_a}]^{-1} \mathbf{\Sigma}_l$$

and

$$\bar{\mathbf{B}}'_l = \mathbf{\Sigma}_l - \beta_l \epsilon_{p,l} \mathbf{\Sigma}_l [\beta_l \epsilon_{p,l} \mathbf{\Sigma}_l + \sigma_r^2 \hat{\mathbf{G}}_{rb} \hat{\mathbf{G}}_{rb}^H + (M_t \eta_e \sigma_r^2 + N_0) \mathbf{I}_{M_a}]^{-1} \mathbf{\Sigma}_l,$$

when radar signal information is not known at the BS.

2.3.2 DoA Estimation at the Radar

The received signal at the radar, in the presence of interference caused due to the pilots transmitted by the users can be expressed as

$$\mathbf{z}[n] = h_{rr} \mathbf{A}(\theta) \mathbf{s}[n] + \sum_{k=1}^{K} \sqrt{\epsilon_{p,k}} \mathbf{g}_{kr} \psi_k[n] + \sqrt{N_0} \mathbf{w}_r[n]. \tag{2.11}$$

The signal received by the radar can now be reduced to the standard desired signal+noise form, where a standard signal processing technique such as the Multiple Signal Classification (MUSIC) algorithm can be used to extract the AoA [47]. Letting $\mathbf{Z} = [\mathbf{z}[1], \mathbf{z}[2], \ldots, \mathbf{z}[N]]$, we can express it as,

$$\mathbf{Z} = h_{rr} \mathbf{A}(\theta) \mathbf{S} + \sum_{k=1}^{K} \sqrt{\epsilon_{p,k}} \mathbf{g}_{kr} \boldsymbol{\psi}_k[N] + \sqrt{N_0} \mathbf{W}_r, \tag{2.12}$$

with $\mathbf{S} = [\mathbf{s}[1], \mathbf{s}[2], \ldots, \mathbf{s}[N]] \in C^{M_t \times N}$, $\mathbf{W} = [\mathbf{w}[1], \mathbf{w}[2], \ldots, \mathbf{w}[N]] \in C^{M_r \times N}$, and $\boldsymbol{\psi}_k[N] = [\psi_k[1], \ldots, \psi_k[N]] \in C^{1 \times N}$. Consequently, we can write the sample covariance matrix of the received radar signal, $\hat{\mathbf{R}}_{zz}$, as,

$$\hat{\mathbf{R}}_{zz} = \mathbf{Z}\mathbf{Z}^H = |h_{rr}|^2 \mathbf{A}(\theta) \mathbf{S}\mathbf{S}^H \mathbf{A}^H(\theta) + \sum_{k=1}^{K} \sum_{l=1}^{K} \sqrt{\epsilon_{p,k}} \sqrt{\epsilon_{p,l}} \mathbf{g}_{kr} \boldsymbol{\psi}_k[N] \boldsymbol{\psi}_l^H[N] \mathbf{g}_{lr}^H$$

$$+ N_0\mathbf{W}_r\mathbf{W}_r^H + 2\Re\left\{h_{rr}\mathbf{A}(\theta)\mathbf{S}\left(\sum_{k=1}^{K}\sqrt{\epsilon_{p,k}}\boldsymbol{\psi}_k^H[N]\mathbf{g}_{kr}^H\right) + \left(\sum_{k=1}^{K}\sqrt{\epsilon_{p,k}}\mathbf{g}_{kr}\boldsymbol{\psi}_k[N]\right)(\sqrt{N_0}\mathbf{W}_r^H) + \sqrt{N_0}h_{rr}^*\mathbf{W}_r\mathbf{S}^H\mathbf{A}^H(\theta)\right\}, \quad (2.13)$$

Considering $N = M_t$, we can reduce $\mathbf{S}\mathbf{S}^H = \sigma_r^2\mathbf{I}_{M_r}$. Consequently, it is easy to show that the actual covariance matrix of $\mathbf{z}[n]$ takes the form

$$\mathbf{R}_{zz} = \sigma_r^2|h_{rr}|^2\mathbf{A}(\theta)\mathbf{A}^H(\theta) + \left(\sum_{k=1}^{K}\epsilon_{p,k}\eta_{rk} + N_0\right)\mathbf{I}_{M_r} \quad (2.14)$$

Now, $\mathbf{A}(\theta)$ is a rank-1 matrix, and so is $\mathbf{A}(\theta)\mathbf{A}^H(\theta)$, therefore, $\mathbf{R}_{zz}$ can still be viewed as the sum of a rank-1 matrix and a multiple of the identity matrix. Consequently, the noise subspace of $\mathbf{R}_{zz}$ consists of the eigenvectors corresponding to the $M_r - 1$ smallest eigenvalues (each being equal to $\sum_{k=1}^{K}\epsilon_{p,k}\eta_{rk} + N_0$). We let the noise subspace of $\mathbf{R}_{zz}$ be represented by the matrix $\mathbf{V}$, and can express the estimate $\hat{\theta}$ of θ as [47],

$$\hat{\theta} = \arg\max_{\phi}\frac{1}{\mathbf{S}^H\mathbf{A}(\phi)^H\mathbf{V}\mathbf{V}^H\mathbf{A}(\phi)\mathbf{S}}. \quad (2.15)$$

Since the MUSIC algorithm is intractable for closed form performance analysis, we will evaluate its performance using Monte Carlo simulations in section 2.6.

2.4 The Uplink Sub-frame

In this section, we analyse the performance of the ICS system during the uplink sub-frame. For this purpose, we first evaluate the rates achievable by the communications subsystem via DE analysis [48, 49], and then derive the radar rate via the CRB on the MSE performance of the radar subsystem.

We can write the received signal at the communication BS as

$$\mathbf{y}[n] = \sum_{k=1}^{K}\sqrt{\beta_k\epsilon_{u,k}}\hat{\mathbf{h}}_k x_k[n] + \sum_{k=1}^{K}\sqrt{\beta_k\epsilon_{u,k}}\tilde{\mathbf{h}}_k x_k[n] + \hat{\mathbf{G}}_{rb}\mathbf{s}[n] + \tilde{\mathbf{G}}_{rb}\mathbf{s}[n] + \sqrt{N_0}\mathbf{w}_b[n]. \quad (2.16)$$

We use MMSE combining at the BS, with the matrix $\mathbf{C} \triangleq \mathbf{R}^{-1}_{yy|\hat{\mathbf{G}}_{rb},\hat{\mathbf{H}}}\hat{\mathbf{H}}$ being the combining matrix, such that, $\mathbf{R}_{yy|\hat{\mathbf{G}}_{rb},\hat{\mathbf{H}}}$ represents the covariance matrix of $\mathbf{y}[n]$ given the availability of the

channel estimates $\hat{\mathbf{G}}_{rb}$ and $\hat{\mathbf{H}}$, and can be expressed as,

$$\mathbf{R}_{yy|\hat{\mathbf{G}}_{rb},\hat{\mathbf{H}}} = \sum_{k=1}^{K} \beta_k \epsilon_{u,k} \hat{\mathbf{h}}_k \hat{\mathbf{h}}_k^H + \sigma_r^2 \hat{\mathbf{G}}_{rb} \hat{\mathbf{G}}_{rb}^H + \sum_{k=1}^{K} \beta_k \epsilon_{u,k} \bar{\mathbf{B}}_k + \left(\sigma_r^2 \eta_e + N_0\right) \mathbf{I}_{M_a}. \tag{2.17}$$

Consequently, the processed signal vector, $\mathbf{r}[n] \in C^{K\times 1}$, at the BS at the nth instant is given by $\mathbf{r}[n] = \mathbf{C}^H \mathbf{y}[n] = \hat{\mathbf{H}}^H \mathbf{R}^{-1}_{yy|\hat{\mathbf{G}}_{rb},\hat{\mathbf{H}}} \mathbf{y}[n]$. Now, letting $r_k[n]$ be the k^{th} component of $\mathbf{r}[n]$, we can write,

$$\begin{aligned} r_k[n] = \sqrt{\beta_k \epsilon_{u,k}} \hat{\mathbf{h}}_k^H \mathbf{R}^{-1}_{yy|\hat{\mathbf{G}}_{rb},\hat{\mathbf{H}}} \hat{\mathbf{h}}_k x_k[n] + \sum_{\substack{l=1 \\ l\neq k}}^{K} \sqrt{\beta_l \epsilon_{u,l}} \hat{\mathbf{h}}_k^H \mathbf{R}^{-1}_{yy|\hat{\mathbf{G}}_{rb},\hat{\mathbf{H}}} \hat{\mathbf{h}}_l x_l[n] + \sum_{l=1}^{K} \sqrt{\beta_l \epsilon_{u,l}} \hat{\mathbf{h}}_k^H \mathbf{R}^{-1}_{yy|\hat{\mathbf{G}}_{rb},\hat{\mathbf{H}}} \tilde{\mathbf{h}}_l x_l[n] \\ + \sum_{i=1}^{M_t} \hat{\mathbf{h}}_k^H \mathbf{R}^{-1}_{yy|\hat{\mathbf{G}}_{rb},\hat{\mathbf{H}}} \hat{\mathbf{g}}_{rb,i} s_i[n] + \hat{\mathbf{h}}_k^H \mathbf{R}^{-1}_{yy|\hat{\mathbf{G}}_{rb},\hat{\mathbf{H}}} \tilde{\mathbf{G}}_{rb} \mathbf{s}[n] + \sqrt{N_0} \hat{\mathbf{h}}_k^H \mathbf{R}^{-1}_{yy|\hat{\mathbf{G}}_{rb},\hat{\mathbf{H}}} \mathbf{w}_b[n]. \end{aligned} \tag{2.18}$$

Here, the first term corresponds to the desired signal, the second to the cancellable inter user interference, the third to the interference due to the channel estimation errors at the BS, the fourth to the cancellable interference from the radar subsystem, the fifth to the non-cancellable interference from the radar subsystem and the last term to the additive white Gaussian noise.

Theorem 1. *The rate achievable by the kth user in the uplink of the communication subsystem of a mMIMO based ICS system can be expressed as*

$$R_k = \log_2(1 + \gamma_{u,k}), \tag{2.19}$$

where $\gamma_{u,k}$ is the SINR for the kth user's signal at the BS, and is given as,

$$\gamma_{u,k} = \frac{\zeta_{s,k}}{\zeta_{I,k} + \zeta_{E,k} + \zeta_{RC,k} + \zeta_{RE,k} + \zeta_{w,k}}. \tag{2.20}$$

Here $\zeta_{s,k}$ corresponds to the desired signal's power and is given by,

$$\zeta_{s,k} = \beta_k \epsilon_{u,k} \frac{|\mu_k|^2}{|1 + \mu_k|^2}, \tag{2.21}$$

such that $\mu_k = Tr\{\mathbf{T}_k(\rho)\mathbf{B}_k\}$, and

$$\mathbf{T}_k(\rho) = \left(\sum_{\substack{m=1, \\ m\neq k}}^{K} \left(\frac{\beta_m \epsilon_{u,m} \mathbf{B}_{M_a}}{1 + \delta_{k,m}(\rho)} + \frac{M_r \sigma_r^2 (\eta_I - \eta_e) \mathbf{I}_{M_a}}{(K-1)(1 + \delta_{k,m}(\rho))} \right) + \mathbf{S} + \rho \mathbf{I}_{M_a} \right)^{-1}, \tag{2.22}$$

with $\delta_{k,m}(\rho) = \lim_{t\to\infty} \delta_{k,m}^{(t)}(\rho)$, such that

$$\delta_{k,m}^{(t)}(\rho) = Tr\Bigg\{\left(\beta_m\epsilon_{u,m}\mathbf{B}_{M_a} + \frac{M_r\sigma_r^2(\eta_I-\eta_e)}{K-1}\mathbf{I}_{M_a}\right)\times\left(\sum_{l=1,\neq k}^{K}\left(\frac{\beta_l\epsilon_{u,l}\mathbf{B}_l}{1+\delta_{k,l}^{t-1}(\rho)} + \frac{M_r\sigma_r^2(\eta_I-\eta_e)\mathbf{I}_{M_a}}{(K-1)(1+\delta_{k,l}^{t-1}(\rho))}\right) + \mathbf{S}+\rho\mathbf{I}_{M_a}\right)^{-1}\Bigg\}, \quad (2.23)$$

having initial values $\delta_{k,m}^{(0)}(\rho) = \frac{1}{\rho}\ \forall m$.

Similarly, $\zeta_{I,k}$ *corresponds to the inter user interference power, and is given as,*

$$\zeta_{I,k} = \sum_{\substack{l=1,\\ l\neq k}}^{K}\frac{\beta_l\epsilon_{u,l}}{|1+\mu_k|^2}\left(\mu_{k,l}^{'} + \frac{(\mu_{k,l}^{'})^2}{|1+\mu_{k,l}|^2} - 2\Re\left\{\frac{(\mu_{k,l}^{'})^{3/2}}{1+\mu_{k,l}}\right\}\right). \quad (2.24)$$

where $\mu_{k,l} = Tr\{\mathbf{T}_{k,l}(\rho)\mathbf{B}_l\}$,

$$\mathbf{T}_{k,l}(\rho) = \left(\sum_{\substack{m=1,\\ m\neq k,l}}^{K}\left(\frac{\beta_m\epsilon_{u,m}\mathbf{B}_{M_a}}{1+\delta_{k,l,m}(\rho)} + \frac{M_r\sigma_r^2(\eta_I-\eta_e)\mathbf{I}_{M_a}}{(K-2)(1+\delta_{k,l,m}(\rho))}\right) + \mathbf{S}+\rho\mathbf{I}_{M_a}\right)^{-1}, \quad (2.25)$$

with $\delta_{k,l,m}(\rho) = \lim_{t\to\infty}\delta_{k,l,m}^{(t)}(\rho)$, *such that*

$$\delta_{k,l,m}^{(t)}(\rho) = Tr\Bigg\{\left(\beta_m\epsilon_{u,m}\mathbf{B}_{M_a} + \frac{M_r\sigma_r^2(\eta_I-\eta_e)}{K-2}\mathbf{I}_{M_a}\right)\times\left(\sum_{\substack{p=1,\\ p\neq k,l}}^{K}\left(\frac{\beta_p\epsilon_{u,p}\mathbf{B}_p}{1+\delta_{k,l,p}^{t-1}(\rho)} + \frac{M_r\sigma_r^2(\eta_I-\eta_e)\mathbf{I}_{M_a}}{(K-2)(1+\delta_{k,l,p}^{t-1}(\rho))}\right) + \mathbf{S}+\rho\mathbf{I}_{M_a}\right)^{-1}\Bigg\}, \quad (2.26)$$

having initial values $\delta_{k,l,m}^{(0)}(\rho) = \frac{1}{\rho}\ \forall m$, *and* $\mu_{k,l}' = Tr\{\mathbf{B}_l\mathbf{T}_{k,l}^{'}(\rho)\}$ *where* $\mathbf{T}_{k,l}^{'}(\rho) \in C^{M\times M}$ *is given by*

$$\mathbf{T}_{k,l}^{'}(\rho) = \mathbf{T}_{k,l}(\rho)\mathbf{B}_k\mathbf{T}_{k,l}(\rho) + \mathbf{T}_{k,l}(\rho)\times\sum_{\substack{m=1,\\ m\neq k,l}}^{K}\left(\frac{\beta_m\epsilon_{u,m}\mathbf{B}_m\delta_m^{'}(\rho)}{(1+\delta_{k,l,m}(\rho))^2} + \frac{M_r\sigma_r^2(\eta_I-\eta_e)\mathbf{I}_{M_a}\delta_m^{'}(\rho)}{(K-2)(1+\delta_{k,l,m}(\rho))^2}\right)\mathbf{T}_{k,l}(\rho), \quad (2.27)$$

and

$\boldsymbol{\delta}^{'}(\rho) = [\delta_1^{'}(\rho)\ldots\delta_K^{'}(\rho)]^T$ *such that* $\boldsymbol{\delta}^{'}(\rho) = (\mathbf{I}-\mathbf{J}(\rho))^{-1}\mathbf{v}(\rho)$,

with

$[\mathbf{J}(\rho)]_{pq} = \frac{1}{(1+\delta_{k,l,p}(\rho))^2}\times Tr\{(\beta_p\epsilon_{u,p}\mathbf{B}_p + \frac{M_r}{K-2}\sigma_r^2(\eta_I-\eta_e)\mathbf{I}_{M_a})\mathbf{T}_{k,l}(\rho)\times(\beta_q\epsilon_{u,q}\mathbf{B}_q + \frac{M_r}{K-2}\sigma_r^2(\eta_I-\eta_e)\mathbf{I}_{M_a})\mathbf{T}_{k,l}(\rho)\}$, *and*

$$[\mathbf{v}(\rho)]_p = Tr\{(\beta_p\epsilon_{u,p}\mathbf{B}_p + \frac{M_r}{K-2}\sigma_r^2(\eta_I-\eta_e)\mathbf{I}_{M_a})\mathbf{T}_{k,l}(\rho)\mathbf{B}_k\mathbf{T}_{k,l}(\rho)\}.$$

The term $\zeta_{E,k}$ *corresponds to the interference power due to channel estimation error and is*

given by

$$\zeta_{E,k} = \sum_{l=1}^{K} \beta_l \epsilon_{u,l} \frac{\mu_k^{'}}{|1+\mu_k|^2}, \tag{2.28}$$

where $\mu_k^{'} = Tr\{\mathbf{T}_k^{'}(\rho)\bar{\mathbf{B}}_l\}$ *and* $\mathbf{T}_k^{'}(\rho) \in C^{M_a \times M_a}$ *is given by*

$$\mathbf{T}_k^{'}(\rho) = \mathbf{T}_k(\rho)\mathbf{B}_k\mathbf{T}_k(\rho) + \mathbf{T}_k(\rho) \times \sum_{\substack{m=1,\\ m\neq k}}^{K} \left(\frac{\beta_m \epsilon_{u,m} \mathbf{B}_m \delta_m^{'}(\rho)}{(1+\delta_{k,m}(\rho))^2} + \frac{M_r \sigma_r^2 (\eta_I - \eta_e)\mathbf{I}_{M_a}\delta_m^{'}(\rho)}{(K-2)(1+\delta_{k,m}(\rho))^2} \right) \times \mathbf{T}_k(\rho), \tag{2.29}$$

with $\mathbf{T}_k(\rho)$ *and* $\boldsymbol{\delta}^{'}(\rho)$ *as defined in* (2.25) *and* (2.27) *respectively.*

$\zeta_{RC,k}$ *corresponds to the interference at the kth user due to the cancellable component of radar generated interference and is given by*

$$\zeta_{RC,k} = \sum_{i=1}^{M_t} \sigma_r^2 \frac{1}{|1+\mu_k|^2} \left\{ \mu_{k,i}^{'} + \frac{(\mu_{k,i}^{'})^{3/2}}{|1+\mu_{k,i}|^2} - 2\Re\left\{ \frac{\mu_{k,i}^{'}}{1+\mu_{k,i}} \right\} \right\}, \tag{2.30}$$

where $\mu_{k,i}^{'} = Tr\{\mathbf{T}_{k,i}^{'}(\rho)(\eta_I - \eta_e)\mathbf{I}_{M_a}\}$, $\mu_{k,i} = Tr\{\mathbf{T}_{k,i}(\rho)(\eta_I - \eta_e)\mathbf{I}_{M_a}\}$ *and* $\mathbf{T}_{k,i}^{'}(\rho) \in C^{M_a \times M_a}$ *is given by*

$$\mathbf{T}_{k,i}^{'}(\rho) = \mathbf{T}_{k,i}(\rho)\mathbf{B}_k\mathbf{T}_{k,i}(\rho) + \mathbf{T}_{k,i}(\rho) \times \sum_{m=1,\neq k}^{K} \left(\frac{\beta_m \epsilon_{u,m} \mathbf{B}_m \delta_{k,i,m}^{'}(\rho)}{(1+\delta_{k,i,m}(\rho))^2} + \frac{(M_r-1)\sigma_r^2(\eta_I - \eta_e)\mathbf{I}_{M_a}\delta_{k,i,m}^{'}(\rho)}{(K-1)(1+\delta_{k,i,m}(\rho))^2} \right) \times \mathbf{T}_{k,i}(\rho), \tag{2.31}$$

and $\mathbf{T}_{k,i}(\rho)$ *is given by*

$$\mathbf{T}_{k,i}(\rho) = \left(\sum_{m=1,\neq k}^{K} \frac{\beta_m \epsilon_{u,m} \mathbf{B}_m}{1+\delta_{k,i,m}(\rho)} + \frac{(M_r-1)\sigma_r^2(\eta_I - \eta_e)\mathbf{I}_{M_a}}{(K-1)(1+\delta_{k,i,m}(\rho))} + \mathbf{S} + \rho\mathbf{I}_{M_a} \right)^{-1}, \tag{2.32}$$

with $\delta_{k,i,m}(\rho) = \lim_{t\to\infty} \delta_{k,i,m}^{(t)}(\rho)$ *being obtained iteratively from*

$$\delta_{k,i,m}^{(t)}(\rho) = Tr\left\{ \left(\beta_m \epsilon_{u,m} \mathbf{B}_m + \frac{(M_r-1)\sigma_r^2(\eta_I - \eta_e)}{K-1}\mathbf{I}_{M_a} \right) \times \left(\sum_{\substack{u=1,\\ u\neq k}}^{K} \left(\frac{\beta_m \epsilon_{u,m}\mathbf{B}_m}{1+\delta_{k,i,u}^{t-1}(\rho)} + \frac{(M_r-1)\sigma_r^2(\eta_I-\eta_e)\mathbf{I}_{M_a}}{(K-1)(1+\delta_{k,i,u}^{t-1}(\rho))} \right) + \mathbf{S} + \rho\mathbf{I}_{M_a} \right)^{-1} \right\}, \tag{2.33}$$

after being initialized as $\delta_{k,i,m}^{(0)}(\rho) = \frac{1}{\rho}\ \forall\, j$, *and* $\boldsymbol{\delta}_{k,i}^{'}(\rho) = [\delta_{k,i,1}^{'}(\rho) \ldots \delta_{k,i,K}^{'}(\rho)]^T$ *such that*

$$\boldsymbol{\delta}_{k,i}^{'}(\rho) = (\mathbf{I}_K - \mathbf{J}_{k,i}(\rho))^{-1}\mathbf{v}_{k,i}(\rho),$$

with

$$[\mathbf{J}_{k,i}(\rho)]_{pq} = \frac{1}{(1+\delta_{k,i,p}(\rho))^2} \times Tr\{(\beta_p \epsilon_{u,p}\mathbf{B}_p + \frac{(M_r-1)}{K-1}\sigma_r^2(\eta_I - \eta_e)\mathbf{I}_{M_a})\mathbf{T}_{k,i}(\rho)(\beta_q \epsilon_{u,q}\mathbf{B}_q + \frac{(M_r-1)}{K-1}\sigma_r^2(\eta_I - \eta_e)\mathbf{I}_{M_a})\mathbf{T}_{k,i}(\rho)\},$$

and

$$[\mathbf{v}_{k,i}(\rho)]_p = Tr\{(\beta_p \epsilon_{u,p}\mathbf{B}_p + \frac{(M_r-1)}{K-1}\sigma_r^2(\eta_I - \eta_e)\mathbf{I}_{M_a})\mathbf{T}_{k,i}(\rho)\mathbf{B}_k\mathbf{T}_{k,i}(\rho)\}.$$

$\zeta_{RE,k}$ corresponds to the interference at the kth user due to error in the estimate of inter-system interference channel between BS and radar and is given by

$$\zeta_{RE,k} = \sum_{i=1}^{M_t} \sigma_r^2 \frac{b_k^2 \eta_e \mu_k^{'}}{|1 + b_k^2 \mu_k|^2}. \tag{2.34}$$

where $\mu_k^{'} = Tr\{\mathbf{T}_k^{'}(\rho)\}$ and is given by (2.29).
$\zeta_{w,k}$ corresponds to the interference at kth user due to additive Gaussian noise and is given by

$$\zeta_{w,k} = N_0 \frac{b_k^2 \mu_k^{'}}{|1 + b_k^2 \mu_k|^2}. \tag{2.35}$$

Proof. See Appendix A.1. □

We can observe that the use of MMSE combining, along with the effects of channel hardening offered by the large number of antennas available at the BS effectively cancels the radar generated interference in the uplink. This effect is illustrated in the results obtained in Fig. 2.9 and Fig. 2.10.

We next quantify the performance of the radar subsystem in terms of the achievable radar rate according the notion developed in [29]. We note that the received signal at the radar takes the form

$$\mathbf{z}[n] = h_{rr}\mathbf{A}(\theta)\mathbf{s}[n] + \sum_{k=1}^{K} \sqrt{\epsilon_{p,k}}\mathbf{g}_{kr}\psi_k[n] + \sqrt{N_0}\mathbf{w}_r[n]. \tag{2.36}$$

Theorem 2. *The radar rate can be expressed as [29],*

$$R_{radar,u} = \log\left(1 + \frac{1}{CRB(\theta)}\right), \tag{2.37}$$

where $CRB(\theta)$ corresponds to the Cramer-Rao bound on the MSE of the AoA estimate at the radar, given as,

$$CRB(\theta) = \frac{N_0 + \sum_{k=1}^{K} \epsilon_{p,k}\eta_r k}{2\sigma_r^2 |h_{rr}|^2} \frac{1}{\Re\{Tr(\dot{\mathbf{A}}(\theta)\dot{\mathbf{A}}^H(\theta))\}}, \tag{2.38}$$

with $\dot{\mathbf{A}}(\theta)$ representing the derivative of $\mathbf{A}(\theta)$ wrt θ.

Proof. See Appendix A.2. □

We can observe in the expression for the CRB that the numerator contains the noise term as well as the interferences from all the communications users, limiting the performance of the radar subsystem. We can obtain the rate regions for the overall ICS system during the uplink communication frame by using Theorems 1 and 2. We next look at the performance of the ICS system during the downlink communication subframe.

2.5 The Downlink Sub-frame

In this section, we analyse the performance of the ICS system during the downlink sub-frame. Letting $\bar{p}_k[n]$ denote the data symbol to be transmitted to the kth user, we can write the data vector to be transmitted by the mMIMO BS in the downlink as $\bar{\mathbf{p}}[n] = [\bar{p}_1[n], \bar{p}_2[n], \ldots, p_K[n], 0, \ldots, 0] \in C^{(K+M_r)\times 1}$. We also let $\bar{\mathbf{H}} = [\hat{\mathbf{H}}\, \hat{\mathbf{G}}_{br}] \in C^{M\times(K+M_r)}$ be the horizontal concatenation of the estimates of the communication channel, and the radar generated interference channel. Using this, we can define the precoder matrix at the BS as, $\mathbf{Q} = (\bar{\mathbf{H}}\bar{\mathbf{H}}^H + \alpha \mathbf{I}_{M_a})^{-1}\hat{\mathbf{H}}^*$, with α being the regularization parameter. This is equivalent to forming a null in the direction of interference channel to the radar. Consequently, the precoded downlink signal transmitted by the BS is expressed as $\mathbf{p}[n] = \mathbf{Q}\text{diag}(\boldsymbol{\epsilon}_d)\bar{\mathbf{p}}[n]$, with $(\boldsymbol{\epsilon}_d) = [\sqrt{\epsilon_{d,1}}, \ldots, \sqrt{\epsilon_{d,K}}]^T$, and $\sqrt{\epsilon_{d,k}}$ representing the downlink energy allocated to the kth user after power control. We can now write the signal received at the kth user as,

$$r_k[n] = \sqrt{\beta_k}\hat{\mathbf{h}}_k^T\mathbf{p}[n] + \sqrt{\beta_k}\tilde{\mathbf{h}}_k^T\mathbf{p}[n] + \mathbf{g}_{rk}^T\mathbf{s}[n] + w_k[n]. \tag{2.39}$$

This can also be written as

$$r_k[n] = \sqrt{\beta_k\epsilon_{d,k}}\hat{\mathbf{h}}_k^T(\bar{\mathbf{H}}\bar{\mathbf{H}}^H + \alpha\mathbf{I}_{M_a})^{-1}\hat{\mathbf{h}}_k^*\bar{p}_k[n] + \sum_{\substack{m=1,\\ m\neq k}}^{K}\sqrt{\beta_k\epsilon_{d,m}}\hat{\mathbf{h}}_k^T(\bar{\mathbf{H}}\bar{\mathbf{H}}^H + \alpha\mathbf{I}_{M_a})^{-1}\hat{\mathbf{h}}_{M_a}^*\bar{p}_{M_a}[n]$$
$$+ \sqrt{\beta_k}\tilde{\mathbf{h}}_k^T(\bar{\mathbf{H}}\bar{\mathbf{H}}^H + \alpha\mathbf{I}_{M_a})^{-1}\hat{\mathbf{H}}^*\bar{\mathbf{p}}[n] + \mathbf{g}_{rk}^T\mathbf{s}[n] + w_k[n]. \tag{2.40}$$

where the first term indicates the desired signal corresponding to the kth user, the second term is the cancellable inter user interference from the data meant for the other users, the third term

corresponds to the interference due to the channel estimation error at the BS, the fourth term is due to the interference from the radar subsystem and the last term is due to additive white Gaussian noise (AWGN).

Theorem 3. *The rate achievable by the kth user in the downlink of the communication subsystem of a ICS system can be expressed as*

$$R_{d,k} = \log_2(1 + \gamma_{d,k}), \tag{2.41}$$

where $\gamma_{d,k}$ is the SINR for the kth user's signal at the BS, and is given as,

$$\gamma_{d,k} = \frac{\zeta_{r,k}}{\zeta_{r,I,k} + \zeta_{r,E,k} + \zeta_{r,RC,k} + \zeta_{r,w,k}}. \tag{2.42}$$

Here $\zeta_{r,k}$ corresponds to the desired signal power and is given by

$$\zeta_{r,k} = \beta_k \epsilon_{d,k} \left| \frac{\mu_{k,\alpha}}{1 + \mu_{k,\alpha}} \right|^2 \tag{2.43}$$

with $\mu_{k,\alpha} = Tr\{\mathbf{T}_k(\alpha)\mathbf{B}_k\}$ such that

$$\mathbf{T}_k(\alpha) = \left(\sum_{\substack{l=1,\\ l\neq k}}^{K} \frac{\mathbf{B}_l}{1 + \delta_{k,l}(\alpha)} + \sum_{l=K+1}^{K+M_r} \frac{(\eta_I - \eta_e)\mathbf{I}_{M_a}}{1 + \delta_{k,l}(\alpha)} + \alpha \mathbf{I}_{M_a} \right)^{-1}, \tag{2.44}$$

and $\delta_{k,l}(\alpha) = \lim_{t\to\infty} \delta_{k,l}^{(t)}(\alpha)$, which is iteratively computed as

$$\delta_{k,l}^{(t)}(\alpha) = Tr\left\{ \mathbf{B}_l \left(\sum_{\substack{m=1,\\ m\neq k}}^{K} \frac{\mathbf{B}_m}{1 + \delta_{k,m}^{(t-1)}(\alpha)} + \sum_{m=K+1}^{K+M_r} \frac{(\eta_I - \eta_e)\mathbf{I}_{M_a}}{1 + \delta_{k,m}^{(t-1)}(\alpha)} + \alpha \mathbf{I}_{M_a} \right)^{-1} \right\} \quad 1 \le l \le K \tag{2.45}$$

$$\delta_{k,l}^{(t)}(\alpha) = Tr\left\{ (\eta_I - \eta_e)\mathbf{I}_{M_a} \left(\sum_{\substack{m=1,\\ m\neq k}}^{K} \frac{\mathbf{B}_m}{1 + \delta_{k,m}^{(t-1)}(\alpha)} + \sum_{m=K+1}^{K+M_r} \frac{(\eta_I - \eta_e)\mathbf{I}_{M_a}}{1 + \delta_{k,m}^{(t-1)}(\alpha)} + \alpha \mathbf{I}_{M_a} \right)^{-1} \right\} \quad K{+}1 \le l \le K{+}M_r \tag{2.46}$$

with initial values $\delta_{k,l}^{(0)}(\alpha) = \frac{1}{\alpha}\ \forall\ l$. The term $\zeta_{r,I,k}$ corresponds to the inter user interference power, and is given as,

$$\zeta_{r,I,k} = \sum_{m=1,m\neq k}^{K} \beta_k \epsilon_{d,m} \frac{1}{|1 + \mu_{k,\alpha}|^2} \times \left\{ (\mu'_{k,m,\alpha}) + \frac{(\mu'_{k,m,\alpha})^2}{|1 + \mu_{k,\alpha}|^2} - 2\Re\left(\frac{(\mu'_{k,m,\alpha})^{3/2}}{1 + \mu_{k,\alpha}} \right) \right\}, \tag{2.47}$$

where $\mu'_{k,m,\alpha} = Tr\{\mathbf{T}'_{k,m}(\alpha)\mathbf{B}_m\}$, such that

$$\mathbf{T}_{k,m}^{'}(\alpha) = \mathbf{T}_{k,m}(\alpha)\mathbf{B}_k\mathbf{T}_{k,m}(\alpha) + \mathbf{T}_{k,m}(\alpha)\left(\sum_{\substack{l=1,\\ l\neq k,m}}^{K} \frac{\mathbf{B}_l\delta_{k,m,l}^{'}(\alpha)}{1+\delta_{k,m,l}(\alpha)} + \sum_{l=K+1}^{K+M_r} \frac{(1-\eta_e)\mathbf{I}_{M_a}\delta_{k,m,l}^{'}(\alpha)}{1+\delta_{k,m,l}(\alpha)}\right)\mathbf{T}_{k,m}(\alpha) \tag{2.48}$$

with

$$\mathbf{T}_{k,m}(\alpha) = \left(\sum_{\substack{l=1,\\ l\neq k,m}}^{K} \frac{\mathbf{B}_l}{1+\delta_{k,m,l}(\alpha)} + \sum_{l=K+1}^{K+M_r} \frac{(\eta_I-\eta_e)\mathbf{I}_{M_a}}{1+\delta_{k,m,l}(\alpha)} + \alpha\mathbf{I}_{M_a}\right)^{-1}, \tag{2.49}$$

and $\delta_{k,m,l}(\alpha) = \lim_{t\to\infty}\delta_{k,m,l}^{(t)}(\alpha)$,

$$\delta_{k,m,l}^{(t)}(\alpha) = Tr\left\{\mathbf{B}_l\left(\sum_{\substack{p=1,\\ p\neq k,m}}^{K} \frac{\mathbf{B}_p}{1+\delta_{k,m,p}^{(t-1)}(\alpha)} + \sum_{p=K+1}^{K+M_r} \frac{(\eta_I-\eta_e)\mathbf{I}_{M_a}}{1+\delta_{k,m,p}^{(t-1)}(\alpha)} + \alpha\mathbf{I}_{M_a}\right)^{-1}\right\} \quad 1\leq l\leq K \tag{2.50}$$

$$\delta_{k,m,l}^{(t)}(\alpha) = Tr\left\{(\eta_I-\eta_e)\mathbf{I}_{M_a}\left(\sum_{\substack{p=1,\\ p\neq k,m}}^{K} \frac{\mathbf{B}_p}{1+\delta_{k,m,p}^{(t-1)}(\alpha)} + \sum_{p=K+1}^{K+M_r} \frac{(\eta_I-\eta_e)\mathbf{I}_{M_a}}{1+\delta_{k,m,p}^{(t-1)}(\alpha)} + \alpha\mathbf{I}_{M_a}\right)^{-1}\right\} \quad K+1\leq l\leq K+M_r \tag{2.51}$$

with initial values $\delta_{k,m,l}^{(0)}(\alpha) = \frac{1}{\alpha}\ \forall\ l$. *Here*

$$\boldsymbol{\delta}_{k,m}^{'}(\alpha) = [\delta_{k,m,1}^{'}(\alpha)\ldots\delta_{k,m,K+M_r-2}^{'}(\alpha)]^T \tag{2.52}$$

such that

$$\boldsymbol{\delta}_{k,m}^{'}(\alpha) = (\mathbf{I}_{K+M_r-2} - \mathbf{J}(\rho))^{-1}\mathbf{v}(\rho), \tag{2.53}$$

where

$$[\mathbf{J}(\alpha)]_{pq} = \frac{Tr\{\mathbf{B}_p\mathbf{T}_{k,m}(\alpha)\mathbf{B}_q\mathbf{T}_{k,m}(\alpha)\}}{(1+\delta_{k,m,p}(\alpha))^2}, \tag{2.54}$$

and

$$[\mathbf{v}(\alpha)]_p = Tr\{\mathbf{B}_p\mathbf{T}_{k,m}(\alpha)\mathbf{T}_{k,m}(\alpha)\}, \tag{2.55}$$

when $p,q = 1,2,\ldots,K,\neq k,m$, *and*

$$[\mathbf{J}(\alpha)]_{pq} = \frac{Tr\{(\eta_I-\eta_e)\mathbf{I}_{M_a}\mathbf{T}_{k,m}(\alpha)(\eta_I-\eta_e)\mathbf{I}_{M_a}\mathbf{T}_{k,m}(\alpha)\}}{(1+\delta_{k,m,p}(\alpha))^2}, \tag{2.56}$$

and

$$[\mathbf{v}(\alpha)]_p = Tr\{(\eta_I-\eta_e)\mathbf{I}_{M_a}\mathbf{T}_{k,m}(\alpha)\mathbf{T}_{k,m}(\alpha)\} \tag{2.57}$$

when $p,q = K+1,\ldots,K+M_r$.

The term $\zeta_{r,E,k}$ *corresponds to the interference power due to channel estimation error and is*

given by

$$\zeta_{r,E,k} = \sum_{l=1}^{K} \beta_k \epsilon_{d,l} \frac{\mu'_{l,\alpha}}{|1+\mu_{l,\alpha}|^2}, \tag{2.58}$$

where $\mu_{l,\alpha} = Tr\{\mathbf{T}_l(\alpha)\mathbf{B}_l\}$ *and* $\mu'_{l,\alpha} = Tr\{\mathbf{T}'_l(\alpha)\mathbf{B}_l\}$ *such that*

$$\mathbf{T}'_l(\alpha) = \mathbf{T}_l(\alpha)\bar{\mathbf{B}}_k\mathbf{T}_l(\alpha) + \mathbf{T}_l(\alpha)\left(\sum_{d=1,\neq l}^{K} \frac{\mathbf{B}_d\delta'_{l,d}(\alpha)}{1+\delta_{l,d}(\alpha)} + \sum_{d=K+1}^{K+M_r} \frac{(\eta_I-\eta_e)\mathbf{I}_{M_a}\delta'_{l,d}(\alpha)}{1+\delta_{l,d}(\alpha)}\right)\mathbf{T}_l(\alpha), \tag{2.59}$$

and

$$\mathbf{T}_l(\alpha) = \left(\sum_{\substack{d=1,\\ d\neq l}}^{K} \frac{\mathbf{B}_d}{1+\delta_{l,d}(\alpha)} + \sum_{d=K+1}^{K+M_r} \frac{(\eta_I-\eta_e)\mathbf{I}_{M_a}}{1+\delta_{l,d}(\alpha)} + \alpha\mathbf{I}_{M_a}\right)^{-1}, \tag{2.60}$$

where $\delta_{l,d}(\alpha) = \lim_{t\to\infty} \delta^{(t)}_{l,d}(\alpha)$,

$$\delta^{(t)}_{l,d}(\alpha) = Tr\left\{\mathbf{B}_d\left(\sum_{\substack{m=1,\\ m\neq l}}^{K} \frac{\mathbf{B}_m}{1+\delta^{(t-1)}_{l,m}(\alpha)} + \sum_{m=K+1}^{K+M_r} \frac{(\eta_I-\eta_e)\mathbf{I}_{M_a}}{1+\delta^{(t-1)}_{l,m}(\alpha)} + \alpha\mathbf{I}_{M_a}\right)^{-1}\right\} \quad 1 \le d \le K \tag{2.61}$$

$$\delta^{(t)}_{l,d}(\alpha) = Tr\left\{(\eta_I-\eta_e)\mathbf{I}_{M_a}\left(\sum_{\substack{m=1,\\ m\neq l}}^{K} \frac{\mathbf{B}_m}{1+\delta^{(t-1)}_{l,m}(\alpha)} + \sum_{m=K+1}^{K+M_r} \frac{(\eta_I-\eta_e)\mathbf{I}_{M_a}}{1+\delta^{(t-1)}_{l,m}(\alpha)} + \alpha\mathbf{I}_{M_a}\right)^{-1}\right\} \quad K+1 \le d \le K+M_r \tag{2.62}$$

with initial values $\delta^{(0)}_{l,d}(\alpha) = \frac{1}{\alpha}\ \forall\ l$, *and*

$$\boldsymbol{\delta}'_{l,d}(\alpha) = (\mathbf{I}_{K+M_r-1} - \mathbf{J}(\alpha))^{-1}\mathbf{v}(\alpha),$$

$$[\mathbf{J}(\alpha)]_{pq} = \frac{Tr\{\mathbf{B}_p\mathbf{T}_l(\alpha)\mathbf{B}_q\mathbf{T}_l(\alpha)\}}{(1+\delta_{l,p}(\alpha))^2},$$

$$[\mathbf{v}(\alpha)]_p = Tr\{\mathbf{B}_p\mathbf{T}_{k,m}(\alpha)\mathbf{T}_{k,m}(\alpha)\},$$

when $p, q = 1, 2, \ldots, K, \neq l$ *and*

$$[\mathbf{J}(\alpha)]_{pq} = \frac{Tr\{(\eta_I-\eta_e)\mathbf{I}_{M_a}\mathbf{T}_l(\alpha)(\eta_I-\eta_e)\mathbf{I}_{M_a}\mathbf{T}_l(\alpha)\}}{(1+\delta_{l,p}(\alpha))^2},$$

$$[\mathbf{v}(\alpha)]_p = Tr\{(\eta_I-\eta_e)\mathbf{I}_{M_a}\mathbf{T}_{k,m}(\alpha)\bar{\mathbf{B}}_k\mathbf{T}_{k,m}(\alpha)\},$$

when $p, q = K+1, \ldots, K+M_r$.
$\zeta_{r,RC,k}$ *corresponds to the interference power due to the presence of radar subsystem is,*

$$\zeta_{r,RC,k} = \sigma_r^2\eta_{r,k} \tag{2.63}$$

$\zeta_{r,W,k}$ corresponds to the interference due to the presence of AWGN and is given by

$$\zeta_{r,W,k} = N_0. \tag{2.64}$$

Proof. See Appendix A.3. □

Here it is important to note that the RZF beamforming by the BS only nulls the interference from the BS to the radar and does not affect the interference from the radar to the users. The radar to user interference, denoted by $\zeta_{r,RC,k}$ in the SINR expression remains unmitigated.

We next analyse the performance of radar subsystem in the downlink subframe. We note that the received signal at the radar is given by

$$\mathbf{z}[n] = h_{rr}\mathbf{A}(\theta)\mathbf{s}[n] + \hat{\mathbf{G}}_{br}^H\mathbf{Q}\text{diag}(\sqrt{\boldsymbol{\epsilon}_d})\bar{\mathbf{p}}[n] + \tilde{\mathbf{G}}_{br}^H\mathbf{Q}\text{diag}(\sqrt{\boldsymbol{\epsilon}_d})\bar{\mathbf{p}}[n] + \sqrt{N_0}\mathbf{w}_r[n]. \tag{2.65}$$

Theorem 4. *The radar rate can be expressed as,*

$$R_{radar,d} = \log\left(1 + \frac{1}{CRB(\theta)}\right), \tag{2.66}$$

where

$$CRB(\theta) = \frac{\sigma_{wr,d}^2}{2\sigma_r^2|h_{rr}|^2}\frac{1}{\Re\{Tr(\dot{\mathbf{A}}(\theta)\dot{\mathbf{A}}^H(\theta))\}}, \tag{2.67}$$

with

$$\sigma_{wr,d}^2 = N_0 + \frac{\mu_{i,\alpha}^{'}}{|1 + \mu_{\hat{\mathbf{g}}_{br,m}}|^2} + \mu_{\alpha}^{'} \tag{2.68}$$

such that $\mu_{\alpha}^{'} = Tr\left\{\mathbf{T}^{'}(\alpha)\left(\sum_{i=1}^{K}\epsilon_{d,i}\mathbf{B}_i\right)\right\}$,

$$\mathbf{T}^{'}(\alpha) = \mathbf{T}(\alpha)(\eta_e\mathbf{I}_{M_a})\mathbf{T}(\alpha) + \mathbf{T}(\alpha)\left(\sum_{l=1}^{K}\frac{\mathbf{B}_l\delta_l^{'}(\alpha)}{1+\delta_l(\alpha)} + \sum_{l=K+1}^{K+M_r}\frac{(\eta_I-\eta_e)\mathbf{I}_{M_a}\delta_l^{'}(\alpha)}{1+\delta_l(\alpha)}\right)\mathbf{T}(\alpha) \tag{2.69}$$

with

$$\mathbf{T}(\alpha) = \left(\sum_{l=1}^{K}\frac{\mathbf{B}_l}{1+\delta_l(\alpha)} + \sum_{l=K+1}^{K+M_r}\frac{(\eta_I-\eta_e)\mathbf{I}_{M_a}}{1+\delta_l(\alpha)} + \alpha\mathbf{I}_{M_a}\right)^{-1}, \tag{2.70}$$

and $\delta_l(\alpha) = \lim_{t\to\infty}\delta_l^{(t)}(\alpha)$,

$$\delta_l^{(t)}(\alpha) = Tr\left\{\mathbf{B}_l\left(\sum_{p=1}^{K}\frac{\mathbf{B}_p}{1+\delta_p^{(t-1)}(\alpha)} + \sum_{p=K+1}^{K+M_r}\frac{(\eta_I-\eta_e)\mathbf{I}_{M_a}}{1+\delta_p^{(t-1)}(\alpha)} + \alpha\mathbf{I}_{M_a}\right)^{-1}\right\} \quad 1 \le l \le K \tag{2.71}$$

$$\delta_l^{(t)}(\alpha) = Tr\left\{(\eta_I-\eta_e)\mathbf{I}_{M_a}\left(\sum_{\substack{p=1,\\ p\neq k,m}}^{K}\frac{\mathbf{B}_p}{1+\delta_p^{(t-1)}(\alpha)}+\sum_{m=K+1}^{K+M_r}\frac{(\eta_I-\eta_e)\mathbf{I}_{M_a}}{1+\delta_p^{(t-1)}(\alpha)}+\alpha\mathbf{I}_{M_a}\right)^{-1}\right\} \quad K{+}1 \leq l \leq K{+}M_r \tag{2.72}$$

such that

$$\delta_l^{(0)}(\alpha) = \frac{1}{\alpha}\ \forall\ l,$$
$$\boldsymbol{\delta}^{'}(\alpha) = [\delta_1^{'}(\alpha)\ldots\delta_{K+M_r-2}^{'}(\alpha)]^T,$$
$$\boldsymbol{\delta}^{'}(\alpha) = (\mathbf{I}_{K+M_r}-\mathbf{J}(\rho))^{-1}\mathbf{v}(\rho),$$

with

$$[\mathbf{J}(\alpha)]_{pq} = \frac{Tr\{\mathbf{B}_p\mathbf{T}(\alpha)\mathbf{B}_q\mathbf{T}(\alpha)\}}{(1+\delta_p(\alpha))^2},$$

$$[\mathbf{v}(\alpha)]_p = Tr\{\mathbf{B}_p\mathbf{T}(\alpha)\eta_e\mathbf{I}_{M_a}\mathbf{T}(\alpha)\},$$

when $p,q = 1,2,\ldots,K$ *and*

$$[\mathbf{J}(\alpha)]_{pq} = \frac{Tr\{(\eta_I-\eta_e)\mathbf{I}_{M_a}\mathbf{T}(\alpha)(\eta_I-\eta_e)\mathbf{I}_{M_a}\mathbf{T}(\alpha)\}}{(1+\delta_p(\alpha))^2},$$

$$[\mathbf{v}(\alpha)]_p = Tr\{(\eta_I-\eta_e)\mathbf{I}_{M_a}\mathbf{T}(\alpha)\eta_e\mathbf{I}_{M_a}\mathbf{T}(\alpha)\},$$

when $p,q = K+1,\ldots,K+M_r$. *Also,*

$$\mu_{i,\alpha}^{'} = Tr\left\{\mathbf{T}_i^{'}(\alpha)\left(\sum_{i=1}^{K}\epsilon_{d,i}\mathbf{B}_i\right)\right\} \tag{2.73}$$

where,

$$\mathbf{T}_i^{'}(\alpha) = \mathbf{T}_{\hat{\mathbf{g}}_{br,m}}(\alpha)(\eta_I-\eta_e)\mathbf{I}_{M_a}\mathbf{T}_{\hat{\mathbf{g}}_{br,m}}(\alpha)+\mathbf{T}_{\hat{\mathbf{g}}_{br,m}}(\alpha)\times\left(\sum_{l=1}^{K}\frac{\mathbf{B}_l\delta_l^{'}(\alpha)}{1+\delta_l(\alpha)}+\sum_{l=K+1}^{K+M_r}\frac{(\eta_I-\eta_e)\mathbf{I}_{M_a}\delta_l^{'}(\alpha)}{1+\delta_l(\alpha)}\right)\mathbf{T}_{\hat{\mathbf{g}}_{br,m}}(\alpha) \tag{2.74}$$

with

$$\mathbf{T}_{\hat{\mathbf{g}}_{br,m}}(\alpha) = \left(\sum_{l=1}^{K}\frac{\mathbf{B}_l}{1+\delta_l(\alpha)}+\sum_{\substack{l=K+1,\\ l\neq m}}^{K+M_r}\frac{(\eta_I-\eta_e)\mathbf{I}_{M_a}}{1+\delta_l(\alpha)}+\alpha\mathbf{I}_{M_a}\right)^{-1}, \tag{2.75}$$

and $\mu_{\hat{\mathbf{g}}_{br,m}} = Tr\{\mathbf{T}_{\hat{\mathbf{g}}_{br,m}}(\alpha)(\eta_I-\eta_e)\mathbf{I}_{M_a}\}$.

Proof. See Appendix A.4. □

Again, the rate regions quantifying the performance of the proposed ICS system can be obtained by using Theorems 3 and 4 in conjunction. In the next section, we present simulation

results to better visualize the ideas presented by these theorems.

2.6 Simulation Results

In this section we validate our derived results using Monte-Carlo simulations and prescribe parameter values for optimized system operation. Here, the communication subsystem consists of single cell mMIMO system having M=128 antennas (with an inter antenna spacing equal to half the carrier wavelength) at a BS that is located at the cell centre serving $K = 8$ users distributed uniformly across the cell, and operating at a carrier frequency $f_c = 3$ GHz. The complex basedband equivalent communications and radar signals are assumed to have a bandwidth of 20 MHz. For this purpose, we assume that the channels to the different antennas are drawn from a spatial first order autoregressive (AR-1) process, with a regression coefficient ν, that is, the channel between the kth UE and the ith BS antenna can be represented as

$$h_{ik} = \nu h_{(i-1)k} + \vartheta_{ik}, \tag{2.76}$$

with ϑ_{ik} being the spatial innovation component having a variance $1 - \nu^2$ and uncorrelated with $h_{(i-1)k}$. This results in a the correlation coefficient among the kth and the lth antenna becoming $\nu^{(k-l)}$

$$\boldsymbol{\Sigma}_k = \begin{bmatrix} 1 & \nu & \nu^2 & \dots & \nu^{M-1} \\ 1 & \nu & \nu^2 & \dots & \nu^{M-1} \\ \vdots & \vdots & \vdots & \ddots & \vdots \\ 1 & \nu & \nu^2 & \dots & \nu^{M-1} \end{bmatrix} \tag{2.77}$$

for the purpose of these simulations we consider $\nu = 0.05$. For simplicity, we assume the cell to be circular, and having a radius 100 m. The communication frame consists of 1024 channel uses with the first $K = 8$ channel uses dedicated for training, and the remaining divided equally for uplink and downlink data transmission. The performance of the communication subsystem, unless stated otherwise is measured in terms of the average per user achievable rate. For the purpose of these experiments, we consider the interference channels to be known at the BS with a 10% error (i.e. $\eta_e = 0.1$) and the variance of AWGN to be unity (i.e. $N_0 = 1$). The large scale

fading path loss in wireless channels is modelled by using the simple path loss model [50] with the path loss exponent being 3.6. We also apply channel inversion based power control in both uplink and downlink.

On the other hand, the radar subsystem consists of a MIMO radar with $M_t = M_r = 8$, transmit and receive antennas. Both the radar subsystem and the target are assumed to be located randomly within the cell and their locations follow the same distribution as the users. Unless stated otherwise, the performance of the radar is quantified in terms of the radar rate derived in the previous sections. All the performance metrics presented in this section are generated by averaging over 10,000 realizations of the system.

2.6.1 CSI Acqusition

Fig. 2.2 plots the MSE of uplink channel estimate as a function of the received pilot SNR for different values of radar transmit power, σ_r^2. This can be calculated in the closed form as $\mathrm{Tr}(\bar{\mathbf{B}})$. We observe that a higher radar transmit power does result in a saturation of the channel estimation MSE, however, since the path loss between the radar transmitter and the BS is significant, the interference due to the radar does not exceed the received pilot power, limiting the MSE to 0.1. The impact of radar generated interference is minimal when both the communication system and the radar are operating at SNRs around 10 dB, which results in a fair channel estimation MSE.

In Fig. 2.3 we plot the mean square estimation error of the AoA at the radar as a function of radar received SNR for three different values of pilot powers transmitted by the communication subsystem. Since this is obtained using the MUSIC algorithm, we cannot have an expression for this MSE in the closed form. We observe that the radar MSE performance degrades as the pilot power of the communication subsystem, and hence the interference to the radar subsystem increases.

2.6.2 Validation of Asymptotic Approximations

In Figs. 2.4 and 2.5 we respectively plot the achievable uplink and downlink rates of the communication subsystem as functions of the received SNR with $\sigma_r^2 = 1$. The theoretical

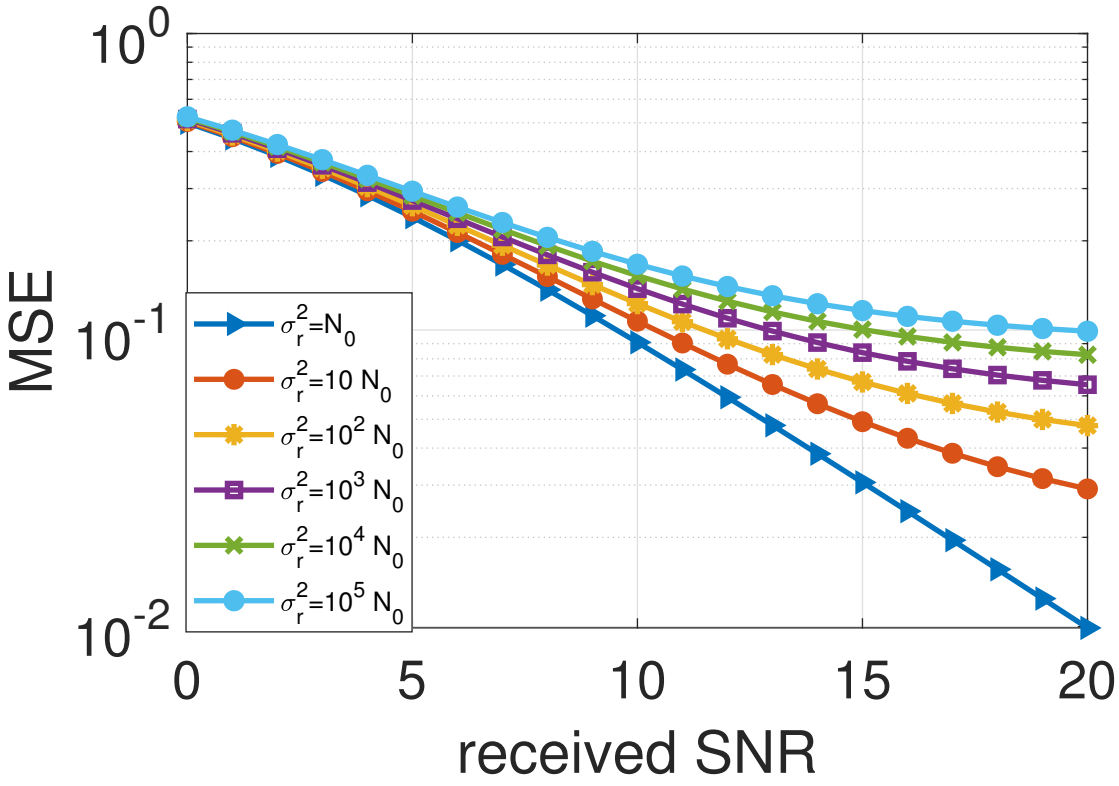

Fig. 2.2: Channel estimation MSE as a function of the received pilot SNR for different values of radar transmit power.

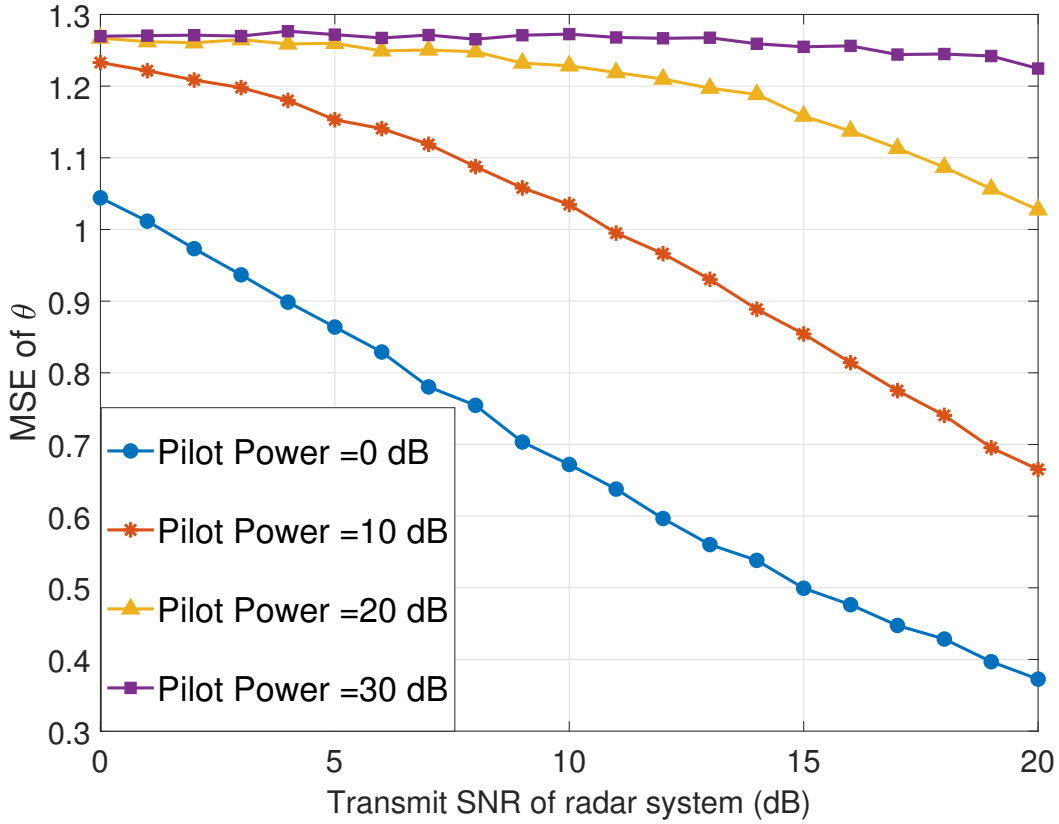

Fig. 2.3: Radar AoA MSE versus radar SNR for different values of transmit pilot power.

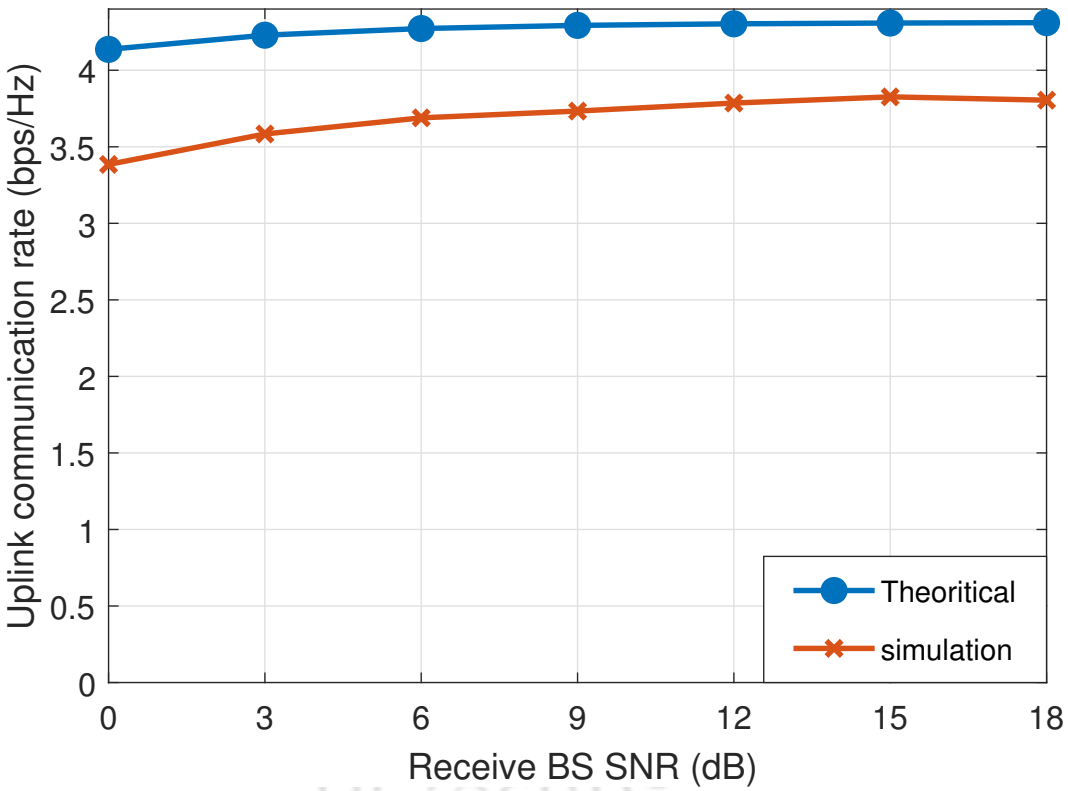

Fig. 2.4: Average uplink communication rate from both theoretical and simulation analysis versus received data SNR for $\sigma_r^2 = N_0$.

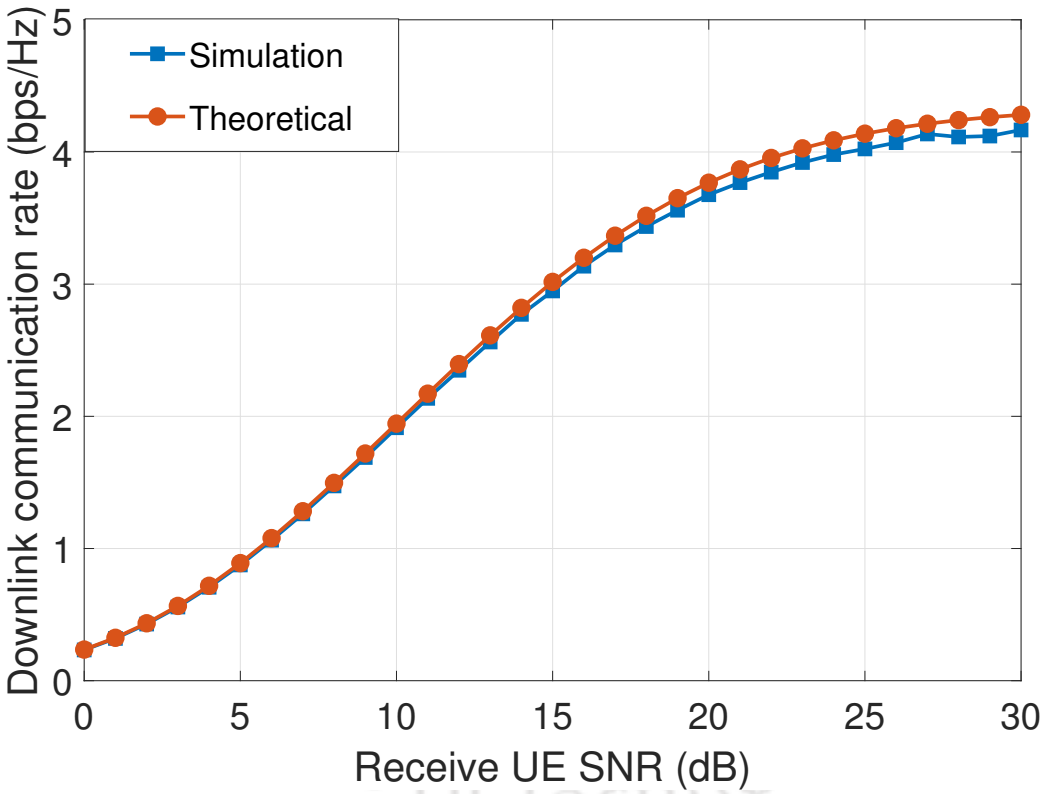

Fig. 2.5: Average communication rate in downlink as a function of the received data SNR from both theoretical and simulation analysis for $\sigma_r^2 = N_0$ radar transmitted power.

values used in these plots are obtained using Theorems 1 and 3 for the uplink and downlink cases respectively. We observe that the simulated results match closely with our derived results, allowing us to use the former for further analysis.

2.6.3 Uplink Data Transmission

Fig. 2.6 plots the achievable communication rate in the uplink subframe as a function of received BS SNR for different levels of interference caused by the radar subsystem. For higher values of received SNR at BS (i.e. $>$ 30 dB) we observe that even a radar SNR of 30 dB results in a negligible loss in the average achievable per user rate for the communication system. This is because of the effective cancellation of the radar generated interference at the BS, as postulated in Theorem 1. Conversely, for low values of BS receive SNR (i.e. $<$ 15 dB) the loss in the average achievable per user rate is significant for the higher values of radar transmit SNR (i.e. $>$ 20 dB), and therefore, it is safe to conclude that under this SNR regime, the system performance is limited by the radar SNR.

Fig. 2.7 illustrates the achievable radar rate in the uplink communication subframe as a function of the received SNR for different levels of interference caused by the communication subsystem. We observe a loss of about 3 bits per channel use when the communication subsystem is operating at a received SNR of 10 dB. This result is in line with Theorem 2, where the radar is shown to face unmitigated interference.

Fig. 2.8 plots the rate region of the ICS system in the uplink communication sub-frame. We observe that the rates achievable by the two subsystems can be traded off with each other, with the dotted line representing the case when the system operates in the time division duplexed mode. We however, observe that the rate region is significantly convex, indicating that the two systems can coexist in a fully shared spectrum with marginal performance losses.

2.6.4 Downlink Data Transmission

Fig. 2.9 illustrates the achievable communication rate in the downlink communication subframe as a function of receive BS SNR for different levels of interference caused by radar subsystem. We observe that in line with the uplink case, the performance degradation is mini-

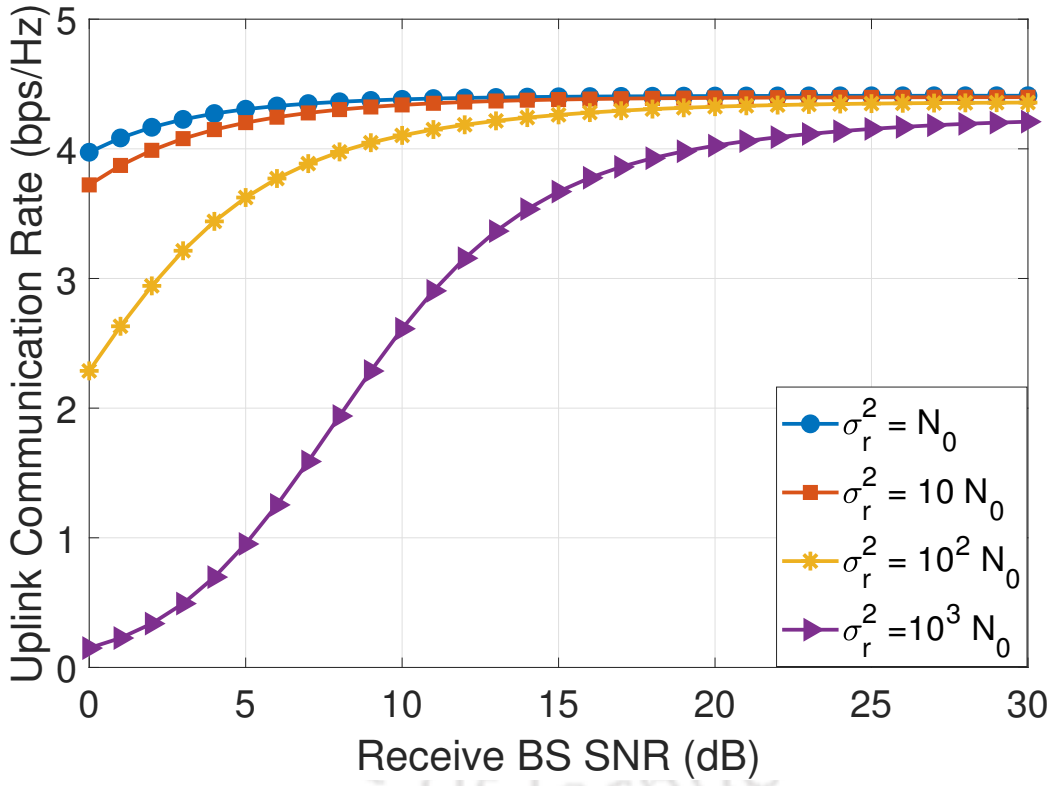

Fig. 2.6: Average uplink communication rate versus received data SNR for different values of radar transmit power.

mal for higher receive UE SNR and the loss is significant for lower values of receive UE SNR. Fig. 2.10 plots the achievable radar rate in the downlink communication subframe as a function of the received SNR for different levels of interference by the communication subsystem. It is clearly visible that the radar rate achievable during the downlink sub-frame is better than that achievable during the uplink subframe, indicating the efficacy of the null being formed in the direction of the radar by the mMIMO BS, as stated in Theorem 4. In Fig. 2.11 we plot the achievable rate region for ICS system during the downlink subframe, with the dotted line representing the case where the two systems are operated in the time division duplexed mode. Similar to the uplink case, this rate region is also convex, validating our hypothesis about the ability of mMIMO systems to coexist with radars.

2.7 Chapter Conclusions

In this chapter, we investigated the performance of ICS system in which both communication and radar sub-systems were operating simultaneously over same spectrum. To evaluate the performance of this system, we modelled it as a multiple access channel with both the subsystems non-cooperatively contending for the available resources. Following this, using results from random matrix theory, and via extensive simulations, we obtained the achievable rate regions for the system considering both uplink and downlink data transmission in the communication subsystem. We have observed these rate regions to be sufficiently convex and can safely conclude that mMIMO systems can coexist with MIMO radars without any significant co-design.

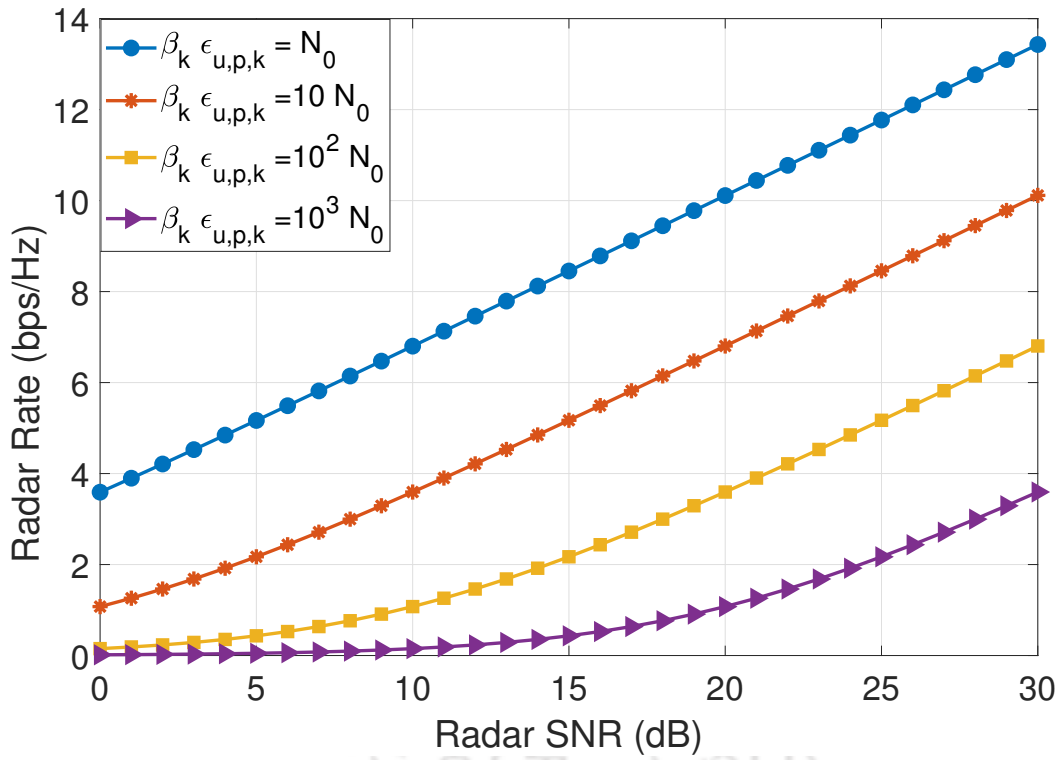

Fig. 2.7: Average uplink radar rate as a function of the radar SNR for different values of uplink data power.

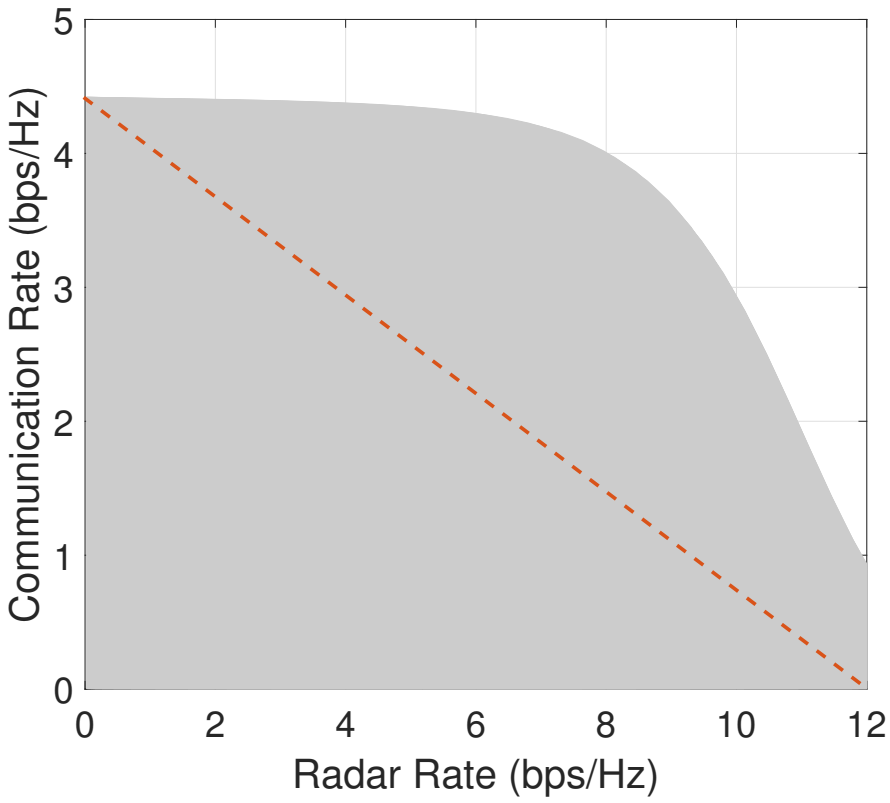

Fig. 2.8: Consolidated Rate Region during the uplink subframe.

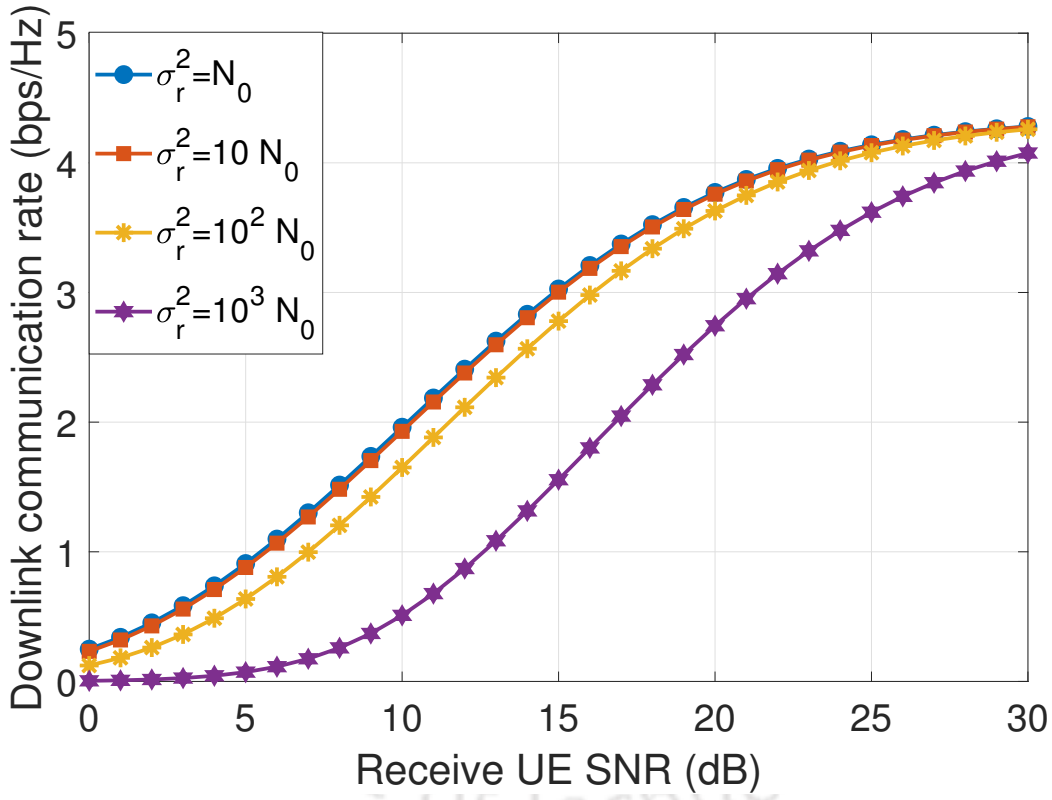

Fig. 2.9: Average communication rate in downlink as a function of the received data SNR for different values of radar transmitted power.

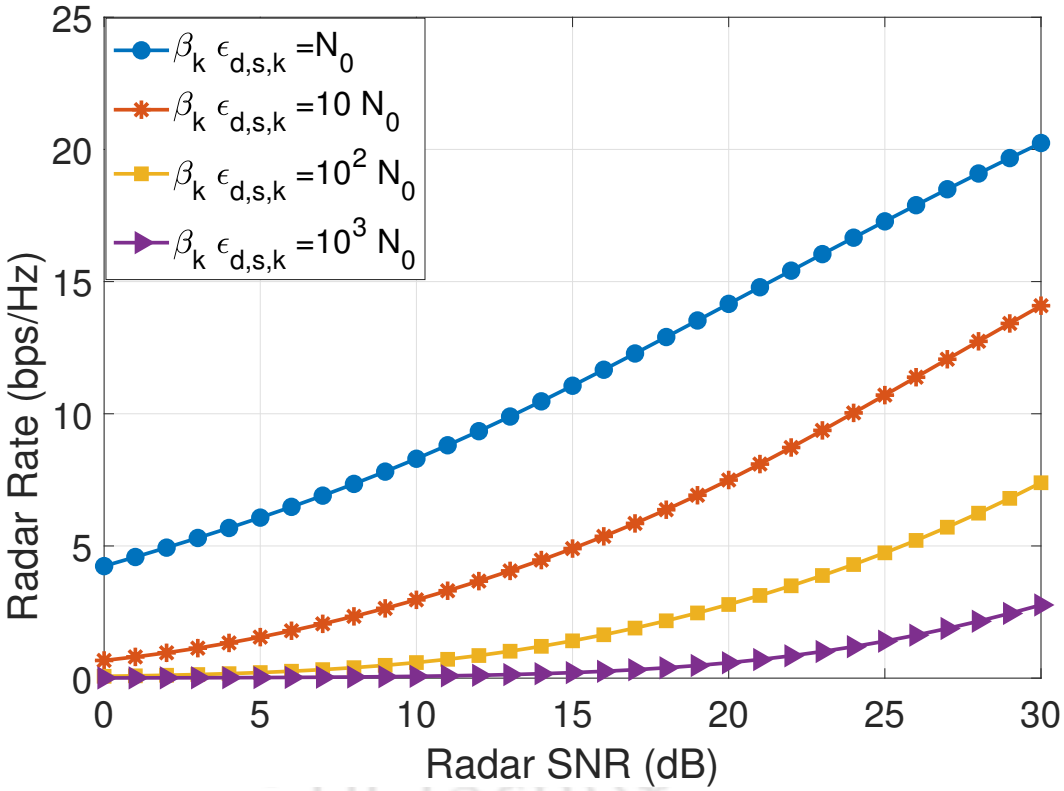

Fig. 2.10: Average radar rate in the downlink as a function of the radar SNR for different values of downlink data power.

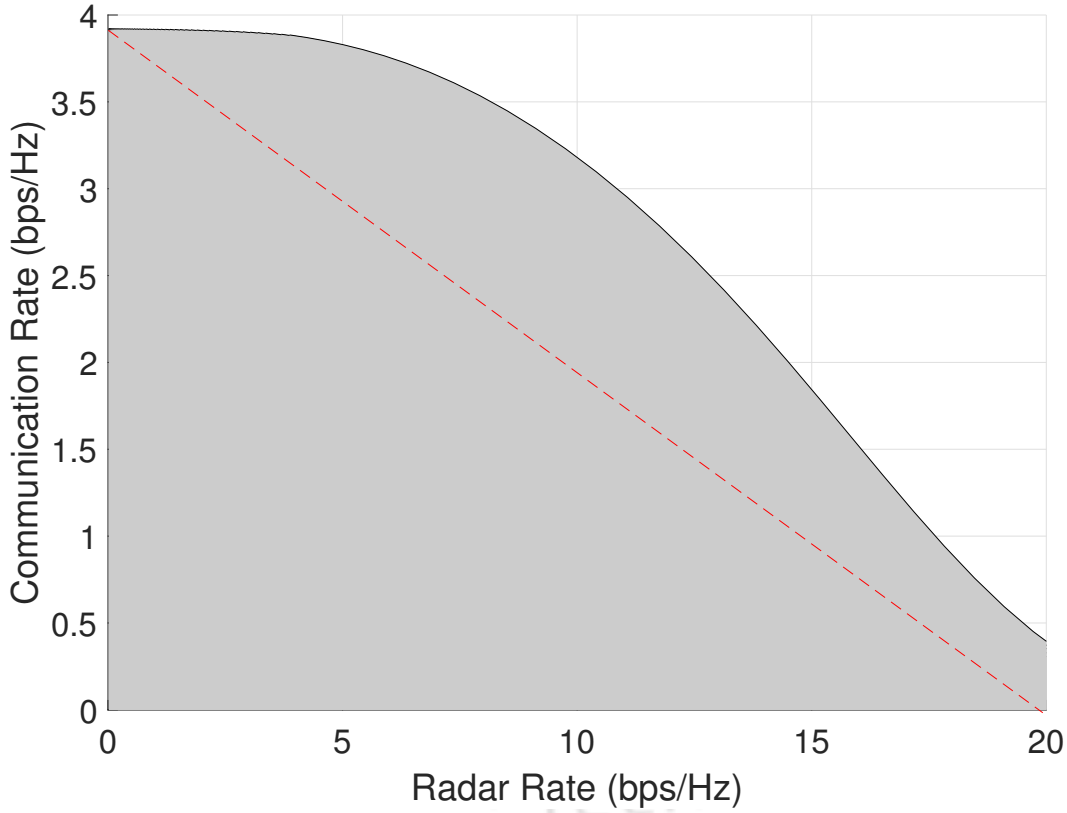

Fig. 2.11: Consolidated Rate Region during the downlink subframe.

3

On the Coexistence of Multi-Static Tracking Radars with Cell Free Massive MIMO

Contents

Recently, CF-mMIMO has emerged as a front runner among enabling technologies for the air interface of beyond 5G (B5G) wireless communications systems [51,52]. The canonical CF-mMIMO system architecture consists of multiple single antenna access points (APs) distributed over a large geographical area, connected to a central processing unit via an instantaneous lossless feedback link [51], making the network deployment simple. The CPU, via these APs serves all the user equipments (UEs) spread over the said geogrophical area. It has been argued that this distributed architecture improves the coverage probability for the users lying on the erstwhile cell edges providing an equitable per user throughput [53–57]. Consequently, it is safe to infer that CF-mMIMO systems combine the high spectral and energy efficiencies offered by cellular mMIMO systems with the diversity and uniform coverage offered by distributed MIMO systems.

As CF-mMIMO offers near uniform coverage to all the users while inheriting the advantages of cellular mMIMO such as power scaling, and high spectral and energy efficiencies [51, 52], the idea of ICS systems built around a CF-mMIMO system have recently been explored [58]. However, these works focus on a co-design approach, and discuss algorithms to optimize the joint operation of the system. Moreover, to the best of our knowledge, there exists no literature on the co-existence of a CF-mMIMO system with a radar. On the other hand we analyse the performance of a co-existence based ICS system comprising a multi-static tracking radar and a CF-mMIMO system.

3.1 Chapter Contributions

Our precise contributions to the study of this system are listed as follows.

(i) We derive the tracking equations for the EKF based tracking radar for both the individual radar sensors as well as the FC considering the interference from the communications subsystem. We also analyse the tracking performance of the underlying EKF, at the sensors and the FC in terms of the corresponding MSE matrices.

(ii) We evaluate the uplink channel estimation performance of the communication subsystem in the presence of the radar generated interference in terms of the mean squared channel

estimation error.

(iii) Using these channel estimates, we derive an expression for the instantaneous achievable rate for each user in the communication subsystem.

(iv) Finally, via detailed numerical simulations we evaluate the system performance for different parameters such as the operating powers of the two subsystems. We also use these results to evaluate the potential operating points of the system and identify the underlying trade-offs.

The key takeaway of this chapter is that a multi-static radar can co-exist with a CF-mMIMO system without causing much deterioration to the performance of either of the two subsystems. We introduce the system model considered by us in the next section.

3.2 System Model

As shown in Fig. 3.1, we consider a CF-mMIMO communication system including N access points (APs), each having M_a antennas and serving K single antenna users in coexistence with a multi-static radar having an M_t antenna transmitter and L single antenna sensors connected to a FC. The multi-static radar is tracking a target moving at a fixed but unknown velocity. Both the communication system and the radar simultaneously operate over the same spectrum resources. All the APs in the communications subsystem are connected to a central processing unit (CPU) via instantaneous feedback links, and are assumed to be fully synchronized. Similarly, all the sensors in the radar subsystem are connected to the FC via an instantaneous wire-line additive white Gaussian noise (AWGN) channel. In the next sub-sections, we describe the system and signal models for both the communication and the sensing subsystems.

3.2.1 The Communication Subsystem

We assume the communication subsystem to operate in the TDD mode with all the APs simultaneously serving all the K users, at a carrier frequency f_c over a common spectrum. The channels between the APs and the users are assumed to be frequency flat rich scattering. Let $\sqrt{\beta_{ik}}\mathbf{h}_{ik} \in C^{M_a \times 1}$ denote the channel between the ith AP and the kth user, with $\sqrt{\beta_{ik}}$ and $\mathbf{h}_{ik} \sim \mathcal{CN}(\mathbf{0}, \mathbf{R}_{ik})$ respectively representing the slow and fast fading components.

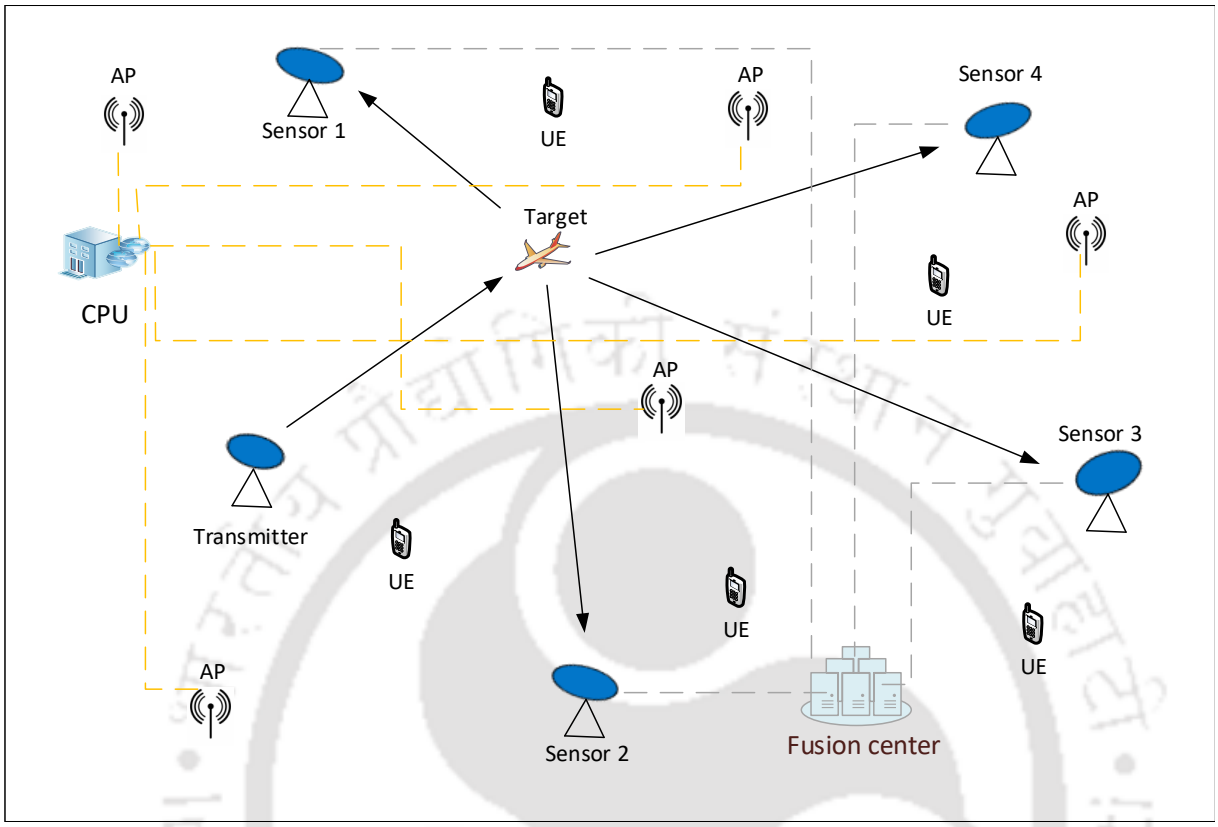

Fig. 3.1: System Model

The communication frame is divided into two sub-frames viz. training and data transmission. During the first sub-frame, the users transmit pilots to the APs that are used by the latter to estimate the underlying channels. Following this, during the data transmission subframe, the UEs transmit uplink data towards the APs, that is detected by the latter using the available channel estimates.

Letting the kth UE transmit the symbol $x_k[n]$ with energy $\epsilon_{u,k}$ at the nth time instant, we can write the signal received by the ith AP, in the absence of radar generated interference as

$$\mathbf{z}_i[n] = \sum_{k=1}^{K} \sqrt{\beta_{ik}} \mathbf{h}_{ik} x_k[n] + \omega_{a,i}[n] \tag{3.1}$$

where $\omega_{a,i}[n] \in C^{M_a \times 1}$ denotes the AWGN at the ith access point. Following this, the APs forward their signals to the CPU, that is assumed to possess the channel state information estimates for minimum mean square error combining based data detection [52].

3.2.2 The Sensing Sub-system and Target Tracking Model

We assume that the L radar sensors jointly detect and track a moving target using multi-static sensing [59]. These sensors are further connected to a FC for signal synchronization and joint processing.

In the absence of any communication subsystem generated interference, the sensing signal received by the lth sensing receiver, at the nth time instant can be expressed as

$$\xi_l[n] = h_{r,l} e^{j2\pi f_{d,l}(n-n_l)} a(\theta_l) \mathbf{a}^H(\theta_t) \boldsymbol{\zeta}[n - n_l] + \omega_{r,l}[n] \tag{3.2}$$

where $h_{r,l}$ is the zero mean circularly symmetric complex Gaussian (ZMCSCG) distributed target to sensor channel coefficient, θ_l is the angle of arrival at the lth sensor and $a(\theta_l)$ is the corresponding antenna response, θ_t is the angle of departure from the transmitter and $\mathbf{a}(\theta_t)$ is the corresponding antenna array response vector, $f_{d,l}$ is the Doppler frequency shift as seen by the lth sensor, n_l is the time delay corresponding to lth sensor, $\boldsymbol{\zeta}[n]$ is the deterministic radar transmit signal at nth time instant having a transmit power P_t, and $\omega_{r,l}[n]$ is the AWGN having variance $\sigma^2_{r,l}$.

The state of target at the nth time instant is given as $\mathbf{s}[n] = [r_x[n], r_y[n], v_x[n], v_y[n]]^T$, where the pairs $(r_x[n], r_y[n])$, and $(v_x[n], v_y[n])$ respectively denote the target's position and velocity in the Cartesian coordinate system. Following the discrete state transition model [60], the state of the target at the nth adaptation cycle can be written as

$$\mathbf{s}[n] = \mathbf{A}\mathbf{s}[n-1] + \mathbf{w}_s[n] \tag{3.3}$$

where $\mathbf{A} = [\mathbf{T} \otimes \mathbf{I}_2]$ is the state transition matrix, with $\mathbf{I}_K$ representing the order K identity matrix, $\mathbf{T} = \begin{bmatrix} 1 & \Delta \\ 0 & 1 \end{bmatrix}$, $\mathbf{w}_s[n]$ being the Gaussian distributed process noise having a covariance matrix $\mathbf{R}_s$, and Δ is the time period of the adaptation cycle.

3.2.3 Interference Channel Models

We assume that the interference channel between the radar transmitter and the ith AP is $\mathbf{G}_{ri} \in \mathbb{C}^{M_a \times M_t}, i \in \{1, 2, \ldots, N\}$. The entries of $\mathbf{G}_{ri}$ are assumed to be independent and identically

distributed (i.i.d.) ZMCSCG random variables having variances $\eta_{Ii} = \min(d_{ri}^{-\alpha}, 1)$ with $\alpha = 3.6$ such that d_{ri} is the distance between the radar transmitter and ith AP. Additionally, we assume that the MMSE estimates of $\mathbf{G}_{ri}$, given by $\hat{\mathbf{G}}_{ri}$ are available at the CPU, such that

$$\mathbf{G}_{ri} = \hat{\mathbf{G}}_{ri} + \tilde{\mathbf{G}}_{ri}, \tag{3.4}$$

with $\tilde{\mathbf{G}}_{ri}$ being the estimation error matrix whose entries are orthogonal to the corresponding entries of $\hat{\mathbf{G}}_{ri}$. The entries of $\tilde{\mathbf{G}}_{ri}$ are also i.i.d. Gaussian and are assumed to have a variance η_{ei}. In case the estimate of an interference channel is not available at the CPU, we set $\hat{\mathbf{G}}_{ri} = 0$, and $\eta_{ei} = \eta_{Ii}$. Similarly, the interference channel between kth UE and lth sensor is denoted by g_{kl}, $k \in \{1, 2, \ldots, K\}$ and $l \in \{1, 2, \ldots, L\}$. The entries of g_{kl} are assumed to be i.i.d ZMCSCG having a variance of η_{kl} that is equal to the large scale fading coefficient between kth user and lth sensor. No information about this channel is assumed at the radar sensors.

3.3 Target Tracking

At each sensing instant, the radar subsystem follows a two step procedure for tracking. During the first step the sensor nodes use the most recent observation to update their respective state estimates, and transmit those to the FC. During the second step the FC assimilates the state estimates from all the sensor nodes to obtain the overall state estimate. In this section, we elaborate on these two steps.

3.3.1 Tracking at the lth sensor node

The signal received by the lth sensing receiver, at the nth time instant, in the presence of communication interference can be expressed as,

$$\xi_l[n] = h_{r,l} e^{j2\pi f_{d,l}(n-n_l)} a(\theta_l) \mathbf{a}^H(\theta_t) \boldsymbol{\zeta}[n - n_l] + \sum_{k=1}^{K} g_{kl} x_k + \omega_{r,l}[n]. \tag{3.5}$$

This can be used to extract the parameter vector $\mathbf{y}_l[n]$ comprising the range, angle and relative speed of the target, that can be expressed as a function of the underlying state $\mathbf{s}[n]$ as,

$$\mathbf{y}_l[n] = \mathbf{f}_l(\mathbf{s}[n]) + \mathbf{w}_{y,l}[n], \tag{3.6}$$

where $\mathbf{w}_{y,l}[n] \sim \mathcal{N}(\mathbf{0}, \mathbf{\Lambda}_{y,l}[n])$, is the observation noise, and $f_l(.)$ is the measurement function expressed as,

$$\begin{aligned} f_l(\mathbf{s}[n]) &= [R_l[n], \theta_l[n], \nu_l[n]]^T \\ &= \begin{bmatrix} \sqrt{(r_x[n]-q_{l,x})^2 + (r_y[n]-q_{l,y})^2} \\ \tan^{-1}\left[\frac{r_y[n]-q_{l,x}}{r_x[n]-q_{l,y}}\right] \\ \frac{(r_x[n]-q_{l,x})v_x[n]+(r_y[n]-q_{l,y})v_y[n]}{\sqrt{(r_x[n]-q_{l,x})^2+(r_y[n]-q_{l,y})^2}} \end{bmatrix} \end{aligned} \tag{3.7}$$

with $(q_{l,x}, q_{l,y})$ representing the location of lth sensor node in Cartesian coordinates, $R_l[n], \theta_l[n]$ and $\nu_l[n]$ respectively being are the target's range, azimuth and velocity. We also note that the matrix $\mathbf{\Lambda}_{y,l}[n]$ takes the form

$$\mathbf{\Lambda}_{y,l}[n] = \text{diag}(\sigma^2_{R,l}[n], \sigma^2_{\theta,l}[n], \sigma^2_{\nu,l}[n]). \tag{3.8}$$

Here, $\sigma^2_{R,l}[n], \sigma^2_{\theta,l}[n]$ and $\sigma^2_{\nu,l}[n]$ are the Cramer-Rao lower bounds on the mean squared estimation error for $R[n], \theta[n]$ and $\nu[n]$ respectively, and are expressed as [61] [62],

$$\begin{aligned} \sigma^2_{R,l}[n] &= \frac{\sum_{k=1}^{K} \epsilon_{u,k}\eta_{kl} + \sigma^2_{r,l}}{h^2_{r,l}P_t} B^{-2} c_R, \\ \sigma^2_{\theta,l}[n] &= \frac{\sum_{k=1}^{K} \epsilon_{u,k}\eta_{kl} + \sigma^2_{r,l}}{h^2_{r,l}P_t} \theta_b^2 c_\theta, \\ \sigma^2_{\nu,l}[n] &= \frac{\sum_{k=1}^{K} \epsilon_{u,k}\eta_{kl} + \sigma^2_{r,l}}{h^2_{r,l}P_t} B^2 c_\nu \end{aligned} \tag{3.9}$$

with B and θ_b being the radar's transmit signal bandwidth and the lth sensor's receive beamwidth respectively, and c_R, c_θ, c_ν being constants. We let $\hat{\mathbf{s}}[n-1|n-1]$ denote the MMSE estimate of the state vector at the $(n-1)$th instant, based on the observations till the $(n-1)$th instant. We let $\mathbf{M}[n-1|n-1] = E[(\mathbf{s}[n-1] - \hat{\mathbf{s}}[n-1|n-1])(\mathbf{s}[n-1] - \hat{\mathbf{s}}[n-1|n-1])^H]$ denote the corresponding MSE matrix. Now, the predicted state vector at the nth instant takes the form $\hat{\mathbf{s}}[n|n-1] = \mathbf{A}\hat{\mathbf{s}}[n-1|n-1]$. Based on this, the MMSE estimate $\hat{\mathbf{y}}_l[n|n-1]$ of $\mathbf{y}_l[n]$, can be expressed as, $\hat{\mathbf{y}}_l[n|n-1] = f_l(\hat{\mathbf{s}}[n|n-1])$ Similarly, the prediction MSE matrix for the nth

adaptation cycle, based on the observations till the $(n-1)$th instant takes the form

$$\mathbf{M}[n|n-1] = \mathbf{A}\mathbf{M}[n-1|n-1]\mathbf{A}^H + \mathbf{R}_s[n]. \tag{3.10}$$

We assume that $\hat{\mathbf{s}}[n|n-1]$ and $\mathbf{M}[n|n-1]$ are all made available at all the sensors by the FC.

Consequently, the innovation component during the nth adaptation cycle is given by, $\boldsymbol{\alpha}_l[n] = \mathbf{y}_l[n] - \hat{\mathbf{y}}_l[n|n-1]$. It is easy to show that the covariance matrix of $\boldsymbol{\alpha}_l[n]$ is

$$\mathbf{R}_{\alpha,l}[n] = \mathbf{F}_l[n]\mathbf{M}[n|n-1]\mathbf{F}_l^H[n] + \sum_{k=1}^{K} \epsilon_{u,k}\eta_{kl}\mathbf{I}_{N_r} + \boldsymbol{\Lambda}_{y,l}[n], \tag{3.11}$$

where $\mathbf{F}_l[n] = \left.\frac{\partial f_l}{\partial \mathbf{s}[n]}\right|_{\mathbf{s}[n]=\hat{\mathbf{s}}[n|n-1]}$. Based on this, we can write the Kalman filtering gain at the lth sensor as

$$\begin{aligned}\boldsymbol{\Gamma}_l[n] = \left(E[\mathbf{s}[n]\boldsymbol{\alpha}_l[n]]\right)\mathbf{R}_{\alpha,l}^{-1}[n] = &\left(\mathbf{M}[n|n-1]\mathbf{F}_l^H[n]\right) \\ &\times \left(\mathbf{F}_l[n]\mathbf{M}[n|n-1]\mathbf{F}_l^H[n] + \sum_{k=1}^{K} \epsilon_{u,k}\eta_{kl}\mathbf{I}_{N_r} + \boldsymbol{\Lambda}_{y,l}[n]\right)^{-1}.\end{aligned} \tag{3.12}$$

Following this, the filtered state vector by the lth sensor node for the nth adaptation cycle is given by

$$\hat{\mathbf{s}}_l[n|n] = \hat{\mathbf{s}}_l[n|n-1] + \boldsymbol{\Gamma}_l[n]\boldsymbol{\alpha}_l[n], \tag{3.13}$$

and the MSE matrix of filtered state, at the lth node $\mathbf{M}_l[n|n] = E[(\mathbf{s}[n] - \hat{\mathbf{s}}_l[n|n])(\mathbf{s}[n] - \hat{\mathbf{s}}_l[n|n])^H]$ takes the form

$$\mathbf{M}_l[n|n] = \left(\mathbf{I} - \boldsymbol{\Gamma}_l[n]\mathbf{F}_l[n]\right)\mathbf{M}[n|n-1]. \tag{3.14}$$

3.3.2 Signal Processing at the FC

The L sensor nodes then communicate their respective filtered estimates, and the corresponding error covariance matrices to the FC via the feedback link. The FC treats these estimates as its observations, to construct the vector

$$\mathbf{y}_f[n] = [\hat{\mathbf{s}}_1^T[n|n], \ldots, \hat{\mathbf{s}}_L^T[n|n]]^T, \tag{3.15}$$

that can be expressed as,

$$\mathbf{y}_f[n] = \mathbf{B}\mathbf{s}[n] + \mathbf{w}_{y,f}[n], \tag{3.16}$$

where $\mathbf{B} = \mathbf{1}_L \otimes \mathbf{I}_4$, with $\mathbf{1}_L$ representing a length L vector containing all 1s, and $\mathbf{w}_{y,fc}$ is the observation noise due to the sensor estimation error, and feedback AWGN, such that $\mathbf{w}_{y,fc}[n] \sim \mathcal{CN}(\mathbf{0}, \mathbf{R}_{y,f})$ where $\mathbf{R}_{y,f}$ is a $4L \times 4L$ block diagonal matrix, containing L 4×4 blocks, such that its lth block is given as $(\mathbf{R}_{y,f})_{l,l} = \mathbf{M}_l[n|n] + \sigma_f^2 \mathbf{I}_4$, with σ_f^2 being the noise variance for the sensor to FC link.

Now, letting

$$\hat{\mathbf{y}}_f[n|n-1] = \mathbf{B}\hat{\mathbf{s}}[n|n-1], \tag{3.17}$$

the innovation component at the FC can be calculated as

$$\boldsymbol{\alpha}_f[n] = \mathbf{y}_f[n] - \hat{\mathbf{y}}_f[n|n-1], \tag{3.18}$$

and its covariance matrix can be obtained as

$$\mathbf{R}_{\alpha,f}[n] = \mathbf{B}\mathbf{M}[n|n-1]\mathbf{B}^H + \mathbf{R}_{y,f}. \tag{3.19}$$

The Kalman filter gain at the FC hence takes the form,

$$\boldsymbol{\Gamma}_f[n] = \left(E[\mathbf{s}[n]\boldsymbol{\alpha}_f^H[n]]\right)\mathbf{R}_{\alpha,f}^{-1}[n] = (\mathbf{M}[n|n-1]\mathbf{B}^H)(\mathbf{B}\mathbf{M}[n|n-1]\mathbf{B}^H + \mathbf{R}_{y,f})^{-1}. \tag{3.20}$$

Based on these, the filtered state vector at the nth adaptation cycle takes the form

$$\hat{\mathbf{s}}[n|n] = \hat{\mathbf{s}}[n|n-1] + \boldsymbol{\Gamma}_f[n]\boldsymbol{\alpha}_f, \tag{3.21}$$

and $\mathbf{M}[n|n]$ can be updated as

$$\mathbf{M}[n|n] = (\mathbf{I} - \boldsymbol{\Gamma}_f[n]\mathbf{B})\mathbf{M}[n|n-1]. \tag{3.22}$$

3.4 Communications Operation

As stated earlier, the communications frame is divided into two subframes, viz. channel estimation and uplink data transmission. In this section we look at the operations performed at

the APs and at the CPU during these two subframes.

3.4.1 The Channel Estimation Sub-frame

Let the kth UE transmit a pilot signal ψ_k such that $\sum_{n=1}^{K} \psi_k[n]\psi_l^*[n] = \rho_{kl}$, with $0 \leq |\rho_{kl}| \leq 1$ representing the correlation coefficient between the pilot sequences transmitted by the kth and the lth users. Consequently, the signal vector received by the CPU at the nth instant can be expressed as

$$\mathbf{z}[n] = \sum_{k=1}^{K} \sqrt{\epsilon_{p,k}}\psi_k[n]\mathbf{h}_k + \mathbf{G}_r\boldsymbol{\zeta}[n] + \mathbf{w}[n], \tag{3.23}$$

where $\mathbf{z}[n] = [\mathbf{z}_1^T[n], \mathbf{z}_2^T[n], \ldots, \mathbf{z}_N^T[n]]^T$, $\mathbf{h}_k = [\sqrt{\beta_{k1}}\mathbf{h}_{k1}^T, \sqrt{\beta_{k2}}\mathbf{h}_{k2}^T, \ldots, \sqrt{\beta_{kN}}\mathbf{h}_{kN}^T]^T$, $\epsilon_{p,k}$ is the uplink transmit pilot power corresponding to kth user, $\mathbf{G}_r = [\mathbf{G}_{r1}^T, \mathbf{G}_{r2}^T, \ldots, \mathbf{G}_{rN}^T]^T$ and $\mathbf{w}[n] = [\mathbf{w}_1^T[n], \mathbf{w}_2^T[n], \ldots, \mathbf{w}_N^T[n]]$. It is easy to show that $\mathbf{h}_k \sim \mathcal{CN}(\mathbf{0}, (\boldsymbol{\beta}_k \otimes \mathbf{1}_{M_aN \times Ma}) \odot \mathbf{R}_k)$, with $\mathbf{R}_k \in C^{M_aN \times M_aN}$ being a block diagonal matrix whose ith block is given as $(\mathbf{R}_k)_{ii} = \mathbf{R}_{ki}$, and $\boldsymbol{\beta}_k = [\beta_{k1}, \ldots, \beta_{kN}]$. We can now define

$$\mathbf{z}_l \triangleq \sum_{n=1}^{K} \mathbf{z}[n]\psi_l[n]. \tag{3.24}$$

The CPU may or may not have the phase synchronization information about $\boldsymbol{\zeta}[n]$. In the former case, the CPU can form $\mathbf{z}_l^{'}$ by subtracting $\sum_{n=1}^{K} \hat{\mathbf{G}}_r\boldsymbol{\zeta}[n]\psi_l[n]$ from $\mathbf{z}_l$ to obtain the vector $\mathbf{z}_l^{'}$. In this case, using the results derived in [63], we can show that the LMMSE estimate of $\mathbf{h}_k$ at the CPU can be expressed as

$$\hat{\mathbf{h}}_\mathbf{k} = \boldsymbol{\Sigma}_{hz,k}\boldsymbol{\Sigma}_{z'z',k}^{-1}\mathbf{z}_k^{'}, \tag{3.25}$$

where $\boldsymbol{\Sigma}_{hz,k} = \sqrt{\epsilon_{p,k}}(\boldsymbol{\beta}_k \otimes \mathbf{1}_{M_aN \times Ma}) \odot \mathbf{R}_k$ and $\boldsymbol{\Sigma}_{z'z',k} = E[\mathbf{z}_k^{'}\mathbf{z}_k^{'H}]$ is a block diagonal matrix whose ith block is given as

$$(\boldsymbol{\Sigma}_{z'z',k})_{ii} = \epsilon_{p,k}\beta_{ki}\mathbf{R}_{ki} + \sum_{\substack{n=1,\\ l\neq k}}^{K} \rho_{nk}^2\epsilon_{p,n}\beta_{ni}\mathbf{R}_{ni} + (P_tN_t\eta_{ei} + N_0)\mathbf{I}_{M_a}. \tag{3.26}$$

It is easy to show that the covariance matrix of $\hat{\mathbf{h}}$ can be expressed as

$$\bar{\mathbf{R}}_k^{'} = \boldsymbol{\Sigma}_{hz,k}\boldsymbol{\Sigma}_{z'z',k}^{-1}\boldsymbol{\Sigma}_{hz,k}^H. \tag{3.27}$$

and the covariance matrix of $\tilde{\mathbf{h}}_k$ is given by

$$\dot{\mathbf{R}}_k^{'} = (\boldsymbol{\beta}_k \otimes \mathbf{1}_{M_aN \times Ma}) \odot \mathbf{R}_k - \bar{\mathbf{R}}_k^{'}. \tag{3.28}$$

Similarly, in case the synchronization information about $\boldsymbol{\zeta}[n]$ is not available at the CPU, then $\hat{\mathbf{h}}_k$ becomes

$$\hat{\mathbf{h}}_{\mathbf{k}} = \boldsymbol{\Sigma}_{hz,k} \boldsymbol{\Sigma}_{zz,k}^{-1} \mathbf{z}_k, \tag{3.29}$$

and $\boldsymbol{\Sigma}_{zz,k} = E[\mathbf{z}_k \mathbf{z}_k^H]$ is a block diagonal matrix whose ith block is given as

$$(\boldsymbol{\Sigma}_{zz,k})_{ii} = \epsilon_{p,k} \beta_{ki} \mathbf{R}_{ki} + \sum_{\substack{n=1, \\ l \neq k}}^{K} \rho_{nk}^2 \epsilon_{p,n} \beta_{ni} \mathbf{R}_{ni} + P_t \hat{\mathbf{G}}_{ri} \hat{\mathbf{G}}_{ri}^H + (P_t N_t \eta_{ei} + N_0) \mathbf{I}_{M_a}. \tag{3.30}$$

In this case, the covariance matrix of $\hat{\mathbf{h}}$ takes the form

$$\bar{\mathbf{R}}_k = \boldsymbol{\Sigma}_{hz,k} \boldsymbol{\Sigma}_{zz,k}^{-1} \boldsymbol{\Sigma}_{hz,k}^H. \tag{3.31}$$

Now, $\mathbf{h}_k$ can be expressed in terms of $\hat{\mathbf{h}}_{\mathbf{k}}$ and an orthogonal estimation error component $\tilde{\mathbf{h}}_k$ as $\mathbf{h}_k = \hat{\mathbf{h}}_k + \tilde{\mathbf{h}}_k$, with $E[\hat{\mathbf{h}}_k \tilde{\mathbf{h}}_k^H]$ being an order MN all zero square matrix, $\tilde{\mathbf{h}}_k$ being a ZMCSCG random vector whose covariance matrix is

$$\dot{\mathbf{R}}_k = (\boldsymbol{\beta}_k \otimes \mathbf{1}_{M_aN \times Ma}) \odot \mathbf{R}_k - \bar{\mathbf{R}}_k. \tag{3.32}$$

3.4.2 Data Transmission

The received signal at the CPU in the presence of radar generated interference can be written as

$$\mathbf{z}[n] = \sum_{l=1}^{K} \sqrt{\epsilon_{u,l}} x_l[n] \hat{\mathbf{h}}_l + \sum_{l=1}^{K} \sqrt{\epsilon_{u,l}} x_l[n] \tilde{\mathbf{h}}_l + \hat{\mathbf{G}}_r \boldsymbol{\zeta}[n] + \tilde{\mathbf{G}}_r \boldsymbol{\zeta}[n] + \sqrt{N_0} \mathbf{w}_z[n]. \tag{3.33}$$

Now, based on the available channel estimates, the CPU can construct the MMSE combining vector corresponding to the kth UE as, $\mathbf{v}_k = \mathbf{R}_{z|\hat{\mathbf{H}},\hat{\mathbf{G}}_r}^{-1} \hat{\mathbf{h}}_k$, where $\mathbf{R}_{z|\hat{\mathbf{H}},\hat{\mathbf{G}}_r}$ is the covariance matrix of $\mathbf{z}[n]$ given the channel estimates $\hat{\mathbf{H}}$ and $\hat{\mathbf{G}}_r$ [52]. This can be expressed as,

$$\mathbf{R}_{z|\hat{\mathbf{H}},\hat{\mathbf{G}}_r} = \sum_{l=1}^{K} \epsilon_{u,l} \left(\hat{\mathbf{h}}_l \hat{\mathbf{h}}_l^H + \dot{\mathbf{R}}_l^{'} \right) + P_t (\hat{\mathbf{G}}_{\mathbf{r}} \hat{\mathbf{G}}_{\mathbf{r}}^H + \mathbf{I}_{M_a} \otimes \mathrm{diag}(\boldsymbol{\eta}_e)) + N_0 \mathbf{I}_{M_aN}, \tag{3.34}$$

where $\boldsymbol{\eta}_e = [\eta_{e,1}, \ldots, \eta_{e,N}]^T$. Consequently, the processed signal vector corresponding to the kth UE, $\mathbf{r}_k[n] = \mathbf{v}_k^H \mathbf{z}[n]$, at the nth instant takes the form

$$\mathbf{r}_k[n] = \sqrt{\epsilon_{u,k}}\hat{\mathbf{h}}_k^H \mathbf{R}^{-1}_{z|\hat{\mathbf{H}},\hat{\mathbf{G}}_r} \hat{\mathbf{h}}_k x_k[n] + \sum_{\substack{l=1,\\ l\neq k}}^{K} \sqrt{\epsilon_{u,l}}\hat{\mathbf{h}}_k^H \mathbf{R}^{-1}_{z|\hat{\mathbf{H}},\hat{\mathbf{G}}_r} \hat{\mathbf{h}}_l x_l[n] + \sum_{l=1}^{K} \sqrt{\epsilon_{u,l}}\hat{\mathbf{h}}_k^H \mathbf{R}^{-1}_{z|\hat{\mathbf{H}},\hat{\mathbf{G}}_r} \tilde{\mathbf{h}}_l x_l[n]$$
$$+ \hat{\mathbf{h}}_k^H \mathbf{R}^{-1}_{z|\hat{\mathbf{H}},\hat{\mathbf{G}}_r} \hat{\mathbf{G}}_r \mathbf{r}[n] + \hat{\mathbf{h}}_k^H \mathbf{R}^{-1}_{z|\hat{\mathbf{H}},\hat{\mathbf{G}}_r} \tilde{\mathbf{G}}_r \mathbf{r}[n] + \sqrt{N_0}\hat{\mathbf{h}}_k^H \mathbf{R}^{-1}_{z|\hat{\mathbf{H}},\hat{\mathbf{G}}_r} \mathbf{w}_z[n]. \quad (3.35)$$

Based on this, the rate achievable by the kth user in the uplink can be expressed as [52],

$$R_k = \log_2(1 + \gamma_k), \quad (3.36)$$

where γ_k is the SINR for the kth user's signal at the CPU and is given as,

$$\gamma_k = \frac{\epsilon_{u,k}|\mathbf{v}_k^H \hat{\mathbf{h}}_k|^2}{\sum_{\substack{l=1,\\ l\neq k}}^{K} \epsilon_{u,l}|\mathbf{v}_k^H \hat{\mathbf{h}}_l|^2 + \sum_{l=1}^{K} \epsilon_{u,l}\mathbf{v}_k^H \dot{\mathbf{R}}_l \mathbf{v}_k + P_t \mathbf{v}_k^H (\hat{\mathbf{G}}_\mathbf{r}\hat{\mathbf{G}}_\mathbf{r}^H + \boldsymbol{\eta}_e \otimes \mathbf{I}_{M_a})\mathbf{v}_k + N_0 \mathbf{v}_k^H \mathbf{v}_k}. \quad (3.37)$$

3.5 Numerical Results

In this section we validate our derived results using Monte-Carlo simulations. Here, the communication subsystem consists of a CF-mMIMO system spread over a circular region with a radius 500 m. We assume both the APs and the users to be distributed uniformly across the cell, and operating at a carrier frequency f_c = 3 GHz. Both the communications and the radar signals are assumed to have a bandwidth of 20 MHz. In this setup, unless stated otherwise, we consider K=16 users and N = 256 APs. The channel covariance matrices at all the APs ($\boldsymbol{\Sigma}_k$) is assumed to be identity. The communication frame consists of 1024 channel uses with the first K channel uses dedicated for training, ensuring orthogonal pilots, and the remaining for uplink data transmission. For the purpose of these experiments, we consider the interference channels to be known at the APs with a 10% error, and the median received SNR for the communications subsystem to be 20 dB. The large scale fading coefficients of the wireless channel (β_{ik}) are modelled as $\beta_{ik} = \min\left(1, \left(\frac{d_{ik}}{d_0}\right)^{-\eta}\right)$ with d_{ik} being the distance between the ith AP and the kth UE,

and $\eta = 3.6$.

On the other hand, the radar subsystem consists of a multi-static radar comprising a transmitter with $M_t = 8$ antennas and L single antenna sensors. The radar sensors are also assumed to be uniformly distributed across the cell. All the performance metrics presented in this section are generated by averaging over 10,000 realizations of the system.

Fig. 3.2 plots the mean square error (MSE) of the estimate of radar target parameter as a function of iteration count for different number of radar sensors (L) when the median received radar SNR is 20 dB for K=16. As expected, the final MSE decreases almost linearly with an the increase in L. To investigate the impact of number of communication users over the performance of the radar, Fig. 3.3 plots the mean square error (MSE) of the estimate of radar target parameter as a function of number of communication users for different number of radar sensors (L) at the 50th iteration for a median received radar SNR of 20 dB. We observe a marginal increase in the MSE with an increase in K.

Fig. 3.4 plots the achievable per user uplink rate as a function of the AP density for different radar received SNRs. We observe that similar to the radar subsystem, the increase in the radar transmit power minimally affects the performance of the communications subsystem.

3.6 Chapter Conclusions

In this chapter, we analysed the coexistence of a cell free massive MIMO communication system with a tracking multi-static radar system. We observed that the radar performance improves significantly with the increase in the number of radar sensors and also observed that the impact of communication system interference over radar system performance is negligible. Similarly, we observed that the performance of the communications subsystem remains largely unaffected by the radar transmit power. This confirms our hypothesis that multi-static radars can coexist with cell free massive MIMO without co-design.

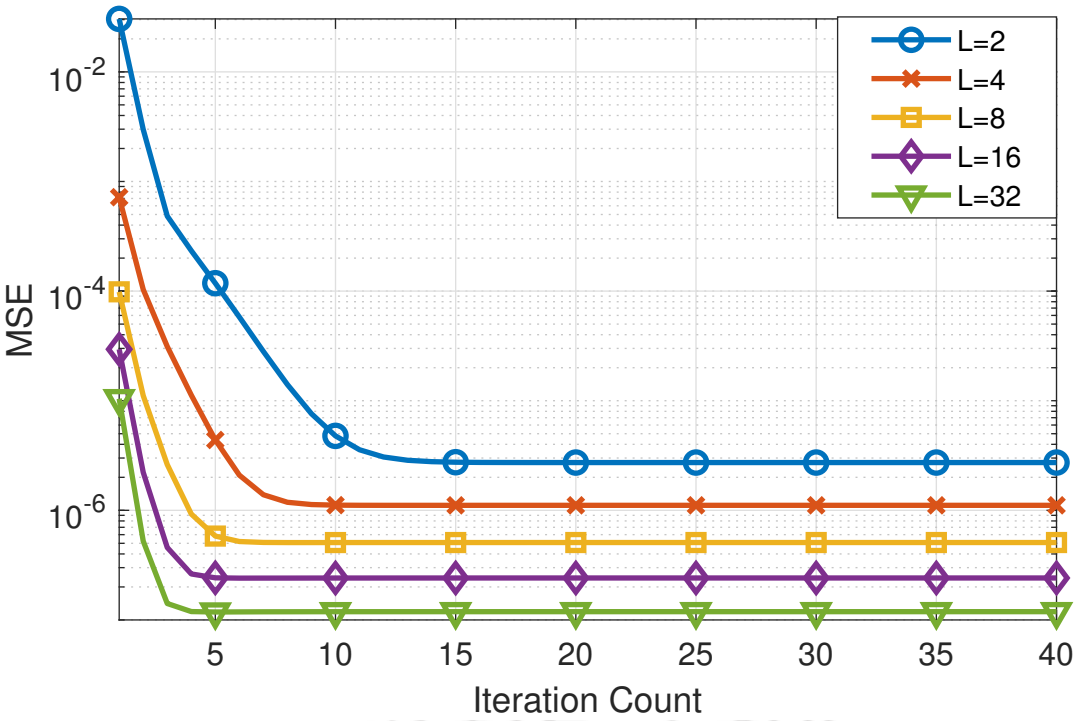

Fig. 3.2: Convergence performance of tracking radar for different numbers of radar sensors (L).

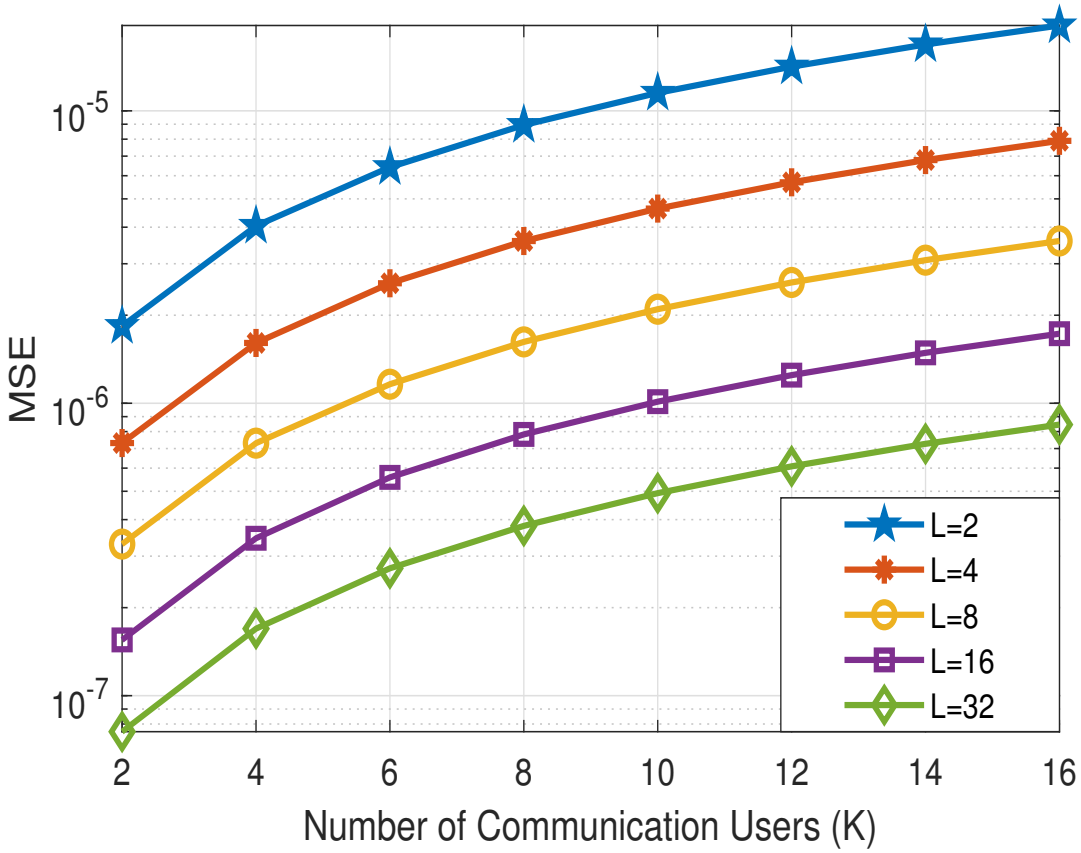

Fig. 3.3: Tracking MSE for different numbers of communication users (K).

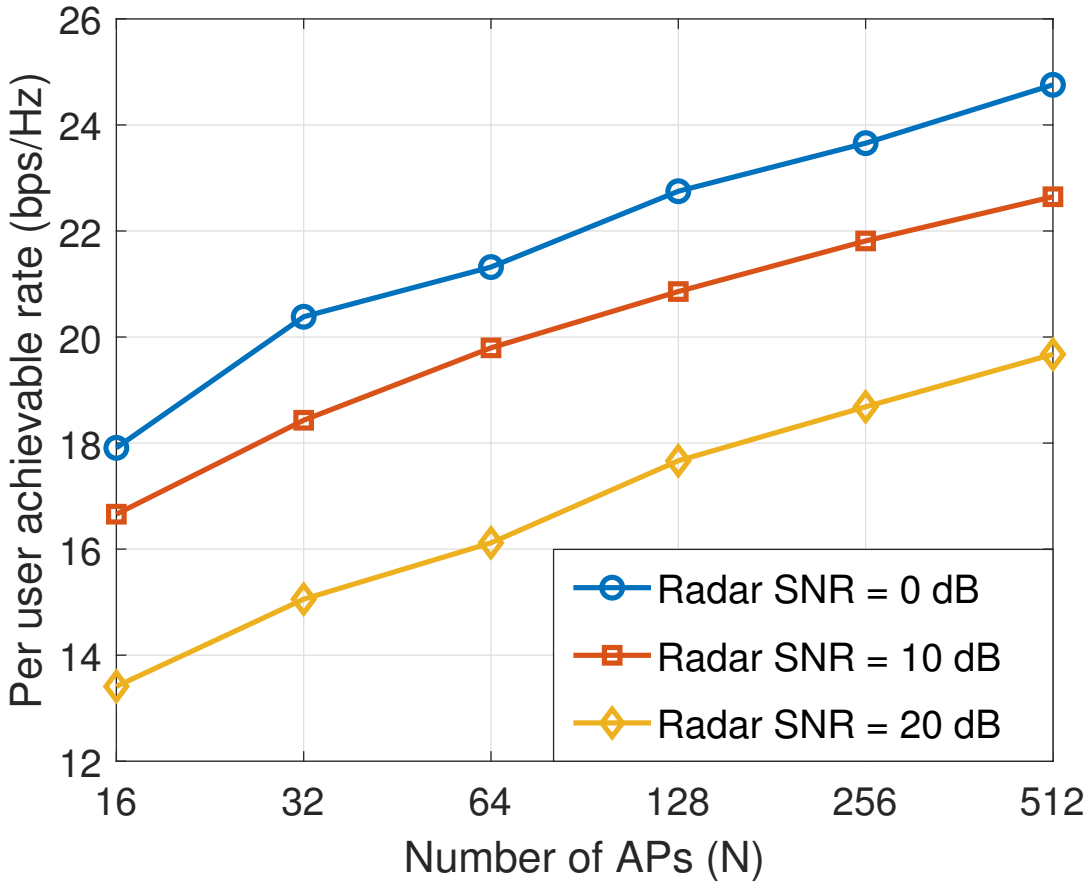

Fig. 3.4: Uplink achievable rate for different number of serving APs (N).

4

Multi-Static Tracking Radars can Coexist with Cell Free Massive MIMO: A Stochastic Geometry Perspective

Contents

A canonical CF-mMIMO system assumes the APs and UEs to be located randomly over the serviced area. In this context, the use of tools from stochastic geometry to model the location of devices leads tractable system-level models as discussed in [64–66]. Consequently, in this chapter, we use tools from stochastic geometry to evalute the performance of the ICS system discussed in the previous chapter.

Here, we extend the discussion from the previous chapter by i.) evaluating the communications and radar performances during in the full communications frame by considering both uplink and downlink and ii.) using tools from stochastic geometry to generalize the results derived in [67] in terms of the AP/ UE/ Sensor deployment. A detailed discussion on the contributions of this work follows in the next subsection.

4.1 Chapter Contributions

In this chapter, we extend the system model from the previous chapter to a stochastic geometry setup. Our precise contributions in this direction are listed as follows

(i) We first discuss channel estimation in the communications subsystem and obtain expression for the LMMSE channel estimate at the APs in the presence of radar generated interference.

(ii) Given the channel estimates, we derive an expression for the instantaneous uplink achievable rate for an arbitrarily placed UE, employing the MRC combining at the APs/ CPU, in contrast to the MMSE combining used in the previous chapter. We then use this instantaneous rate to obtain the coverage probability for an arbitrarily located UE in the uplink, and evaluate the effects of the radar generated interference.

(iii) We then obtain the tracking equations for the EKF based tracking radar for both the individual radar sensors, as well as the FC considering the interference from the communications subsystem. We also analyse the tracking performance of the underlying EKF, at the sensors and the FC in terms of the corresponding MSE matrices.

(iv) Similarly, we evaluate the downlink instantaneous per user achievable rate and coverage probability for each user in the presence of radar generated interference for the commu-

nications subsystem, and derive the effects of the communications generated interference on the radar tracking performance.

(v) Finally, via detailed numerical simulations, we evaluate the system performance for different parameters such as the operating powers of the two subsystems. We also use these results to evaluate the potential operating points of the system and identify the underlying trade-offs.

4.2 System Model

As shown in Fig. 4.1, we consider a CF-mMIMO communication system coexisting with a multi-static radar. The radar subsystem is assumed to consist of an M_t antenna transmitter, and multiple physically separated single antenna sensors connected to an FC. This radar subsystem is tracking a target moving at a fixed but unknown velocity. We assume all the radar sensors to be connected to the FC via an instantaneous wire-line AWGN channel. Similarly, the communications subsystem consists of randomly distributed single antenna APs and UEs, all communicating over the same time frequency resources as the radar. All the APs in the communications subsystem are connected to a CPU via instantaneous feedback links, and are assumed to be fully synchronized. Since the APs, the UEs and the radar sensors are all randomly distributed, we can assume their locations to be distributed as 2D homogeneous Poisson point processes (PPPs) Φ_a, Φ_u, and Φ_s having densities λ_a [APs/m^2], λ_u [UEs/m^2] and λ_s [sensors/m^2] respectively. In the following sub-sections, we elaborate on the models for the two subsystems and discuss the interference channel model.

4.2.1 The Communications Subsystem

We assume the communication subsystem to operate in the TDD mode with all the APs simultaneously serving all users, at a carrier frequency f_c over a common spectrum. The channels between the APs and the UEs are assumed to be frequency flat rich scattering and independent. We let h_{ki} denote the channel between the AP located at $a_i \in \Phi_a$ and the user at $u_k \in \Phi_u$, such that and $h_{ki} \sim \mathcal{CN}(0, \beta(d_{ki}))$,

$$\beta(d_{ki}) = \min\{(d_{ki})^{-\alpha}, 1\} \tag{4.1}$$

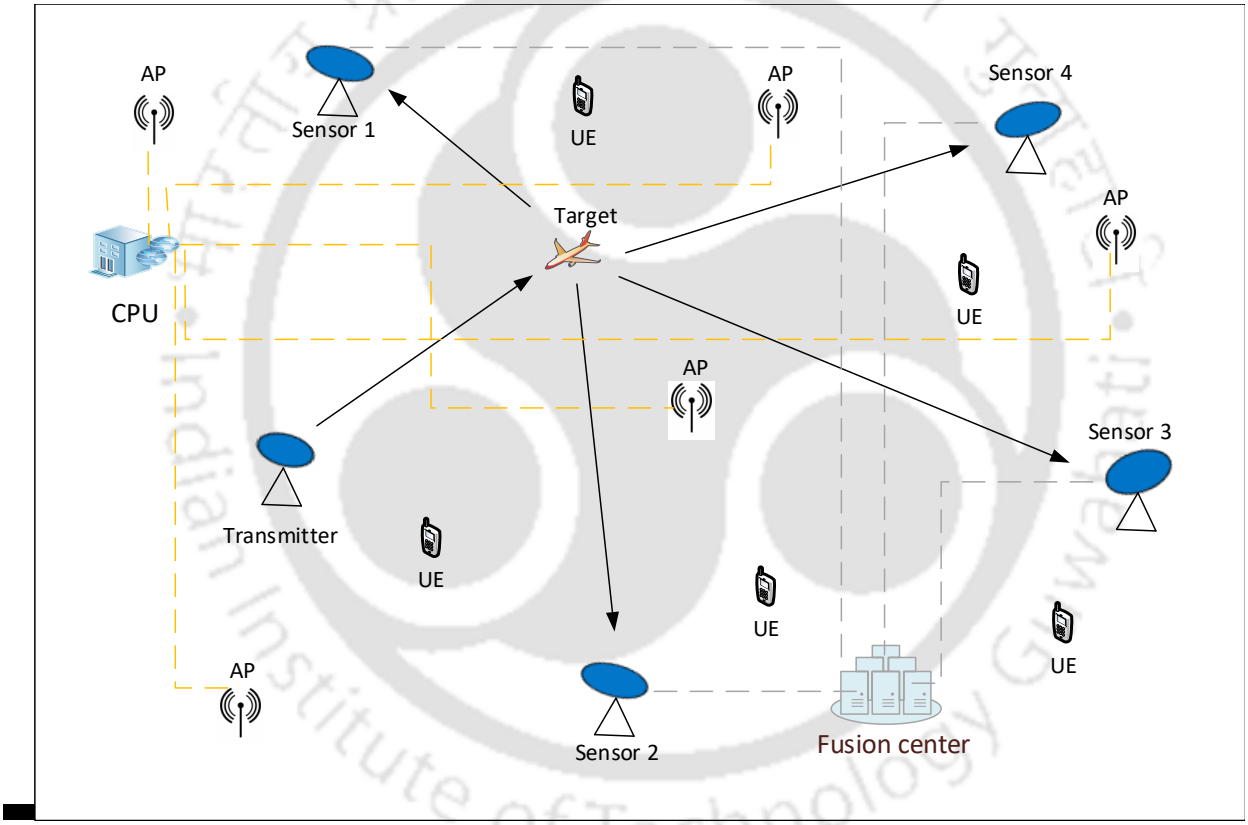

Fig. 4.1: System Model

with d_{ki} representing the distance between the AP located at a_i and the user located at u_k, and α being the path loss exponent. For ease of notation we let $\beta_{ki} = \beta(d_{ki})$. Furthermore, we assume the communication frame is divided into three sub-frames, viz. channel estimation, uplink data transmission, and downlink data transmission. In the first sub-frame, spanning $K = card(\Phi_a)$ channel uses, the users transmit orthogonal pilot signals that are received at all the APs. These pilots are used by the APs to form the MMSE estimates of the underlying channels. Following this, during the uplink data transmission sub-frame, spanning τ_u channel uses, the users transmit uplink data, that is received by APs. Following this, the APs perform maximal ratio combining (MRC) on the received data and forward it to the CPU. Finally, during the downlink data transmission sub-frame, spanning τ_d channel uses, the APs forward the data received from the CPU to the UEs, under the assumption of channel reciprocity, by performing matched filter precoding (MFP). We discuss the signal models for these subframes in the sequel.

4.2.1.1 Channel Estimation

Let the UE located at u_k transmit the pilot symbol $\psi_k[n]$ such that $(E[\psi_k[n]\psi_p^*[m]] = \delta[n-m]\delta[k-p])$ with uplink pilot power $\epsilon_{p,k}$. We can write the signal received by the APs, in the absence of radar generated interference as,

$$\mathbf{z}[n] = \sum_{u_k \in \Phi_u} \sqrt{\epsilon_{p,k}}\mathbf{h}_k\psi_k[n] + \sqrt{N_0}\mathbf{w}_z[n], \tag{4.2}$$

where $\mathbf{z}[n] = [z_1[n], z_2[n], \ldots, z_N[n]]^T$, $\mathbf{h}_k = [\sqrt{\beta_{k1}}h_{k1}, \sqrt{\beta_{k2}}h_{k2}, \ldots, \sqrt{\beta_{kN}}h_{kN}]^T$ with $N = card(\Phi_a)$, $\mathbf{w}_z[n] = [w_{z1}[n], w_{z2}[n], \ldots, w_{zN}[n]]$ denotes the temporally and spatially white ZMCSCG noise with unit variance.

4.2.1.2 Uplink Transmission

Let the UE located at u_k transmit the symbol $x_k[n]$ with uplink transmit power $\epsilon_{u,k}$, at the nth instant, based on this, we can write the signal received at the CPU in the absence of any radar generated interference as,

$$\mathbf{z}[n] = \sum_{u_l \in \Phi_u} \sqrt{\epsilon_{u,l}}\mathbf{h}_l x_l[n] + \sqrt{N_0}\mathbf{w}_z[n]. \tag{4.3}$$

4.2.1.3 Downlink Transmission

Let ϵ_d denote the downlink transmit power and $t_k[n]$ the downlink transmit symbol corresponding to the user located at u_k at nth time instant, using matched filter precoding at each AP, we can write the downlink signal transmitted by the AP located at a_m as

$$b_m[n] = \sum_{u_i \in \Phi_u} p_{im} \sqrt{\epsilon_d} t_i[n], \tag{4.4}$$

with $p_{im} = \frac{\hat{h}_{im}^*}{\sqrt{E|\hat{h}_{im}|^2}}$. Here the precoding vector is being scaled to simplify the subsequent analysis, and does not affect the underlying SINR distribution [68]. Now, the signal received by the user located at u_k can be written as,

$$y_{d,k} = \sum_{a_l \in \Phi_a} h_{kl} b_l[n] + w_y[n], \tag{4.5}$$

where $w_k[n]$ is the ZMCSCG noise with unit variance.

4.2.2 The Radar Subsystem

We assume the radar sensors to be connected to an FC for joint processing. In the absence of any communication subsystem generated interference, the sensing signal received by the sensing receiver located at $s_l \in \Phi_s$, at the nth time instant can be expressed as

$$\xi_l[n] = h_{r,l} e^{j2\pi f_{d,l}(n-n_l)} a(\theta_l) \mathbf{a}^H(\theta_t) \boldsymbol{\zeta}[n - n_l] + w_{r,l}[n], \tag{4.6}$$

where $h_{r,l}$ is the ZMCSCG distributed target to sensor channel coefficient incorporating the effects of random radar cross section and path loss, θ_l is the angle of arrival at the sensing receiver located at s_l and $a(\theta_l)$ is the corresponding antenna response, θ_t is the angle of departure from the transmitter and $\mathbf{a}(\theta_t)$ is the corresponding antenna array response vector, $f_{d,l}$ is the Doppler frequency shift as seen by the sensing receiver located at s_l, n_l is the time delay, $\boldsymbol{\zeta}[n]$ is the deterministic radar transmit signal at nth time instant having a transmit power P_t, and $w_{r,l}[n]$ is the AWGN having variance $\sigma_{r,l}^2$. We also define the state of target at the nth instant as $\mathbf{s}[n] = [r_x[n], r_y[n], v_x[n], v_y[n]]^T$, where the pairs $(r_x[n], r_y[n])$, and $(v_x[n], v_y[n])$ correspond to the Cartesian coordinates of the represent target's position and velocity respectively. Now,

using the discrete state transition model from [60], we can express the the state of the target during the nth adaptation cycle as

$$\mathbf{s}[n] = \mathbf{A}\mathbf{s}[n-1] + \mathbf{w}_s[n] \tag{4.7}$$

where $\mathbf{A} = [\mathbf{T} \otimes \mathbf{I}_2]$ is the state transition matrix, with $\mathbf{I}_K$ being the order K identity matrix, $\mathbf{T} = \begin{bmatrix} 1 & \Delta \\ 0 & 1 \end{bmatrix}$, $\mathbf{w}_s[n]$ is the Gaussian distributed process noise having a covariance matrix $\mathbf{R}_s$, and Δ is the time period of the adaptation cycle.

4.2.3 Interference Channel Models

We let $\mathbf{g}_{ri} \in C^{M_t \times 1}$ denote the interference channel between the radar transmitter and the AP located at a_i. The entries of $\mathbf{g}_{ri}$ are assumed to be independent and identically distributed (i.i.d.) ZMCSCG random variables having variances β_{ri}, such that $\beta_{ri} = \beta(d_{ri})$ corresponds to the path loss function with d_{ri} is the distance between radar transmitter and the AP located at a_i. Additionally, we assume that the MMSE estimates of $\mathbf{g}_{ri}$, given by $\hat{\mathbf{g}}_{ri}$ are available at the CPU, such that

$$\mathbf{g}_{ri} = \hat{\mathbf{g}}_{ri} + \tilde{\mathbf{g}}_{ri}, \tag{4.8}$$

with $\tilde{\mathbf{g}}_{ri}$ being the estimation error matrix whose entries are orthogonal to the corresponding entries of $\hat{\mathbf{g}}_{ri}$. The entries of $\tilde{\mathbf{g}}_{ri}$ are also i.i.d. Gaussian and are assumed to have a variance $\eta_{ei} = \eta_e \beta(d_{ri})(0 \leq \eta_e \leq 1)$. In case the estimate of an interference channel is not available at the CPU, we set $\hat{\mathbf{g}}_{ri} = 0$, and $\eta_e = 1$. Similarly, the interference channel between the UE located at u_k and sensor located at s_l is denoted by g_{kl}, $u_k \in \Phi_u$ and $s_l \in \Phi_s$. The entries of g_{kl} are assumed to be i.i.d ZMCSCG having a variance equal to the large scale fading coefficient between the UE located at u_k and sensor located at s_l. No information about this channel is assumed at the radar sensors. Moreover, we assume that the interference channel between the user located at u_k and the radar transmit array is represented by g_{kr}. g_{rk} are assumed to consist of i.i.d. ZMCSCG entries with a variance equal to the large scale fading coefficient between the radar and user located at u_k. Similarly, the interference channel between the AP located at r_i and the radar sensor located at s_l is represented by g_{il}, and has a variance that is proportional

to the underlying slow fading component.

4.3 The Channel Estimation Subframe

As stated earlier, the first subframe in the larger communications frame is the channel estimation subframe. Therefore, in this section, we look at the operations performed at the APs and at the CPU during this subframe. Let the UE at u_k transmit a pilot signal $\psi_k[n]$ at the nth time instant such that $\sum_{n=1}^{K} \psi_k[n]\psi_l^*[n] = \delta[k-l]$. Consequently, the signal received by the CPU corresponding to the AP located at a_i at the nth instant can be expressed as

$$z_i[n] = \sum_{u_k \in \Phi_u} \sqrt{\epsilon_{p,k}}\psi_k[n]\sqrt{\beta_{ki}}h_{ki} + \sum_{r_m \in \Phi_a} \mathbf{g}_{mi}^T \boldsymbol{\zeta}_m[n] + w_{zi}[n], \tag{4.9}$$

Based on this, we can now define,

$$z_{li} \triangleq \sum_{n=1}^{K} z_i[n]\psi_l^*[n]. \tag{4.10}$$

Now, the CPU may or may not have the phase synchronization information about $\boldsymbol{\zeta}[n]$. In the former case, the CPU can form $z_l^{'}$ by subtracting $\sum_{n=1}^{K} \hat{\mathbf{g}}_{ri}^T \boldsymbol{\zeta}[n]\psi_l[n]$ from z_{li} to obtain the vector $z_{li}^{'}$. In this case, using the results derived in [63], we can show that the LMMSE estimate of h_{ki} at the CPU can be expressed as

$$\hat{h}_{ki} = \frac{\sqrt{\epsilon_{p,k}}\beta_{ki}}{\epsilon_{p,k}\beta_{ki} + P_t\eta_{ei} + N_0} z_{ki}^{'}, \tag{4.11}$$

It is easy to show that the variance of $\hat{h}_{ki}$ can be expressed as

$$\sigma_{ki}^2 = \frac{\epsilon_{p,k}\beta_{ki}^2}{\epsilon_{p,k}\beta_{ki} + P_t\eta_{ei} + N_0}. \tag{4.12}$$

equivalently, we can write σ_{ki}^2 as a function of the distance d_{ki}, and express it as

$$\sigma_{ki}^2(d_{ki}, d_{ri}) = \frac{\epsilon_{p,k}\beta^2(d_{ki})}{\epsilon_{p,k}\beta(d_{ki}) + P_t\eta_e\beta(d_{ri}) + N_0}. \tag{4.13}$$

Now, h_{ki} can be expressed in terms of $\hat{h}_{ki}$ and an orthogonal estimation error component $\tilde{h}_{ki}$ as $h_{ki} = \hat{h}_{ki} + \tilde{h}_{ki}$, with $E[\hat{h}_{ki}\tilde{h}_{ki}^H] = 0$, and $\tilde{h}_{ki}$ being a ZMCSCG random variable having a variance

given as

$$\bar{\sigma}_{ki}^2 = \beta_{ki} - \sigma_{ki}^2 \tag{4.14}$$

Similarly, in case the synchronization information about $\zeta[n]$ is not available at the CPU, then

$$\hat{h}_{ki} = \frac{\sqrt{\epsilon_{p,k}}\beta_{ki}}{\epsilon_{p,k}\beta_{ki} + P_t\eta_{ei} + N_0} z_{ki}. \tag{4.15}$$

and

$$\sigma_{ki}^2 = \frac{\epsilon_{p,k}\beta_{ki}^2}{\epsilon_{p,k}\beta_{ki} + P_t\eta_{Ii} + N_0}, \tag{4.16}$$

that is,

$$\sigma_{ki}^2(d_{ki}, d_{ri}) = \frac{\epsilon_{p,k}\beta^2(d_k i)}{\epsilon_{p,k}\beta(d_{ki}) + P_t\eta_e\beta(d_{ri}) + N_0}. \tag{4.17}$$

We note that the pilots are being transmitted in the uplink, i.e. by the UEs to the APs, therefore, from the point of view of the radar subsystem, the interference generated by pilot transmission is identical to the interference generated by uplink data transmission albeit with a different power level. As a consequence, we can evaluate the effect of pilot transmission on the radar subsystem simultaneously with the effect of uplink data transmission, and have relegated that discussion to the next section.

4.4 The Uplink Data Transmission Sub-frame

In this section, we determine the performance of the ICS system by individually evaluating the performances of the two subsystems and accounting for the effects of the mutual interference. For this purpose, we use the coverage probability of the communication sub-system, and the tracking MSE of the radar target as performance metrics. We first obtain the performance metric of the communication sub-system in the next sub-section.

4.4.1 Coverage analysis for the Communications Sub-system

Here, in order to evaluate the performance of the communication sub-system during the uplink frame, we will first evaluate the uplink rate achievable by each user for a given system deployment, and then apply results from stochastic geometry to obtain the coverage probability.

The received signal at the CPU in the presence of radar generated interference can be written as

$$\mathbf{z}[n] = \sum_{u_l \in \Phi_u} \sqrt{\epsilon_{u,l}} x_l[n] \hat{\mathbf{h}}_l + \sum_{u_l \in \Phi_u} \sqrt{\epsilon_{u,l}} x_l[n] \tilde{\mathbf{h}}_l + \hat{\mathbf{G}}_r^H \boldsymbol{\zeta}[n] + \tilde{\mathbf{G}}_r^H \boldsymbol{\zeta}[n] + \sqrt{N_0} \mathbf{w}_z[n], \tag{4.18}$$

where $\hat{\mathbf{G}}_r = [\hat{\mathbf{g}}_{\mathbf{r1}}, \hat{\mathbf{g}}_{\mathbf{r1}}, \ldots, \hat{\mathbf{g}}_{\mathbf{rN}}]$ and $\tilde{\mathbf{G}}_r = [\tilde{\mathbf{g}}_{\mathbf{r1}}, \tilde{\mathbf{g}}_{\mathbf{r1}}, \ldots, \tilde{\mathbf{g}}_{\mathbf{rN}}]$. Now, based on the available channel estimates, the CPU performs MRC combining with $v_k[n] = \sum_{a_i \in \Phi_a} \hat{h}_{ki}^* z_i[n]$ being the processed signal corresponding to the UE located at u_k that takes the form

$$v_k[n] = \sum_{a_i \in \Phi_a} \hat{h}_{ki}^* \sqrt{\epsilon_{u,k}} x_k[n] \hat{h}_{ki} + \sum_{a_i \in \Phi_a} \hat{h}_{ki}^* \sqrt{\epsilon_{u,k}} x_k[n] \tilde{h}_{ki} + \sum_{a_i \in \Phi_a} \sum_{u_l \in \Phi_u \setminus u_k} \hat{h}_{ki}^* \sqrt{\epsilon_{u,l}} x_l[n] h_{li} + \sum_{a_i \in \Phi_a} \hat{h}_{ki}^* (\tilde{\mathbf{g}}_{ri}^T \boldsymbol{\zeta}[n]) + \sum_{a_i \in \Phi_a} \hat{h}_{ki}^* \sqrt{N_0} w_{zi}[n]. \tag{4.19}$$

Here, the first term indicates desired signal corresponding to the user located at u_k, the second term indicates interference due to channel estimation error, the third term indicates inter user interference, the fourth term indicates radar generated interference and the last term corresponds to the effect of additive noise.

Lemma 1. *The SINR corresponding to the user located at u_k is given as*

$$\gamma_{u,k} = \frac{\xi_{s,k}}{\xi_{E,k} + \xi_{I,k} + \xi_{RC,k} + \xi_{w,k}}. \tag{4.20}$$

where

$$\xi_{s,k} = \epsilon_{u,k} \left(\sum_{a_i \in \Phi_a} \sigma_{ki}^4 + \sum_{a_n \in \Phi_a} \sum_{a_m \in \Phi_a} \sigma_{km}^2 \sigma_{kn}^2 \right), \tag{4.21}$$

denotes the desired signal power,

$$\xi_{E,k} = \epsilon_{u,k} \sum_{a_i \in \Phi_a} \bar{\sigma}_{ki}^2 \sigma_{ki}^2, \tag{4.22}$$

denotes the channel estimation error power,

$$\xi_{I,k} = \sum_{a_i \in \Phi_a} \sum_{u_l \in \Phi_u \setminus u_k} \epsilon_{u,l} \beta_{li} \sigma_{ki}^2, \tag{4.23}$$

denotes the inter user interference power,

$$\xi_{RC,k} = P_t \sum_{a_i \in \Phi_a} \eta_{ei} \sigma_{ki}^2, \tag{4.24}$$

denotes the interference power due to radar sub-system and

$$\xi_{w,k} = N_0 \sum_{a_i \in \Phi_a} \sigma_{ki}^2 \tag{4.25}$$

denotes the effect of additive Gaussian noise. Hence,

$$\gamma_{u,k} = \frac{\epsilon_{u,k}\left(\sum_{a_i\in\Phi_a} 2\sigma_{ki}^4 + 2\sum_{a_n\in\Phi_a\setminus a_m}\sum_{a_m\in\Phi_a}\sigma_{km}^2\sigma_{kn}^2\right)}{\epsilon_{u,k}\sum_{a_i\in\Phi_a}\sigma_{ki}^2\bar{\sigma}_{ki}^2 + \sum_{a_i\in\Phi_a}\sum_{u_l\in\Phi_u\setminus u_k}\epsilon_{u,l}\beta_{li}\sigma_{ki}^2 + P_t\sum_{a_i\in\Phi_a}\eta_{ei}\sigma_{ki}^2 + N_0\sum_{a_i\in\Phi_a}\sigma_{ki}^2}. \tag{4.26}$$

Proof. See Appendix B.1. □

Theorem 5. *The coverage probability of an arbitrarily located UE operating in the communications subsystem, with all the UEs transmitting at a fixed power ρ_u, for an coverage rate $R_{u,0}$ can be expressed as* (4.27)*, where*

$$P_{cov,u}(R_{u,0}) = \int_0^\infty\int_0^\infty\int_0^\infty \mathbb{1}\left[\epsilon_{u,k}\left((2\pi\lambda_a)^2\int_x^\infty\int_x^\infty\int_y^\infty\int_y^\infty \sigma^2(r,t)\sigma^2(s,v)dtdvdrds + \int_x^\infty\int_y^\infty(\sigma^4(r,t)+\gamma_0\sigma^2(r,t))dtdr\right) \geq \gamma_0\left(\int_y^\infty\int_x^\infty \sigma^2(r,t)\left(\rho_u\bar{\sigma}^2(r,t) + I_1(z) + P_t\eta_e\beta(t) + N_0\right)drdt\right)\right] p_{d_{u1}}(z)p_{d_{k1}}(x)p_{d_{r1}}(y)dzdxdy. \tag{4.27}$$

$$I_1(z) = 2\pi\lambda_u\rho_u\left(\int_z^\infty \beta(u)udu\right) \tag{4.28}$$

$$\sigma^2(r,t) = \frac{\rho_p\beta^2(r)rt}{\rho_p\beta(r) + P_t\eta_e\beta(t) + N_0} \tag{4.29}$$

$$\bar{\sigma}^2(r,t) = rt\beta(r)\frac{P_t\eta_e\beta(t) + N_0}{\rho_p\beta(r) + P_t\eta_e\beta(t) + N_0} \tag{4.30}$$

$$p_{d_{k1}}(x) = 2\pi\lambda_a x e^{-\pi\lambda_a x^2}, \tag{4.31a}$$

$$p_{d_{r1}}(y) = 2\pi\lambda_a y e^{-\pi\lambda_a y^2}, \tag{4.31b}$$

$$p_{d_{u1}}(z) = 2\pi\lambda_u y e^{-\pi\lambda_u z^2}, \tag{4.31c}$$

and $\gamma_0 = (2^{R_{u,0}} - 1)$.

Proof. See Appendix B.2 □

We note that the integrals in (4.27) cannot be solved in closed form, and need to be evaluated numerically [66].

4.4.2 Tracking performance

We now seek to quantify the performance of the radar subsystem in terms of the MSE of the radar target parameters. For this purpose, we note that signal processing operations at the radar receiver are carried out in in two phases, viz. at individual sensor nodes, and at the FC. Therefore, we quantify the performances of these two stages separately.

Lemma 2. *The covariance matrix for the observation noise at the radar receiver is given as,*

$$\boldsymbol{\Lambda}_{y,l}[n] = diag(\sigma^2_{R,l}[n], \sigma^2_{\theta,l}[n], \sigma^2_{v,l}[n]), \tag{4.32}$$

where $\sigma^2_{R,l}[n], \sigma^2_{\theta,l}[n]$ and $\sigma^2_{v,l}[n]$ are the Cramer-Rao lower bounds on the mean squared estimation error for $R[n], \theta[n]$ and $v[n]$ respectively [62], and take the form

$$\sigma^2_{R,l}[n] = \frac{2\pi\rho_u\lambda_u \int_0^\infty \int_u^\infty \beta(r) r dr p_{d_{l0}}(u) du + \sigma^2_{r,l}}{T_d P_t} B^{-2} c_R, \tag{4.33a}$$

$$\sigma^2_{\theta,l}[n] = \frac{2\pi\rho_u\lambda_u \int_0^\infty \int_u^\infty \beta(r) r dr p_{d_{l0}}(u) du + \sigma^2_{r,l}}{T_d P_t} \theta_b^2 c_\theta, \tag{4.33b}$$

$$\sigma^2_{v,l}[n] = \frac{2\pi\rho_u\lambda_u \int_0^\infty \int_u^\infty \beta(r) r dr p_{d_{l0}}(u) du + \sigma^2_{r,l}}{T_d P_t} B^{-2} c_v, \tag{4.33c}$$

such that,

$$p_{d_{l0}}(u) = 2\pi\lambda_k u e^{-\pi\lambda_u u^2}, \tag{4.34}$$

with T_d being the dwell time of the radar sensing receiver located at s_l on the radar target, B and θ_b being the radar's transmit signal bandwidth and the receive beam-width of the sensor node located at s_l respectively, and c_R, c_θ, c_v being constants.

Proof. See Appendix B.3. □

Theorem 6. *Given that a estimate of the system state at the nth instant based on the samples collected till the $(n-1)$th instant, $\hat{\mathbf{s}}[n|n-1]$ and the corresponding state estimation MSE matrix $\mathbf{M}[n|n-1]$ are made available to all the sensors by the FC, the updated MMSE estimate of the system state at the lth sensor is given as*

$$\hat{\mathbf{s}}_l[n|n] = \hat{\mathbf{s}}[n|n-1] + \boldsymbol{\Gamma}_l[n]\boldsymbol{\alpha}_l[n], \tag{4.35}$$

where

$$\boldsymbol{\Gamma}_l[n] = \left(\mathbf{M}[n|n-1]\mathbf{F}_l^H[n]\right) \times \left(\mathbf{F}_l[n]\mathbf{M}[n|n-1]\mathbf{F}_l^H[n] + \sum_{u_k \in \Phi_u} \epsilon_{x,k}\eta_{kl}\mathbf{I}_{N_r} + \boldsymbol{\Lambda}_{y,l}[n]\right)^{-1} \tag{4.36}$$

represents the Kalman filtering gain, such that,

$$\mathbf{F}_l[n] = \left.\frac{\partial f_l}{\partial \mathbf{s}[n]}\right|_{\mathbf{s}[n]=\hat{\mathbf{s}}[n|n-1]}, \tag{4.37}$$

and

$$\boldsymbol{\alpha}_l[n] = \mathbf{y}_l[n] - \hat{\mathbf{y}}_l[n|n-1] \tag{4.38}$$

is the innovation component having a covariance matrix,

$$\mathbf{R}_{\alpha,l}[n] = \left(\mathbf{F}_l[n]\mathbf{M}[n|n-1]\mathbf{F}_l^H[n] + \sum_{u_k \in \Phi_u} \epsilon_{x,k}\eta_{kl}\mathbf{I}_{N_r} + \boldsymbol{\Lambda}_{y,l}[n] \right), \tag{4.39}$$

with

$$\hat{\mathbf{y}}_l[n|n-1] = f_l(\hat{\mathbf{s}}[n|n-1]). \tag{4.40}$$

Proof. We note that each radar sensor node is essentially using an EKF for signal tracking, where the current state estimate supplied by the FC is used to form the estimate of $\mathbf{y}_l[n]$ as (4.40). Following this, the innovation component is calculated as (4.38), that is used to update the available state estimate as (4.35), with the Kalman filtering gain calculated as,

$$\boldsymbol{\Gamma}_l[n] = \left(E[\mathbf{s}[n]\boldsymbol{\alpha}_l[n]]\right)\mathbf{R}_{\alpha,l}^{-1}[n] \tag{4.41}$$

where $\mathbf{R}_{\alpha,l}[n]$ is the correlation matrix of the innovation component and is given by

$$\mathbf{R}_{\alpha,l}[n] = E[\boldsymbol{\alpha}_l[n]\boldsymbol{\alpha}_l^H[n]]. \tag{4.42}$$

The interested reader can find a detailed derivation of the general EFK in [69, Section 13.7]. □

Theorem 7. *The MSE matrix of filtered state, at the lth node and at the nth time instant takes the form*

$$\mathbf{M}_l[n|n] = \left(\mathbf{I} - \boldsymbol{\Gamma}_l[n]\mathbf{F}_l[n]\right)\mathbf{M}[n|n-1]. \tag{4.43}$$

Proof. The MSE matrix at the lth sensor node is given by

$$\mathbf{M}_l[n|n] = E[(\mathbf{s}[n] - \hat{\mathbf{s}}_l[n|n])(\mathbf{s}[n] - \hat{\mathbf{s}}_l[n|n])^H], \tag{4.44}$$

that can be simplified to the (4.43) using the procedure detailed in [69, Section 13.7]. The procedure is fairly standard and is omitted for brevity. □

Following this, the L sensor nodes then communicate their respective filtered estimates, and the corresponding error covariance matrices to the FC via the feedback link. The FC treats these estimates as its observations, to construct the vector

$$\mathbf{y}_f[n] = [\hat{\mathbf{s}}_1^T[n|n], \ldots, \hat{\mathbf{s}}_L^T[n|n]]^T, \tag{4.45}$$

that can be expressed as,

$$\mathbf{y}_f[n] = \mathbf{B}\mathbf{s}[n] + \mathbf{w}_{y,f}[n], \tag{4.46}$$

where $\mathbf{B} = \mathbf{1}_L \otimes \mathbf{I}_4$, with $\mathbf{1}_L$ representing a length L vector containing all 1s, and $\mathbf{w}_{y,fc}$ is the observation noise due to the sensor estimation error, and feedback AWGN, such that $\mathbf{w}_{y,fc}[n] \sim \mathcal{CN}(\mathbf{0}, \mathbf{R}_{y,f})$ where $\mathbf{R}_{y,f}$ is a $4L \times 4L$ block diagonal matrix, containing L 4×4 blocks, such that its lth block is given as $(\mathbf{R}_{y,f})_{l,l} = \mathbf{M}_l[n|n] + \sigma_f^2 \mathbf{I}_4$, with σ_f^2 being the noise variance for the sensor to FC link.

Theorem 8. *The state correction equation at the FC for the nth adaptation cycle is given by*

$$\hat{\mathbf{s}}[n|n] = \hat{\mathbf{s}}[n|n-1] + \boldsymbol{\Gamma}_f[n]\boldsymbol{\alpha}_f, \tag{4.47}$$

where

$$\boldsymbol{\Gamma}_f[n] = (\mathbf{M}[n|n-1]\mathbf{B}^H)(\mathbf{B}\mathbf{M}[n|n-1]\mathbf{B}^H + \mathbf{R}_{y,f})^{-1} \tag{4.48}$$

is the Kalman filtering gain and

$$\boldsymbol{\alpha}_f[n] = \mathbf{y}_f[n] - \hat{\mathbf{y}}_f[n|n-1], \tag{4.49}$$

is the innovation component, such that

$$\hat{\mathbf{y}}_f[n|n-1] = \mathbf{B}\hat{\mathbf{s}}[n|n-1]. \tag{4.50}$$

Finally the predicted state vector is calculated as,

$$\hat{\mathbf{s}}[n|n-1] = \mathbf{A}\hat{\mathbf{s}}[n-1|n-1], \tag{4.51}$$

and communicated with all the sensors.

Proof. The proof follows a pattern similar to the proof of Theorem 6 and is omitted for brevity. □

Theorem 9. *The MSE matrix of the state vector,* $\mathbf{M}[n|n] = E[(\mathbf{s}[n] - \hat{\mathbf{s}}[n|n])(\mathbf{s}[n] - \hat{\mathbf{s}}[n|n])^H]$ *is given by*

$$\mathbf{M}[n|n] = (\mathbf{I} - \boldsymbol{\Gamma}_f[n]\mathbf{B})\mathbf{M}[n|n-1]. \tag{4.52}$$

Based on this, the minimum prediction MSE matrix of the state vector based on $n-1$ previous observations, $\mathbf{M}[n|n-1] = E[(\mathbf{s}[n] - \hat{\mathbf{s}}[n|n-1])(\mathbf{s}[n] - \hat{\mathbf{s}}[n|n-1])^H]$ is calculated as

$$\mathbf{M}[n|n-1] = \mathbf{A}\mathbf{M}[n-1|n-1]\mathbf{A}^H + \mathbf{R}_s[n], \tag{4.53}$$

and shared with all the sensors.

4.5 The Downlink Sub-frame

In this section we analyze the performance of the ICS system during the downlink sub-frame in the presence of mutual interference of the two sub-systems. Similar to the uplink case, we first evaluate the coverage probability of the communication sub-system, and then the tracking MSE of radar subsystem.

4.5.1 Coverage analysis for the communication sub-system

In this sub-section we first calculate the per user achievable rate in the presence of radar generated interference, and use this to obtain the coverage probability. We note that, the signal received by the user located at u_k can be expressed as

$$y_{d,k} = \sum_{a_l \in \Phi_a} h_{kl} b_l[n] + \mathbf{g}_{rk}^T \zeta[n] + \sqrt{N_0} w_y[n] \tag{4.54}$$

$$= \sum_{a_l \in \Phi_a} \hat{h}_{kl} \frac{\hat{h}_{kl}^*}{\sqrt{E|\hat{h}_{kl}|^2}} \sqrt{\epsilon_d} t_k + \sum_{a_l \in \Phi_a} \tilde{h}_{kl} \frac{\hat{h}_{kl}^*}{\sqrt{E|\hat{h}_{kl}|^2}} \sqrt{\epsilon_d} t_k + \sum_{a_l \in \Phi_a} \sum_{u_i \in \Phi_u \setminus u_k} h_{kl} \frac{\hat{h}_{il}^*}{\sqrt{E|\hat{h}_{il}|^2}} \sqrt{\epsilon_d} t_i + \mathbf{g}_{rk}^T \boldsymbol{\zeta}[n] + w_y[n]. \tag{4.55}$$

Here, the first term indicates the desired signal corresponding to the user, the second term corresponds to channel estimation error interference, the third term is due to the inter user interference, the fourth term is because of the interference from the radar subsystem and the last term is due to the AWGN.

Lemma 3. *The SINR corresponding to the user located at u_k is given as*

$$\gamma_{d,k} = \frac{\xi_{d,s,k}}{\xi_{d,E,k} + \xi_{d,I,k} + \xi_{d,RC,k} + N_0}, \tag{4.56}$$

where

$$\xi_{d,s,k} = \epsilon_d \sum_{a_l \in \Phi_a} 2\sigma_{kl}^2 + \epsilon_d \sum_{a_m \in \Phi_a \setminus a_n} \sum_{a_n \in \Phi_a} \sqrt{\sigma_{km}^2 \sigma_{kn}^2} \tag{4.57}$$

denotes the desired signal power,

$$\xi_{d,E,k} = \epsilon_d \sum_{a_l \in \Phi_a} (\bar{\sigma}_{kl}^2) \tag{4.58}$$

denotes the channel estimation error power,

$$\xi_{d,I,k} = \epsilon_d \sum_{a_l \in \Phi_a} \sum_{u_i \in \Phi_u \setminus u_k} \beta_{kl} \tag{4.59}$$

denotes the inter user interference power, and

$$\xi_{d,RC,k} = P_t \eta_{ek} \tag{4.60}$$

denotes the radar generated interference power and N_0 is the noise variance.

Proof. See Appendix B.4 □

Theorem 10. *The downlink coverage probability of an arbitrarily located UE for a given threshold $R_{d,1}$ can be expressed as,*

$$P_{cov,d}(R_{d,1}) = \int_0^\infty \int_0^\infty \int_0^\infty \mathbf{1}\Big(\rho_d (2\pi\lambda_a)^2 \int_x^\infty \int_y^\infty \sigma^2(r,t) dr dt + \rho_d (2\pi\lambda_a)^4 \int_x^\infty \int_y^\infty \int_x^\infty \int_y^\infty \sigma(r,t)\sigma(s,u) dr dt ds du \geq 4\pi^2 \lambda_a \lambda_u \int_z^\infty \int_x^\infty \beta(r) r t dr dt + P_t \eta_e \beta(z) + N_0\Big) p_{d_{u1}}(z) p_{d_{k1}}(x) p_{d_{r1}}(y) dz dx dy \tag{4.61}$$

where

$$p_{d_{k1}}(x) = 2\pi\lambda_a x e^{-\pi\lambda_a x^2}, \tag{4.62a}$$

$$p_{d_{r1}}(y) = 2\pi\lambda_a y e^{-\pi\lambda_a y^2}, \tag{4.62b}$$

$$p_{d_{u1}}(z) = 2\pi\lambda_u y e^{-\pi\lambda_u z^2}, \tag{4.62c}$$

and

$$\gamma_1 = 2^{R_{d,1}} - 1 \tag{4.63}$$

Proof. See Appendix B.5 □

4.5.2 Target Tracking

The signal received by the sensing receiver located at s_l, at the nth time instant, in the presence of downlink communication interference can be expressed as,

$$\xi_l[n] = h_{r,l} e^{j2\pi f_{d,l}(n-n_l)} a(\theta_l) \mathbf{a}^H(\theta_t) \boldsymbol{\zeta}[n - n_l] + \sum_{a_i \in \Phi_a} g_{il} b_i + \omega_{r,l}[n]. \tag{4.64}$$

The parameter vector $\mathbf{y}_l[n]$ can be obtained via a procedure similar to the one described in Section 4.4.2. However, since we consider the radar operation in the downlink subframe instead of the uplink subframe, the observation noise covariance matrix $\boldsymbol{\Lambda}_{y,l}[n]$ is expressed as in Lemma 4.

Lemma 4. *In the presence of downlink communication signal the matrix* $\boldsymbol{\Lambda}_{y,l}[n]$ *takes the form*

$$\boldsymbol{\Lambda}_{y,l}[n] = diag(\sigma^2_{R,l}[n], \sigma^2_{\theta,l}[n], \sigma^2_{v,l}[n]). \tag{4.65}$$

where

$$\begin{aligned}
\sigma^2_{R,l}[n] &= \frac{\int_0^\infty 2\pi\lambda_a(\int_{d_{Nl}}^\infty \beta(r) r dr) p_{d_{Nl}}(u) du + \sigma^2_{r,l}}{h^2_{r,l} P_t} B^{-2} c_R, \\
\sigma^2_{\theta,l}[n] &= \frac{\int_0^\infty 2\pi\lambda_a(\int_{d_{Nl}}^\infty \beta(r) r dr) p_{d_{Nl}}(u) du + \sigma^2_{r,l}}{h^2_{r,l} P_t} \theta_b^2 c_\theta, \\
\sigma^2_{v,l}[n] &= \frac{\int_0^\infty 2\pi\lambda_a(\int_{d_{Nl}}^\infty \beta(r) r dr) p_{d_{Nl}}(u) du + \sigma^2_{r,l}}{h^2_{r,l} P_t} B^2 c_v,
\end{aligned} \tag{4.66}$$

such that

$$p_{d_{Nl}}(u) = \frac{2}{\Gamma(N)} (\pi\lambda_a)^N u^{2N-1} e^{-\pi\lambda_a u^2}. \tag{4.67}$$

Following this, given the FC generated estimate vector $\hat{\mathbf{s}}[n]$ and the corresponding MSE matrix $\mathbf{M}[n, n-1]$, the lth sensor can update its local estimate using Theorem 6, and the corresponding MSE as Theorem 7. Similarly, based on the local estimates supplied by the sensors, the FC may use Theorems 8 and 9.

4.6 Simulation Results

In this section we validate our derived results using Monte-Carlo simulations. Here, the communication subsystem consists of a CF-mMIMO system spread over a circular region with a radius 500 m. We assume both the APs and the users to be distributed as PPP across the cell, and operating at a carrier frequency f_c. Both the communications and the radar signals are assumed to have a bandwidth of 20 MHz. The communication frame consists of 1024 channel uses with the first K channel uses dedicated for training, ensuring orthogonal pilots, and the remaining for uplink data transmission. For the purpose of these experiments, we consider the interference channels to be known at the APs with a 10% error. On the other hand, the radar subsystem consists of a multi-static radar comprising a transmitter with $M_t = 10$ antennas and single antenna sensors. The radar sensors are also assumed to be distributed as PPP with intensity λ_s across the cell. All the performance metrics presented in this section are generated by averaging over 10,000 realizations of the system.

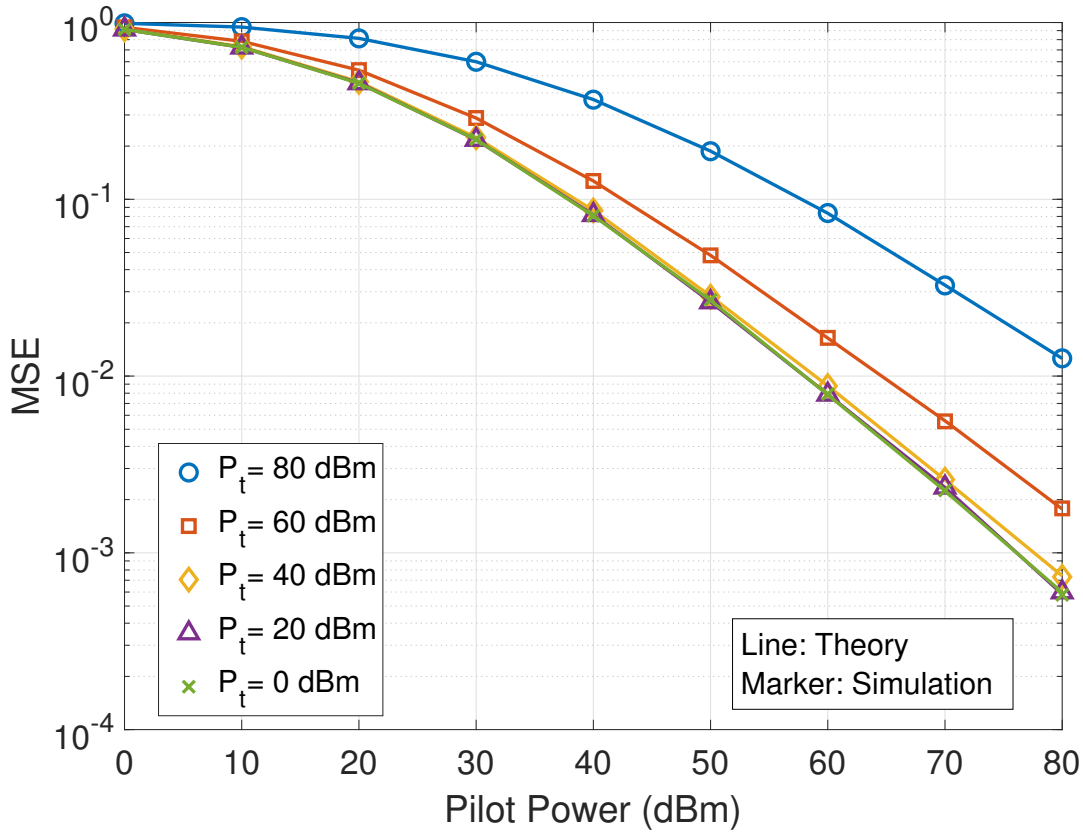

Fig. 4.2: Channel Estimation MSE as a function of the pilot power for different radar transmit powers

Table 4.1: Simulation parameters.

Parameter	Values
Cell radius (r)	500 m
Propagation constant (α)	-3.6
Interference channel MSE(η_e)	0.1
Radar Transmit antennas (M_t)	10
Carrier frequency (f_c)	3 GHz
AP density (λ_a)	$1024 \times 10^{-6}\text{m}^{-2}$
UE density (λ_u)	$32 \times 10^{-6}\text{m}^{-2}$
Radar sensor density (λ_s)	$8 \times 10^{-6}\text{m}^{-2}$
Bandwidth	20 MHz
Ambient Temperature	300K
T_d	0.1 s
θ_b	2.5°

Fig. 4.2 plots the MSE of the uplink channel estimate as a function of uplink pilot power for different values of radar transmit power. We observe the MSE decreases with the increase in the uplink pilot power. Below 20 dBm the impact of radar generated interference onto the channel estimation MSE is negligible, however, above 20 dBm it increases slightly with the increase in the radar transmit power.

Fig. 4.3 illustrates the CDF of the per user uplink achievable rate for different uplink transmit power and different AP densities, in this case, we have fixed $\lambda_u = 32 \times 10^{-6}$. We observe that the CDF shifts right with an increase in the AP densities, which is an expected behaviour for CF mMIMO systems, and it marginally shifts left with an increase in the radar generated interference. Therefore, it is safe to conclude that the uplink receive diversity in CF-mMIMO systems counter acts the detrimental effects of radar generated interference, allowing minimal deterioration in the communications performance.

In Fig. 4.4 we plot the uplink rate coverage probability as a function of the rate threshold for different values of UE densities and radar transmit power. We again observe that the effect of UE densities on the per user achievable rate is much more pronounced that that of the radar transmit power indicating the possibility of coexistence between CF systems and multistatic radars. We evaluate the plots marked "theory" using the N nearest user approximation discussed in [66].

Fig. 4.5 plots the MSE performance of the two level EKF as a function of the iterations, for different UE densities and radar transmit powers with a radar sensor density of $\lambda_s = 8{\times}10^{-6}m^{-2}$.

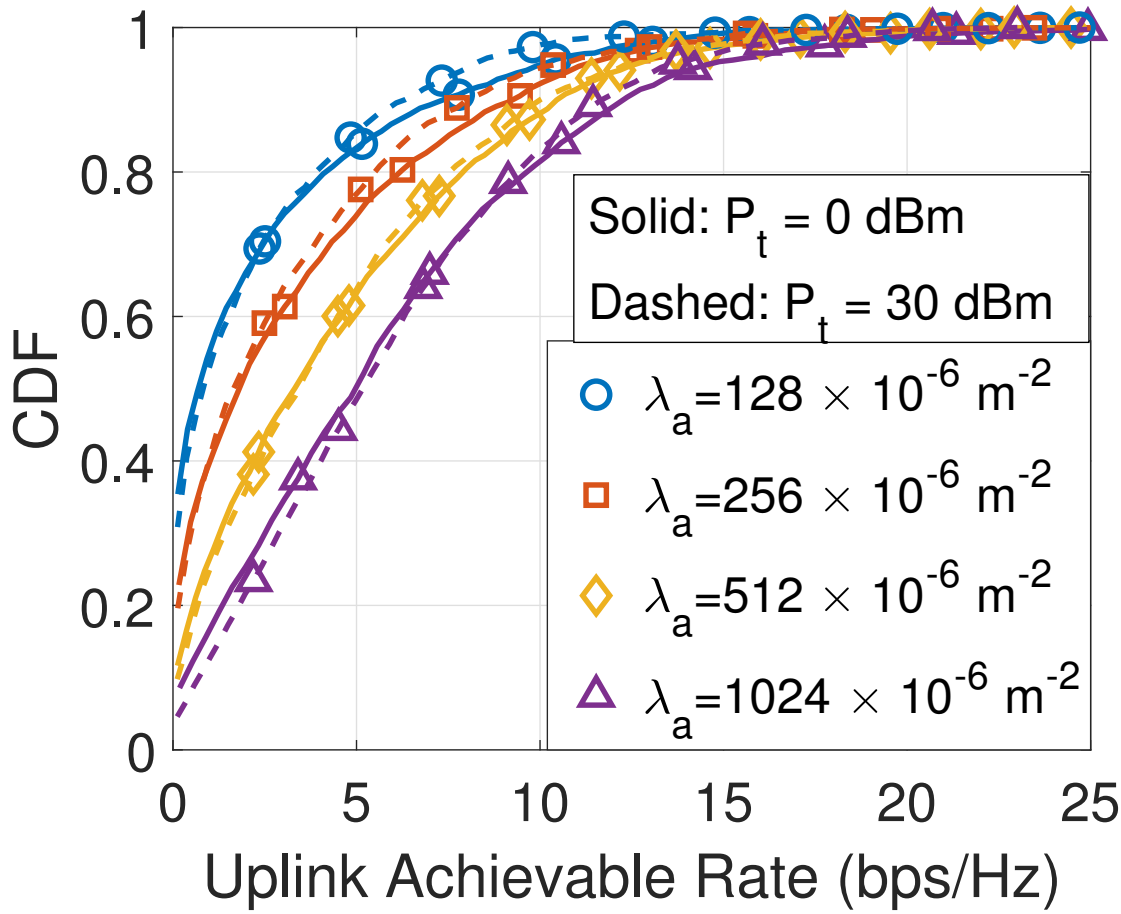

Fig. 4.3: Rate coverage probability as a function of the rate threshold for different radar SNRs at $\lambda_u = 32 \times 10^{-6} m^{-2}$ with the uplink transmit power ρ_u being 0dBm.

.

We note that the MSE converges to the same value in all the cases, with the speed of convergence depending on the UE density and the radar transmit power.

We evaluate the effect of varying the sensor densities on the convergence performance of the two level Kalman filtering setup in Fig. 4.6. We note that the final MSE decreases with an increase in the sensor density. However, the MSE converges to the same value, regardless the amount of interference generated by the UEs.

In Figs. 4.7 and 4.8 we plot the rate coverage probabilities of the communications subsystem in the downlink sub-frame for different amounts of radar generated interference, for different UE (Fig. 4.7) and AP (Fig. 4.8) densities. From both these figures, we note that the effect of radar generated interference is more pronounced in the downlink as compared to the uplink. This can be attributed to the lack of receive diversity in the downlink. However, while the performance losses in the downlink are pronounced, they are still not severe enough to render the communications subsystem unusable, indicating the feasibility of our initial hypothesis of coexistence between CF-mMIMO systems and multistatic tracking radars. Finally, in Fig. 4.9 we evaluate the performance of the EKF based tracking radar in the downlink for different AP and sensor densities. We note that while an increased AP generated interference leads to a slower convergence in this case, the final value of the MSE remains unchanged.

4.7 Chapter Conclusions

In this chapter, we considered the coexistence of a CF-mMIMO system with a multi-static EKF based tracking radar. Using tools from stochastic geometry, we derived expressions for the rate coverage probabilities of the communications subsystem both in the uplink and the downlink. We also evaluated the performance of a two level federated EKF based tracking radar and evaluated its performance for randomly deployed sensors and randomly generated interference sources. Via extensive simulation we found that the effect of inter system interference is minimal for the radar subsystem and negligible in the uplink of the communications subsystem. The communications subsystem does see some performance loss during the downlink subframe due to the loss in diversity, but that still allows coexistence between the two subsystems.

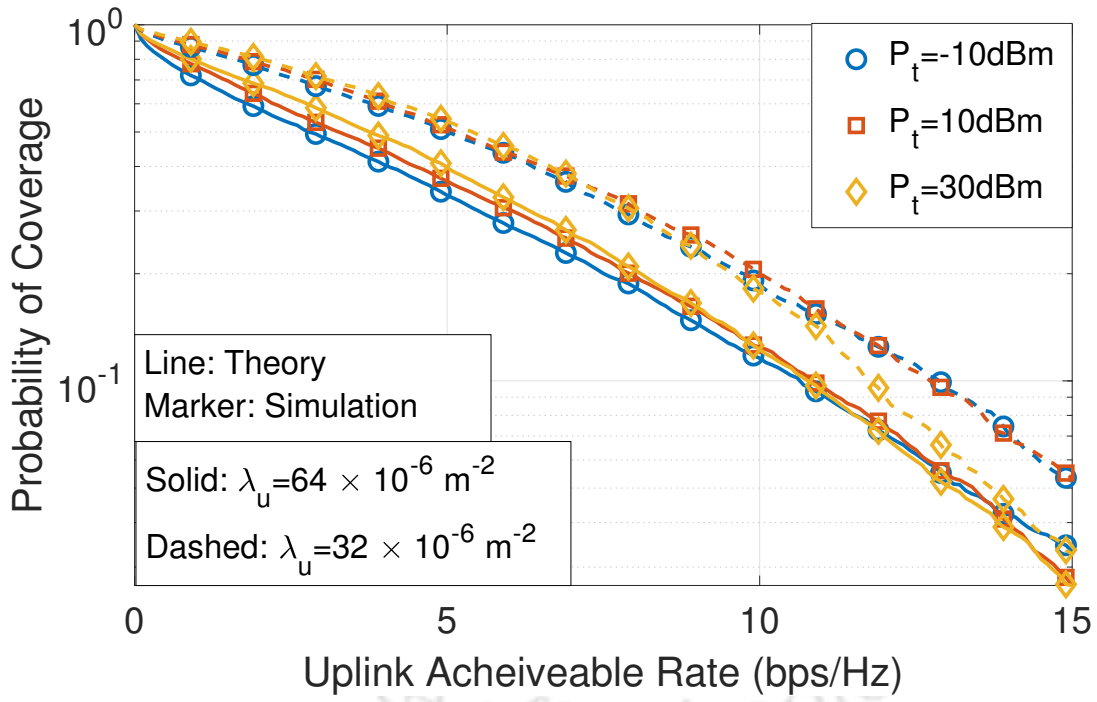

Fig. 4.4: Rate coverage probability as a function of the rate threshold for different UE densities for ρ_u = 0dBm and $\lambda_a = 1024 \times 10^{-6} m^{-2}$.

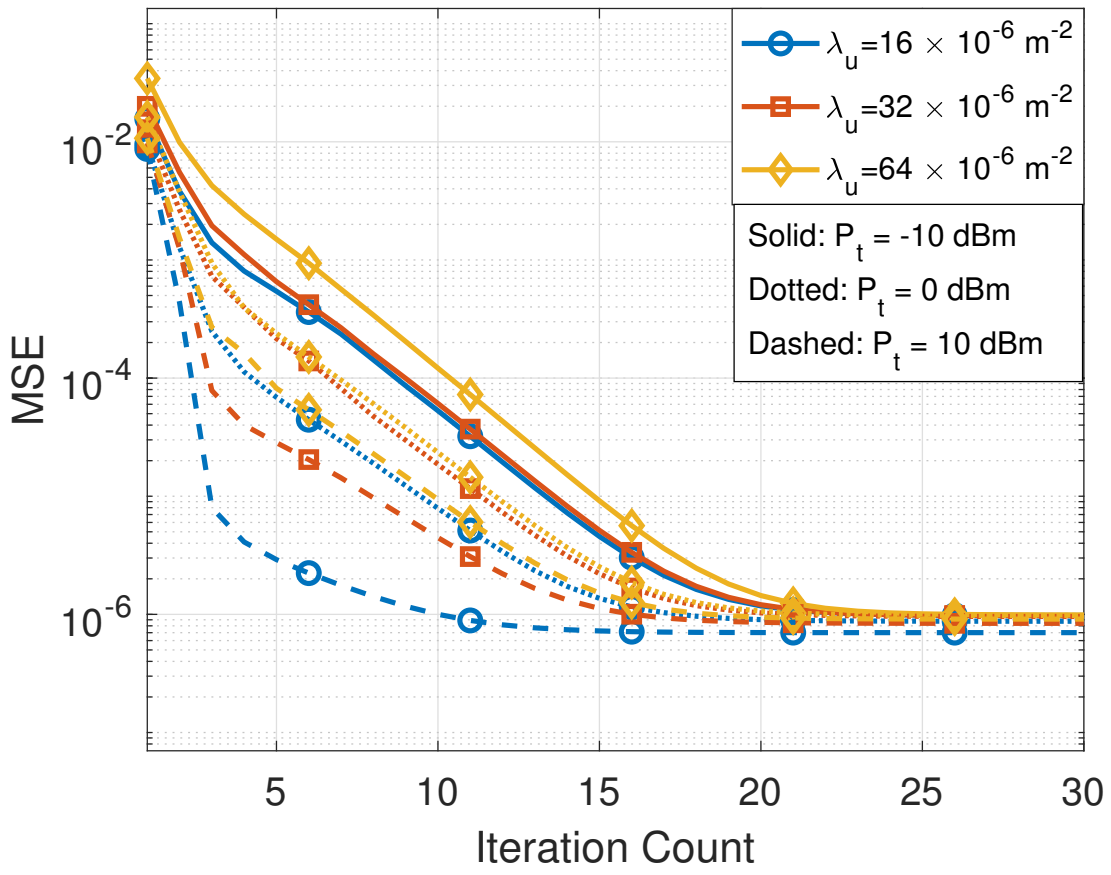

Fig. 4.5: MSE Performance of the EKF for different UE densities and Radar Transmit Powers at $\lambda_s = 8 \times 10^{-6} m^{-2}$ for $\epsilon_{u,k} = 0dBm$.

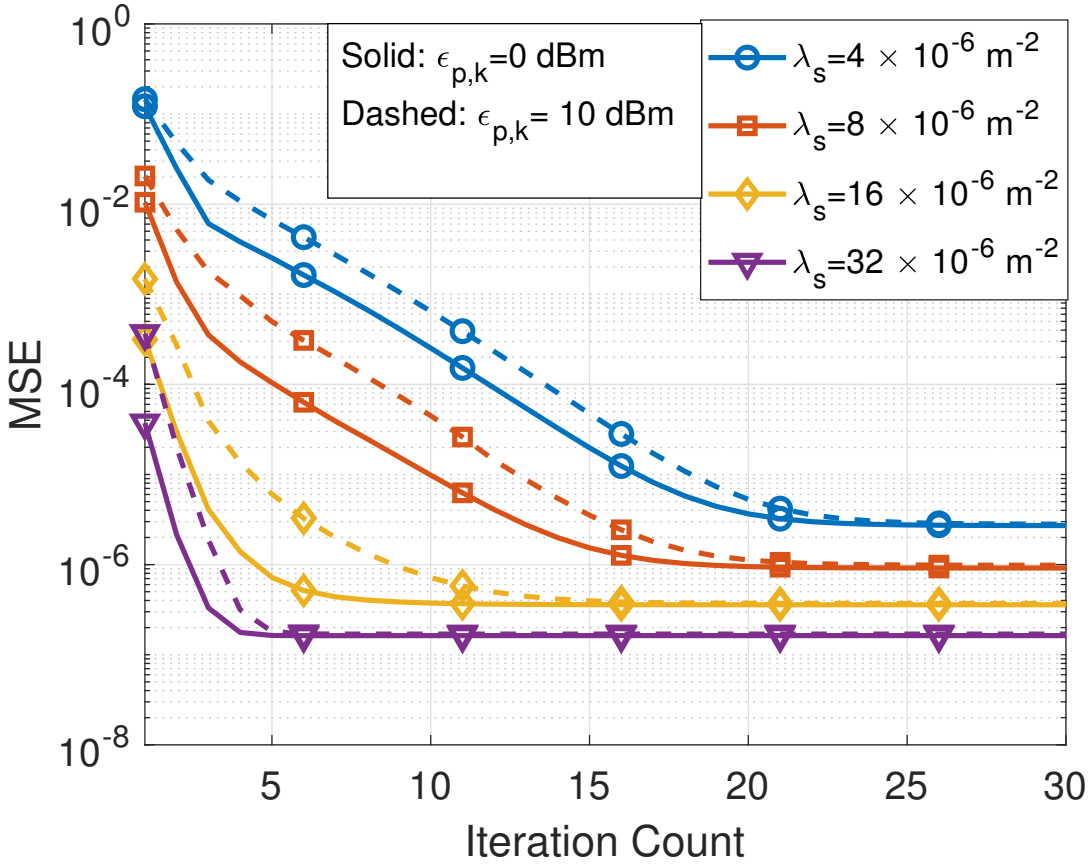

Fig. 4.6: MSE Performance of the EKF for different radar sensor densities and uplink signal Powers at $\lambda_u = 32 \times 10^{-6} m^{-2}$ for $Pt = 0dBm$.

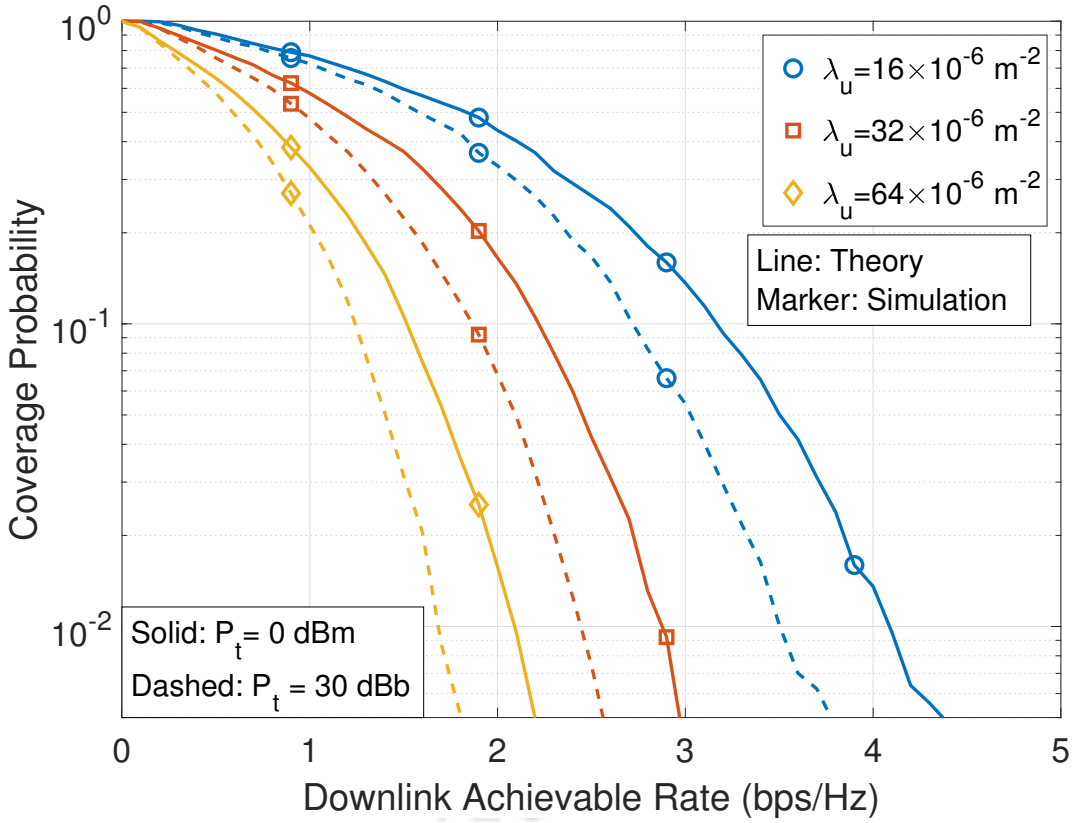

Fig. 4.7: Downlink rate coverage probability as a function of the rate threshold for different radar transmit powers and UE densities $\lambda_a = 1024 \times 10^{-6} m^{-2}$ for $\rho_d = 0 dBm$.

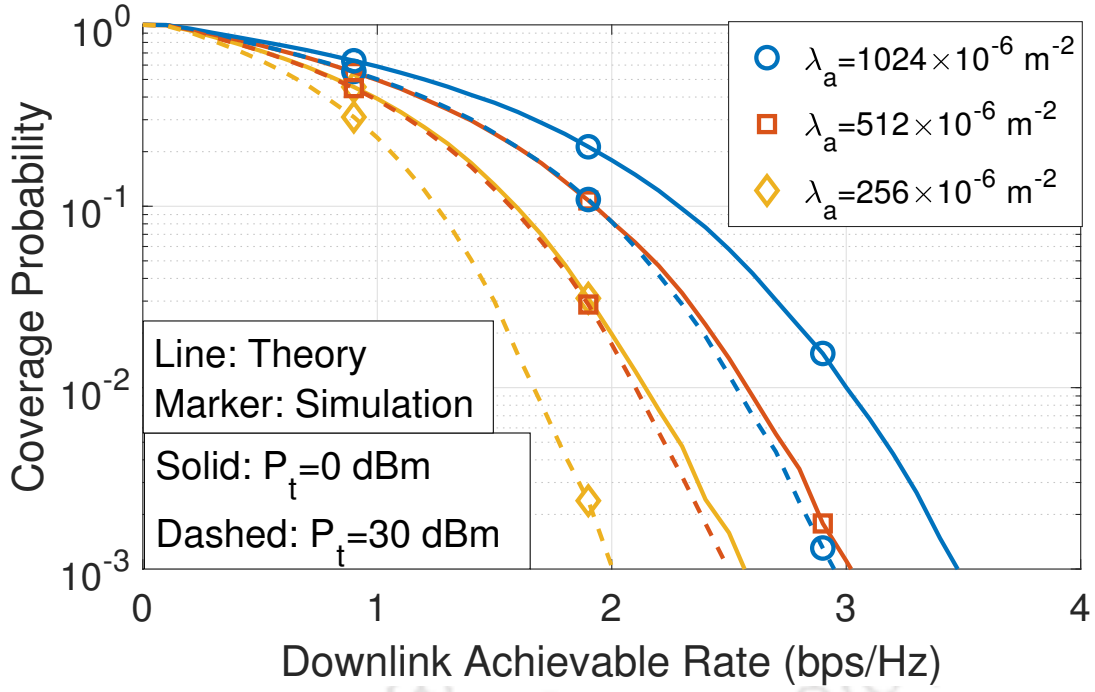

Fig. 4.8: Downlink rate coverage probability as a function of the rate threshold for different radar transmit powers and AP densities $\lambda_u = 32 \times 10^{-6} m^{-2}$ for $\rho_d = 0 dBm$.

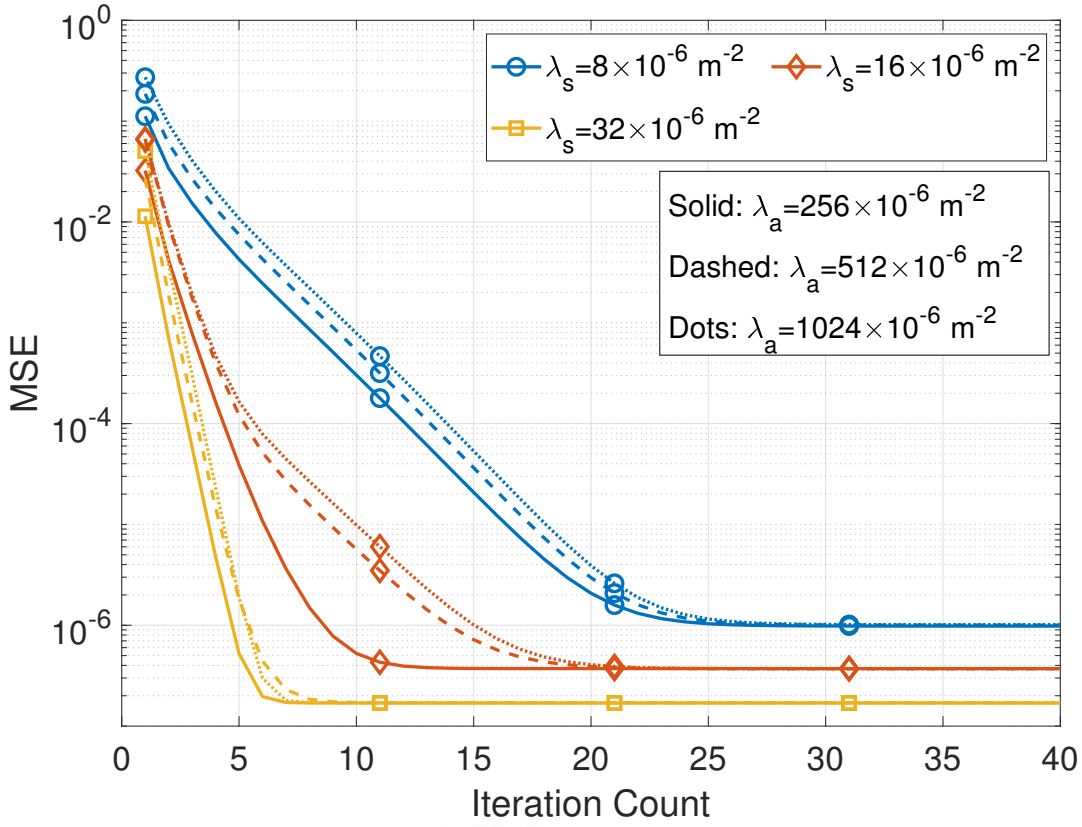

Fig. 4.9: MSE Performance of the EKF during the downlink subframe for different radar sensor densities and AP densities at $Pt = 0dBm$ and $\rho_d = 10dBm$.

5

Communication IRSs Can Enable radar Communication Coexistence

Contents

IRSs, that essentially are large, nearly passive surfaces made out of meta-materials are also being recognized as a key enabling technology for next generation wireless communications systems, especially in the millimeter wave (mmWave) bands [70–72]. This is mainly because IRSs, with the choice of an appropriate phase shift matrix, offer a step towards controllable propagation, and to some extent a performance superior to an inverse-square-law governed channel [72]. However, it is important to note that while an IRS can be tuned to improve the performance of a given communication link, it will continue to reflect all the signals, that lie within the desired frequency range. Consequently, a radar co-existing with an IRS based communications systems will also receive echoes from the proximal IRS in addition to the intended target. As elaborated in Section 5.2, depending on the information about the IRS available at the radar receiver, these additional echoes can either improve the radar performance or deteriorate it.

5.1 Chapter Contributions

In this work, we study effect of the information available about the IRS on the the radar performance in terms of the angle of arrival (AoA) estimation performance. Our precise contributions can be listed as follows,

(i) Assuming the availability of exact IRS parameters at the radar receiver, we derive the Cramer-Rao bound (CRB) on the AoA estimate at the radar receiver. We observe that in this case, the IRS generated echos can actually be used to aid the radar.

(ii) Considering the case where the IRS parameters are not available at the radar receiver we note that the additional reflections generated by the IRS will add to the clutter and lead to a misspecified system model. Consequently, in this case, we derive the misspecified CRB (MCRB) [73] on the performance of the radar system.

(iii) Considering the radar as a source of interference for the IRS based communications subsystem, we write an expression for the achievable rate of the communications subsystem.

(iv) Finally, we evaluate the performance of the ICS system via detailed Monte-Carlo simulations, and find appropriate operating points for the system.

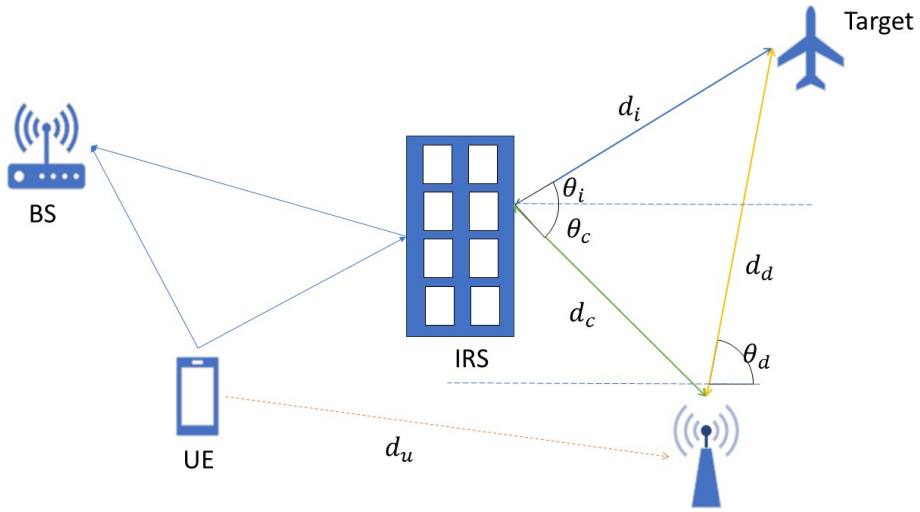

Fig. 5.1: The System Model

The key idea of this chapter is to argue that an IRS being deployed to enhance the performance of a communications system can also enable coexistence with a radar system by reducing the transmit power requirements of the communications subsystem, and causing minimal clutter to the radar subsystem. We next discuss the system model considered by us.

5.2 System Model

We consider a coexistence based ICS system consisting of a mono-static MIMO radar co-existing with an IRS aided single user communications system operating in the millimeter spectrum. The radar subsystem consists of two collocated arrays of M_t transmit and M_r receive antennas, and is estimating the parameters of an arbitrarily located target. Similarly, the communications subsystem consists of an M_a antenna BS communicating with an N_U antenna user aided by an P element IRS. We consider only the uplink sub-frame of the communications subsystem, i.e. the UE is transmitting while the BS is receiving. We assume that the BS is located at the centre of the circular area being served, all the other elements are distributed randomly within this circular area having a radius r_0. This setup is illustrated in Fig. 5.1.

The deterministic signal transmitted by the radar at time t is given by $\mathbf{p}(t)$, and is assumed to have a pulse repetition interval T. This signal is reflected both by the IRS and the target, as well as by several other objects located in the vicinity, and is received at the radar, making

the effective radar channel similar to multipath. Ignoring all the signal reflections, except those from the target and the IRS, we can consider the radar echo to consist of four components, viz. 1. the direct path echo from the target; 2. the clutter generated by the IRS; 3. the echo generated by the target and reflected by the IRS; 4. the echo from the target that is reflected by the IRS; we briefly discuss these in the sequel.

We can write the echo generated by the target as

$$\mathbf{z}_d(t) = \alpha_d e^{j2\pi f_{D,d} t} \mathbf{a}_{r,r}(\theta_d) \mathbf{a}_{r,t}^H(\theta_d) \mathbf{p}(t - \tau_d). \tag{5.1}$$

Here α_d is the complex coefficient of the direct path accounting for the path losses and the radar cross section of the target. This can be assumed to be deterministic but unknown [74]. The vectors $\mathbf{a}_{r,r}(\theta)$ $\mathbf{a}_{r,t}(\theta)$ respectively represent the receive and transmit array responses of the radar with θ_d, being the DoA, that needs to be estimated. $f_{D,d}$ represents the Doppler shift for the direct path, and $\tau_d = 2\frac{d_d}{c}$, with c being the velocity of light, is the lag for the direct path.

Next, we can express the clutter generated by the IRS as,

$$\mathbf{z}_c(t) = \alpha_c \mathbf{a}_{r,r}(\theta_c) \mathbf{a}_{I,t}^H(\theta_c) \mathbf{Q}_P \mathbf{a}_{I,r}(\theta_c) \mathbf{a}_{r,t}^H(\theta_c) \mathbf{p}(t - \tau_c), \tag{5.2}$$

where $\mathbf{a}_{I,r}^H(\theta)$ and $\mathbf{a}_{I,t}^H(\theta)$ represent the receive and transmit array response vectors for the IRS, with θ_c being the angle between the IRS and the radar, $\mathbf{Q}_P$ is the reflection coefficient matrix of the IRS, defined as $\mathbf{Q}_P = \text{diag}(\mathbf{q})$, with $\mathbf{q} = [q_1, \ldots, q_L]^T$, such that $q_l = \eta_l e^{j\phi_l}$ is the reflection coefficient of the lth IRS element, with η_l being the absorption coefficient and ϕ_l being the reflection phase of the lth element [75]. Finally, α_c is another deterministic but unknown constant characterizing the path loss between the IRS and the Radar. The lag of the IRS generated clutter is given by $\tau_c = 2\frac{d_c}{c}$. Note that since we assume both the radar and the IRS to be stationary, there is no Doppler shift in the clutter component. We write the signal echoed by the target and reflected by the IRS as,

$$\mathbf{z}_1(t) = \sqrt{\alpha_c}\omega_1 \sqrt{\alpha_d} e^{j2\pi f_{D,1} t} \mathbf{a}_{r,r}(\theta_c) \mathbf{a}_{I,t}^H(\theta_c) \times \mathbf{Q}_P \mathbf{a}_{I,r}(\theta_i) \mathbf{a}_{r,t}^H(\theta_d) \mathbf{p}\left(t - \frac{\tau_c}{2} - \frac{\tau_d}{2} - \tau_i\right), \tag{5.3}$$

where ω_1 is the deterministic but unknown complex path gain coefficient from the target to the

IRS. $f_{D,i}$ is the Doppler shift caused by the target. $\tau_i = \frac{d_i}{c}$ denotes the propagation lag between the target and the IRS.

Finally, the signal reflected by the IRS and then echoed by the target takes the form,

$$\mathbf{z}_2(t) = \sqrt{\alpha_c}\omega_2 \sqrt{\alpha_d} e^{j2\pi f_{D,2} t} \mathbf{a}_{r,r}(\theta_d)\mathbf{a}_{I,t}(\theta_i) \times \mathbf{Q}_P \mathbf{a}_{I,r}(\theta_c)\mathbf{a}_t^T(\theta_c)\mathbf{p}\left(t - \frac{\tau_c}{2} - \frac{\tau_d}{2} - \tau_i\right), \tag{5.4}$$

where ω_2 is the complex path gain coefficient from the IRS to the target also assumed to be deterministic but unknown. In addition to this, the radar subsystem will receive the signal transmitted by the UE in the communications subsystem as interference from the direct path, as well as via the IRS. Consequently, the overall interference channel between the radar and the communications UE can be expressed as

$$\mathbf{H}_I = \mathbf{H}_u + \sqrt{\alpha_c}\mathbf{a}_{r,r}(\theta_c)\mathbf{a}_{I,t}^H(\theta_c)\mathbf{Q}\mathbf{H}_1, \tag{5.5}$$

with $\mathbf{H}_u = \sum_{l=1}^{C_u} \alpha_{u,l}\mathbf{a}_{r,r}(\theta_{u,l})\mathbf{a}_{u,t}^H(\phi_{1,l})$, and $\mathbf{H}_1 = \sum_{i=1}^{C_1} \alpha_{1,l}\mathbf{a}_{I,r}(\theta_{1,l})\mathbf{a}_{u,t}^H(\phi_{1,l})$, such that C_u and C_1 are the numbers of dominant propagation paths for the respective channels, $\alpha_{x,l}$ is the ZMCSCG distributed path gain for the lth path between the UE and the radar ($x = u$)/ IRS ($x = 1$) whose variance is a function of the inverse square of the distance between the UE and the radar; and $\theta_{x,l}$ is the angle of arrival at the radar/IRS, and $\phi_{x,l}$ is the angle of departure from the UE. Based on these, and representing the signal transmitted by the UE by $\mathbf{s}(t)$, we can write the signal received by the radar as,

$$\begin{aligned}
\mathbf{z}(t) =& \alpha_d e^{j2\pi f_{D,d} t}\mathbf{a}_{r,r}(\theta_d)\mathbf{a}_{r,t}^H(\theta_d)\mathbf{p}(t-\tau_d) + \alpha_c \mathbf{a}_{r,r}(\theta_c)\mathbf{a}_{I,t}^H(\theta_c)\mathbf{Q}_P\mathbf{a}_{I,r}(\theta_c)\mathbf{a}_{r,t}^H(\theta_c)\mathbf{p}(t-\tau_c) + \sqrt{\alpha_c} e^{j2\pi f_{D,i} t} \times \\
& \sqrt{\alpha_d}\left(\omega_1 \mathbf{a}_{r,r}(\theta_c)\mathbf{a}_{I,t}^H(\theta_c)\mathbf{Q}_P\mathbf{a}_{I,r}(\theta_i)\mathbf{a}_{r,t}^H(\theta_d) + \omega_2 \mathbf{a}_{r,r}(\theta_d)\mathbf{a}_{I,t}(\theta_i)\mathbf{Q}_P\mathbf{a}_{I,r}(\theta_c)\mathbf{a}_t^T(\theta_c)\right) \times \\
& \mathbf{p}\left(t - \frac{\tau_c}{2} - \frac{\tau_d}{2} - \tau_i\right) + \mathbf{H}_I\mathbf{s}(t) + \mathbf{w}(t), \\
=& \mathbf{z}_d(t) + \mathbf{z}_c(t) + \mathbf{z}_1(t) + \mathbf{z}_2(t) + \mathbf{H}_I\mathbf{s}(t) + \mathbf{w}(t),
\end{aligned} \tag{5.6}$$

with $\mathbf{w}(t)$ being the ZMCSCG distributed noise vector having a covariance matrix $N_0\mathbf{I}_{M_r}$.

Now, the radar receiver is interested in estimating the angle of arrival θ_d at the radar, based on the observations of $\mathbf{z}(t)$. In this case, it is important to note that the clutter parameters α_c, τ_c, $\mathbf{Q}_P$, θ_c, $\mathbf{a}_{I,t}(\theta)$ and $\mathbf{a}_{I,r}(\theta)$ may or may not be known at the radar. In case these parameters are

known at the radar, the IRS generated clutter $\mathbf{z}_c(t)$ may simply be subtracted from $\mathbf{z}(t)$, and the two echos viz. $\mathbf{z}_1(t)$ and $\mathbf{z}_2(t)$ may be treated as functions of θ_d. In this case, we utilize all the information available from both the direct path and the IRS generated echos, and minimize the sources of interference. Consequently, the radar performance in this case acts as an upper bound on the performance of the overall radar subsystem. Similarly, in case the clutter parameters are not known at the radar receiver, then neither can the clutter component be subtracted from $\mathbf{z}(t)$, nor can $\mathbf{z}_1(t)$ and $\mathbf{z}_2$ be treated as deterministic functions of θ_d, thus reducing all the components of $\mathbf{z}(t)$ to interference and noise. Naturally, this represents the worst case performance of the radar subsystem, and acts as a lower bound on its performance. We next derive the system performance for the two above mentioned cases.

5.3 Best Case Performance

Subtracting the clutter component $\mathbf{z}_c$ from $\mathbf{z}$, and considering just one range Doppler cell for simplicity, we can write the residual signal as

$$\begin{aligned}\mathbf{y} &= \mathbf{z} - \mathbf{z}_c \\ &= \alpha_d\omega_d\mathbf{a}_{r,r}(\theta_d)\mathbf{a}_{r,t}^H(\theta_d)\mathbf{p} + \sqrt{\alpha_c}\left(\omega_1\mathbf{A}_{\mathbf{I},\mathbf{R}}(\theta_c)\mathbf{a}_{I,r}(\theta_i)\mathbf{a}_{r,t}^H(\theta_d) + \omega_2\mathbf{a}_{r,r}(\theta_d)\mathbf{a}_{I,t}(\theta_i)\mathbf{A}_{R,I}(\theta_c)\right)\mathbf{p} + \mathbf{H}_I\mathbf{s} + \mathbf{w},\end{aligned} \tag{5.7}$$

where $\mathbf{A}_{\mathbf{I},\mathbf{R}}(\theta_c) = \mathbf{a}_{r,r}(\theta_c)\mathbf{a}_{I,t}^H(\theta_c)\mathbf{Q}_P$ and $\mathbf{A}_{R,I}(\theta_c) = \mathbf{Q}_P\mathbf{a}_{I,r}(\theta_c)\mathbf{a}_{r,t}^H(\theta_c)$.

Now, given θ_c, θ_i is a deterministic function of θ_d, we can define, $\mathbf{B}_d(\theta_d) \triangleq \mathbf{a}_{r,r}(\theta_d)\mathbf{a}_{r,t}^H(\theta_d)$, $\mathbf{B}_1(\theta_d) \triangleq \mathbf{a}_{I,r}(\theta_i)\mathbf{a}_{r,t}^H(\theta_d)$ and $\mathbf{B}_2(\theta_d) \triangleq \mathbf{a}_{r,r}(\theta_d)\mathbf{a}_{I,t}^H(\theta_i)$, and write

$$\mathbf{y} = \alpha_d\omega_d\mathbf{B}_d(\theta_d)\mathbf{p} + \sqrt{\alpha_c}\left(\omega_1\mathbf{A}_{\mathbf{I},\mathbf{R}}(\theta_c)\mathbf{B}_1(\theta_d) + \omega_2\mathbf{B}_2(\theta_d)\mathbf{A}_{R,I}(\theta_c)\right)\mathbf{p} + \mathbf{H}_I\mathbf{s}(t) + \mathbf{w}(t). \tag{5.8}$$

Again, since we are interested in the radar performance only in the terms of the AoA, all parameters other than θ_d can be assumed to be known[1], and the received signal becomes

$$\mathbf{y} = \xi_d\mathbf{B}_d(\theta_d)\mathbf{p} + \xi_1\mathbf{A}_{I,R}(\theta_c)\mathbf{B}_1(\theta_d)\mathbf{p} + \xi_2\mathbf{B}_2(\theta_d)\mathbf{A}_{R,I}(\theta_c)\mathbf{p} + \mathbf{H}_I\mathbf{s} + \mathbf{w} = \boldsymbol{\zeta}(\theta_d) + \mathbf{v}. \tag{5.9}$$

[1]We note that these parameters include the path gains and the RCS; however we are evaluating the best case performance, and can assume the system to be oracle supported.

Here, the vector function $\boldsymbol{\zeta}(\theta_d)$ and the noise component $\mathbf{v}$ are defined implicitly. Now, assuming that the noise covariance matrix is given as $E[\mathbf{w}\mathbf{w}^H] = N_0\mathbf{I}_{M_r}$, and assuming $E[\mathbf{s}\mathbf{s}^H] = \mathcal{E}_s\mathbf{I}_K$, we get,

$$\begin{aligned}\boldsymbol{\Sigma}_C &\triangleq E[\mathbf{H}_I\mathbf{s}\mathbf{s}^H\mathbf{H}_I^H] \\ &= \mathcal{E}_s\left(\sum_{i=1}^{C_I}\gamma_{I,i}\mathbf{I}_{M_r} + \left(\sum_{i=1}^{C_2}\gamma_{2,i}\right)\left(\mathbf{b}_r(\theta_c)\mathbf{a}_I^H(\pi-\theta_c-\theta_d)\times\mathbf{Q}_P\mathbf{Q}_P^H\mathbf{a}_I(\pi-\theta_c-\theta_d)\,\mathbf{b}_r^H(\theta_c)\right)\right),\end{aligned} \tag{5.10}$$

we can write the overall noise and interference covariance matrix seen by the radar as $\boldsymbol{\Sigma}_v = N_0\mathbf{I}_{M_r} + \boldsymbol{\Sigma}_C$. Consequently, we can write the pdf of $\mathbf{y}$ as

$$f(\mathbf{y};\theta_d) = \frac{1}{|\pi\boldsymbol{\Sigma}_v|}\exp\left(-(\mathbf{y}-\boldsymbol{\zeta}(\theta_d))^H\boldsymbol{\Sigma}_v^{-1}(\mathbf{y}-\boldsymbol{\zeta}(\theta_d))\right), \tag{5.11}$$

and hence,

$$\ell(\mathbf{y};\theta_d) = -\log(\det(\pi\boldsymbol{\Sigma}_v)) - (\mathbf{y}-\boldsymbol{\zeta}(\theta_d))^H\boldsymbol{\Sigma}_v^{-1}(\mathbf{y}-\boldsymbol{\zeta}(\theta_d)). \tag{5.12}$$

Let $\dot{\boldsymbol{\zeta}}(\theta_d)$ represent the derivative of $\boldsymbol{\zeta}(\theta_d)$ with respect to θ_d, the consequent fisher information can be expressed as

$$\mathcal{I}(\theta_d) = E_{\mathbf{y}}\left[\dot{\boldsymbol{\zeta}}^H(\theta_d)\boldsymbol{\Sigma}_v^{-1}(\mathbf{y}-\boldsymbol{\zeta}(\theta_d))(\mathbf{y}-\boldsymbol{\zeta}(\theta_d))^H\boldsymbol{\Sigma}_v^{-1}\dot{\boldsymbol{\zeta}}^H(\theta_d)\right]. \tag{5.13}$$

Since $\boldsymbol{\zeta}$ is a deterministic function of θ_d, it is easy to argue that the CRB on the variance of an estimate of θ_d, for a given range-Doppler cell within all the clutter parameters known, is given as

$$\sigma_e^2 = \frac{1}{\mathcal{I}(\theta_d)} = \frac{1}{\dot{\boldsymbol{\zeta}}^H(\theta_d)\boldsymbol{\Sigma}_v^{-1}\dot{\boldsymbol{\zeta}}(\theta_d)}. \tag{5.14}$$

As stated earlier, this is the best case CRB and acts as an upper bound on the radar performance. We next discuss the lower bound on the radar subsystem performance in terms of the MCRB on the AoA.

5.4 The Worst Case Performance

We now consider the case when the clutter parameters are not known at the radar. In this case, the radar receiver ignores the existence of the IRS, and the consequent multipath, mak-

ing the model misspecified and the clutter parameters can not be directly subtracted from $\mathbf{z}(t)$. Therefore, in this case we will derive the misspecified CRB (MCRB) on the AoA, as discussed in [73].

We can write the misspecified received signal $\mathbf{x}$ as

$$\mathbf{x} = \xi_d \mathbf{B}_d(\theta_d)\mathbf{p} + \mathbf{H}_I\mathbf{s} + \mathbf{w} = \boldsymbol{\psi}(\theta_d)\mathbf{p} + \mathbf{v}, \tag{5.15}$$

and can rewrite $\mathbf{z}$ as,

$$\mathbf{z} = \boldsymbol{\psi}(\theta_d)\mathbf{p} + \boldsymbol{\mu}(\theta_c, \theta_d)\mathbf{p} + \mathbf{v}, \tag{5.16}$$

with $\boldsymbol{\mu}(\theta_c, \theta_d) = \alpha_c \mathbf{a}_{r,r}(\theta_c)\mathbf{a}_{I,t}^H(\theta_c)\mathbf{Q}_P\mathbf{a}_{I,r}(\theta_c)\mathbf{a}_{r,t}^H(\theta_c) + \xi_1\mathbf{A}_{I,R}(\theta_c)\mathbf{B}_1(\theta_d) + \xi_2\mathbf{B}_2(\theta_d)\mathbf{A}_{R,I}(\theta_c)$.
Naturally,

$$f(\mathbf{x};\theta_d) = \frac{1}{|\pi\boldsymbol{\Sigma}_v|}\exp\left(-(\mathbf{x}-\boldsymbol{\psi}(\theta_d)\mathbf{p})^H\boldsymbol{\Sigma}_v^{-1}(\mathbf{x}-\boldsymbol{\psi}(\theta_d)\mathbf{p})\right), \tag{5.17}$$

and consequently, the misspecified Fisher information is given as $\mathcal{I}_m(\theta_d) = \sigma_p^2\left(\dot{\boldsymbol{\psi}}^H(\theta_d)\boldsymbol{\Sigma}_v^{-1}\dot{\boldsymbol{\psi}}(\theta_d)\right)$. Now, analogous to the notation defined in [73], we can define the signal to multipath ratio as $\eta = \frac{\|\boldsymbol{\psi}(\theta_d)\mathbf{p}\|^2}{\|\boldsymbol{\mu}(\theta_c,\theta_d)\mathbf{p}\|^2}$, and denote the phase difference between the first elements of $\boldsymbol{\psi}(\theta_d)$ and $\boldsymbol{\mu}(\theta_c,\theta_d)$ as Δ. Based on this, we can write the MCRB in the absence of the knowledge of any clutter parameters at the radar receiver as

$$\sigma_m^2 = M_{\theta_d} + B_{\theta_d}, \tag{5.18}$$

such that

$$M_{\theta_d} = \frac{1}{\mathcal{I}_m(\theta_d)}\frac{E_{\dot{\mathbf{B}}_d}\left(\left|\mathrm{tr}\left(\dot{\mathbf{B}}_d^H(\theta_d)\boldsymbol{\mu}(\theta_c,\theta_d)\right)\right|^2 + \eta E_{\dot{\mathbf{B}}_d}\right)}{\left(\mathrm{Re}\left\{\mathrm{tr}\left(\ddot{\mathbf{B}}_d^H(\theta_d)\boldsymbol{\mu}(\theta_c,\theta_d)\right)e^{-j\Delta}\right\} - \sqrt{\eta}E_{\dot{\mathbf{B}}_d}\right)^2}, \tag{5.19}$$

where

$$E_{\dot{\mathbf{B}}_d} = \mathrm{tr}\left(\dot{\mathbf{B}}_d(\theta_d)\dot{\mathbf{B}}_d^H(\theta_d)\right), \tag{5.20}$$

($\dot{\mathbf{B}}_d(\theta_d)$ and $\ddot{\mathbf{B}}_d^H(\theta_d)$ respectively represent the first and second derivatives of $\mathbf{B}_d^H(\theta_d)$ w.r.t θ_d, and

$$B_{\theta_d} = \theta_d - \theta_d^{'}, \tag{5.21}$$

with $\theta_d^{'}$ being chosen such that it maximizes the inner product between $\mathbf{z}_d$ and $\mathbf{z}_c + \mathbf{z}_1 + \mathbf{z}_2$ as

$$\theta_d^{'} = \arg\max_{\theta_a} \left\{ \left| \text{tr}\left(\mathbf{B}_d^H(\theta_a)\mathbf{B}_d(\theta_d)\right) + \frac{1}{1+\sqrt{\eta}}\text{tr}\left(\mathbf{B}_d^H(\theta_a)\boldsymbol{\mu}(\theta_c,\theta_d)\right) \right|^2 \right\}. \tag{5.22}$$

We have considered the case $\theta_d = \theta_d'$, similar to the method discussed in [73].

5.5 Communications Rate Analysis

We can write the effective communication channel between the BS and UE as,

$$\mathbf{H}_B = \mathbf{H}_0 + \mathbf{H}_2\mathbf{Q}\mathbf{H}_1, \tag{5.23}$$

with $\mathbf{H}_0 = \sum_{l=1}^{C_0} \alpha_{0,l}\mathbf{a}_{b,r}(\theta_{b,l})\mathbf{a}_{u,t}^H(\theta_{u,l})$, and $\mathbf{H}_2 = \sum_{i=1}^{C_2} \alpha_{2,l}\mathbf{a}_{I,r}(\theta_{u,l})\mathbf{a}_{u,t}^H(\theta_{u,l})$, such that $\alpha_{x,l}$ is the ZMCSCG distributed path gain for the ith path between the BS and the UE ($x = 0$)/ IRS ($x = 2$) whose variance is a function of the inverse square of the distance between the BS and the UE/IRS, $\theta_{b,l}$ is the angle of arrival at the BS, and $\phi_{x,l}$ is the angle of departure from the UE/IRS. Similarly the interference channel between the radar transmitter and the BS is given as

$$\mathbf{H}_J = \mathbf{H}_x + \mathbf{H}_2\mathbf{Q}_P\mathbf{a}_{I,r}(\theta_c)\mathbf{a}_{r,t}^H(\theta_c), \tag{5.24}$$

with the direct path channel $\mathbf{H}_x = \sum_{l=1}^{C_x} \alpha_{x,l}\mathbf{a}_{b,r}(\theta_{b,l})\mathbf{a}_{r,t}^H(\theta_{r,l})$, such that $\alpha_{x,l}$ is the ZMCSCG distributed path gain for the ith path between the radar and the BS whose variance is a function of the inverse square of the distance between the BS and the radar, $\theta_{b,l}$ is the angle of arrival at the BS, and $\theta_{r,l}$ is the angle of departure from the radar. Based on these, the signal received by the BS becomes

$$\mathbf{r} = \mathbf{H}_B\mathbf{s} + \mathbf{H}_J\mathbf{p} + \mathbf{w}_B \tag{5.25}$$

with $\mathbf{w}_B(t)$ being the ZMCSCG distributed noise vector having a covariance matrix $N_0\mathbf{I}_{M_a}$. Treating the radar generated interference as noise [76] and defining $\sigma_x^2 = N_0 + \text{Tr}\{E\left[\mathbf{H}_J\mathbf{p}\mathbf{p}^H\mathbf{H}_J^H\right]\}$, we can lower bound the rate achievable by the communications subsystem as

$$R(\mathbf{H}_B) = \log\det\left(\mathbf{I}_{M_a} + \frac{\mathcal{E}_s}{\sigma_x^2}\mathbf{H}_B\mathbf{H}_B^H\right). \tag{5.26}$$

5.6 Performance Evaluation

In this section, we evaluate the performance of the system under consideration via detailed Monte-Carlo simulations. We assume that the coexistence based system is located within a circular region with a radius of $r_0 = 50\,m$, with the BS positioned at its centre. We assume the IRS, the communications user, the radar, and the target to be placed randomly (according to a uniform distribution) within the operating region, and operating at a carrier frequency of 30 GHz. We consider $M_t = M_r = 12$, radar transmit/ receive antennas $P = 64$ IRS elements, $M_a = 8$ BS antenna elements and $N_U = 1$ indicating a single antenna user. All the performance metrics provided in this section are obtained by averaging across $50,000$ realizations of the system. The IRS phase matrix has been calculated according to the algorithm discussed [77].

In Fig. 5.2, we plot the best case and worst case radar CRBs as a function of the radar received SNR for different uplink communication transmit powers (σ_p^2). As expected, the CRB decreases with the increase in the radar receive SNR while it increases with the increase of σ_p^2, showing a linear trend in the logarithmic scale. We also observe a negligible difference in the best case CRB and MCRB due to a very weak IRS reflected signal towards the radar receiver. We have found the signal to multi-path ratio to be of the order of 10^5 in our simulations.

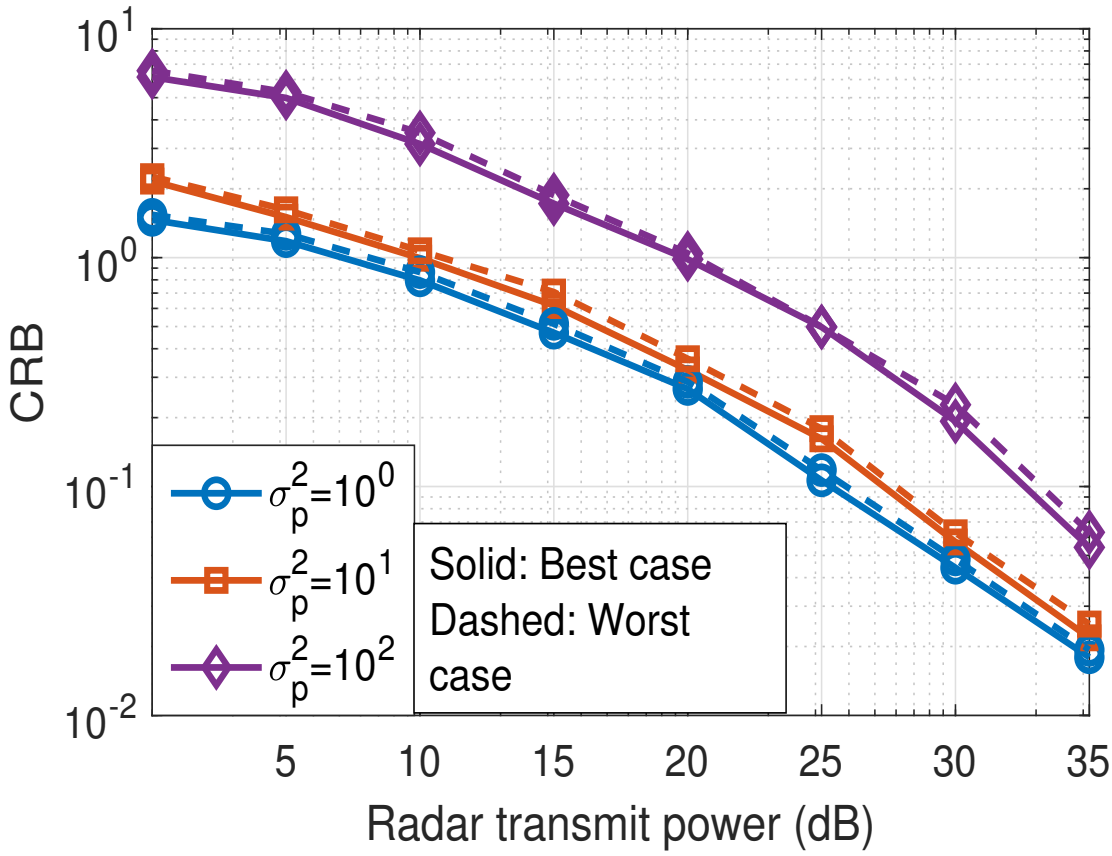

Fig. 5.2: Best case and worst case CRB as a function of the radar transmit power for different values of communication system transmit power.

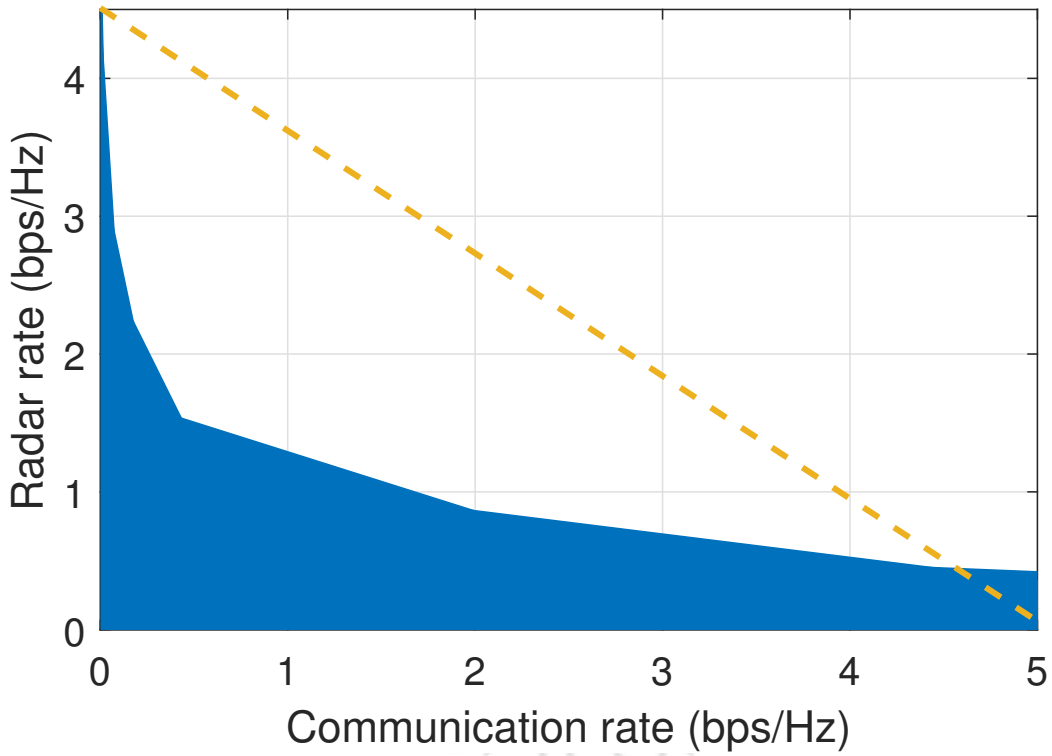

Fig. 5.3: Rate region for the proposed co-existence based ICS system without IRS.

In Figs. 5.3 and 5.4 we use the notion of radar rate as in [78] to evaluate the rate region for the proposed coexistence based ICS system without and with an IRS respectively. In Fig 5.3, we observe the rate region without the presence of an IRS to be significantly concave, indicating the in-feasibility of coexistence of the two sub-systems. On the other hand, Fig. 5.4 shows that the this rate region is highly convex in the presence of an IRS, signifying the ability of the two subsystems to co-exist. This behavior can be attributed to the fact that the presence of an IRS reduces the amount of transmit signal power that is needed to achieve a given rate for the communications subsystem, leading to reduced interference for the radar subsystem. We can therefore conclude that the presence of a communications IRS, not only enhances the performance of a communications system, but also allows for radar-communications coexistence.

5.7 Chapter Conclusions

In this chapter, we have considered an ICS system operating in the co-existence mode, and comprising an IRS based communications subsystem and a MIMO radar by modelling the mutual interference caused by the operation of the two subsystems. We have argued that the existence of the IRS can either help or hinder the radar subsystem performance based on the availability of various parameters. Through extensive simulations, we have shown that the average multi-path caused by the presence of an IRS is much weaker as compared to the direct path, and hence the effect of the IRS on the radar system performance can be ignored. This reinforces the conclusion that while the presence of an IRS significantly improves the communication subsystem performance, leading to lower transmit powers for the communications subsystem, it barely affects the performance of the radar subsystem, thereby enabling co-existence based ICS. Future work may include the analysis of dependence of the CSI quality at the IRS controller on the achievable rate regions.

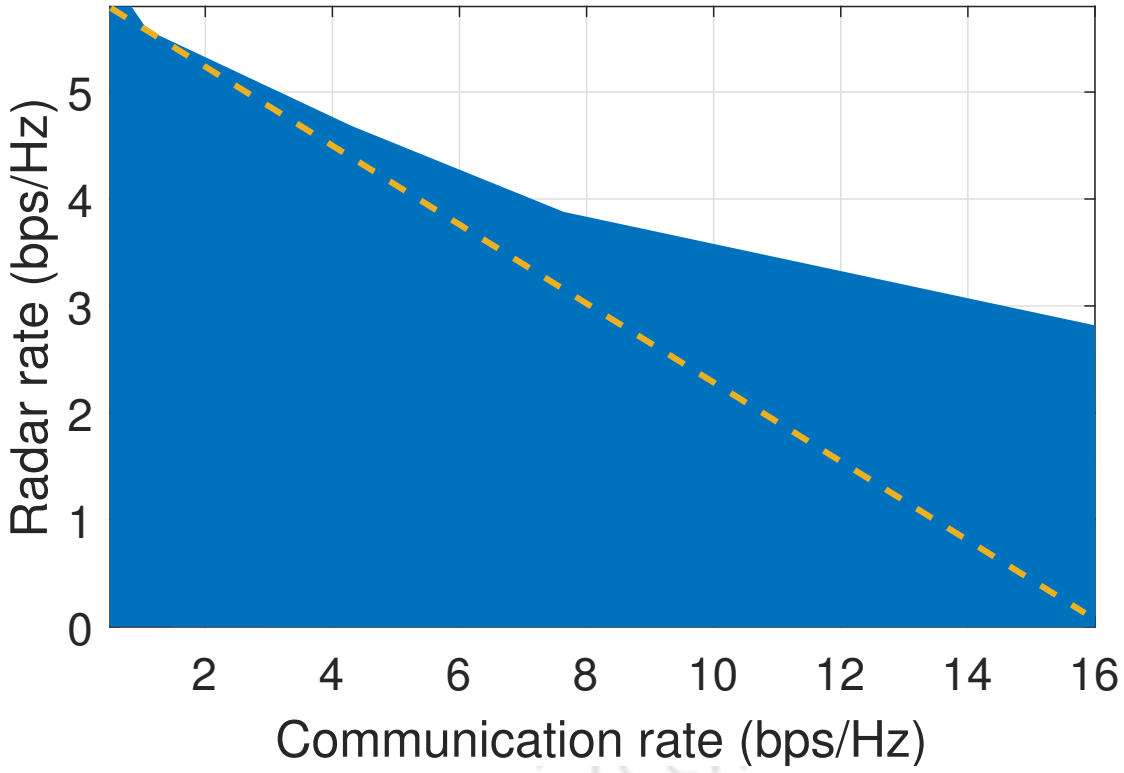

Fig. 5.4: Rate region for the proposed co-existence based ICS system.

6

Conclusions and Future Work

Contents

This thesis considered the study and analysis of co-existence based ICS systems. The following sections list the conclusions drawn in this thesis and, some open problems in this area from the perspective of future research.

6.1 Conclusions

In the second chapter, we modelled a mMIMO communication system in coexistence with a mono-static MIMO radar. We utilized the NSP based technique proposed in [20] to project the communication waveform onto the null space of the interference channel. We utilized DE analysis to derive the detailed expressions of uplink and downlink achievable rates for the communication sub-system. Through extensive numerical simulations, we observed that the use of MMSE combining along with a large number of antenna elements at the BS effectively mitigates the radar generated interference in the uplink. We also observed that the obtained rate regions in the uplink and the downlink communication sub-frames are convex enough to ensure that mMIMO communication systems can coexist with MIMO radars without an extensive redesign.

In the third chapter, we modelled an ICS consisting of a multi static tracking radar and a CF-mMIMO communication system. Here, the radar and communication sub-systems simultaneously operated over the same spectrum. Assuming that the radar sensors, APs and UEs have distributed uniformly across a circular cell of radius 500 m, we evaluated the ICS system performance for uplink communication subframe. The radar receiver performed two stage EKF based target tracking. In the first stage, radar sensors estimated the target state and forwarded it to the FC. During the second stage, using these forwarded target states the FC further estimated the final target state. In the communication system, first the APs performed the uplink channel estimation using the uplink pilot transmission and used these estimated channels to obtain the expression for instantaneous per user achievable rate in the uplink communication frame. Via Monte Carlo simulations, we observed that increase in the number of radar sensors improved the radar system performance. We also observed that the communication system performance gets minimally affected by the increase in the radar transmit power. In Chapter 4, we extended

the work of Chapter 3 to a stochastic geometry setup. Here, we have evaluated the performance of ICS system in terms of the coverage probability for the communication subsystem and the estimation MSE for the radar subsystem in both the uplink and the downlink communication subframes using tools from stochastic geometry.

In the fifth chapter, we modelled a mono-static MIMO radar in co-existence with an IRS aided single user communication system in an ICS system. Here, both the radar and communication sub-systems operated in the mmWave spectrum. We obtained the performance of the radar sub-system in two cases: in the first case, we assumed that the exact IRS clutter parameters are available at the radar receiver, to give an upper bound on the radar system performance and second when they are not available at the radar receiver. We derived performance metrics for both the subsystems. For the radar subsystem, we obtained the CRB on the AoA estimate at the radar receiver for both the best and worst case performance. For communication subsystem, we derived the per user uplink rate in the presence of radar generated interference. Via simulations, we have observed that the difference between the best case and worst case CRB is negligible. Thus, the presence of IRS has improved the performance of communication subsystem while minimally impacting the performance of the radar subsystem.

6.2 Directions for Future Work

In this thesis, we analysed the coexistence of mMIMO and cell free mMIMO communication systems with MIMO radar in a single carrier wireless transmission system. It can be extended to a broadband, multi carrier wireless transmission system to further improve the spectral efficiencies. Power controlled transmission is another potential direction for the future work for efficient spectrum usage in an underlay spectrum sharing scenario.

mMIMO radar technology is capable of fulfilling the increased requirements of complex functionalities like multiple target detection. Because of large diversity and spatial resolution, they can detect much smaller size objects (like unmanned aerial vehicles) in comparison to conventional radars [79]. Therefore, it may be interesting to analyse the coexistence of mMIMO radar and communication system.

A

Appendix

A.1 Proof of Theorem 1

Treating interference as noise [80], we can write the SINR of the received signal as the ratio of the mean squared value of the desired component to the sum of the mean squared values of all other components. In this context, we can write,

$$\zeta_{s,k} = \beta_k \epsilon_{u,k} E\{|\hat{\mathbf{h}}_k^H \mathbf{R}^{-1}_{yy|\hat{\mathbf{G}}_{rb},\hat{\mathbf{H}}} \hat{\mathbf{h}}_k|^2\} \tag{A.1}$$

Now,

$$\hat{\mathbf{h}}_k^H \mathbf{R}^{-1}_{yy|\hat{\mathbf{G}}_{rb},\hat{\mathbf{H}}} \hat{\mathbf{h}}_k = \frac{\hat{\mathbf{h}}_k^H \mathbf{R}^{-1}_{yy|\hat{\mathbf{G}}_{rb},\hat{\mathbf{H}}_k} \hat{\mathbf{h}}_k}{1 + \hat{\mathbf{h}}_k^H \mathbf{R}^{-1}_{yy|\hat{\mathbf{G}}_{rb},\hat{\mathbf{H}}_k} \hat{\mathbf{h}}_k} \tag{A.2}$$

where $\hat{\mathbf{H}}_k \in C^{M_a \times (K-1)}$ contains all columns of $\hat{\mathbf{H}}$ except $\hat{\mathbf{h}}_k$. Thus, $\mathbf{R}_{yy|\hat{\mathbf{G}}_{rb},\hat{\mathbf{H}}_k}$ can be expressed as

$$\mathbf{R}_{yy|\hat{\mathbf{G}}_{rb},\hat{\mathbf{H}}_k} = \sum_{\substack{m=1,\\ m\neq k}}^{K} \beta_m \epsilon_{u,m} \hat{\mathbf{h}}_m \hat{\mathbf{h}}_m^H + \sigma_r^2 \hat{\mathbf{G}}_{rb} \hat{\mathbf{G}}_{rb}^H + \sum_{m=1}^{K} \beta_m \epsilon_{u,m} \bar{\mathbf{B}}_m^2 + \left(\sigma_r^2 \eta_e + N_0\right) \mathbf{I}_{M_a}. \tag{A.3}$$

Now, since $\hat{\mathbf{h}}_k$ and $\mathbf{R}^{-1}_{yy|\hat{\mathbf{G}}_{rb},\hat{\mathbf{H}}_k}$ are independent,

$$\hat{\mathbf{h}}_k^H \mathbf{R}^{-1}_{yy|\hat{\mathbf{G}}_{rb},\hat{\mathbf{H}}_k} \hat{\mathbf{h}}_k \xrightarrow[M\to\infty]{a.s.} \mathrm{Tr}\{\mathbf{R}^{-1}_{yy|\hat{\mathbf{G}}_{rb},\hat{\mathbf{H}}_k} \mathbf{B}_k\}. \tag{A.4}$$

Letting $\rho = \sigma_r^2\eta_e + N_0$, $\mathbf{S} = \sum_{m=1}^{K}\beta_m\epsilon_{u,m}\bar{\mathbf{B}}_m^2$ and $\mathbf{D}_k$ be a diagonal matrix, such that its mth diagonal element $d_{k,m}$ is given by $d_{k,m} = \beta_m\epsilon_{u,m}$ where $m \in \{1, 2, \ldots, k-1, k+1, \ldots, K\}$. We can now write,

$$\mathbf{R}_{yy|\hat{\mathbf{G}}_{rb},\hat{\mathbf{H}}_k} = \hat{\mathbf{H}}_k\mathbf{D}_{k,\beta\epsilon_{u,s}}\hat{\mathbf{H}}_k^H + \sigma_r^2\hat{\mathbf{G}}_{rb}\hat{\mathbf{G}}_{rb}^H + \mathbf{S} + \rho\mathbf{I}_{M_a}. \tag{A.5}$$

Since $\mathbf{S} \in C^{M\times M}$ is a non negative definite matrix, $\hat{\mathbf{H}}_k \in C^{M\times(K-1)}$ is a random matrix and $\rho > 0$, [48],

$$\mathrm{Tr}\{\mathbf{R}^{-1}_{yy|\hat{\mathbf{G}}_{rb},\hat{\mathbf{H}}_k}\mathbf{B}_k\} \xrightarrow[M\to\infty]{a.s.} \mu_k. \tag{A.6}$$

Back substituting the expression for $\zeta_{s,k}$ results in (2.21). Now,

$$\zeta_{I,k} = \left(\sum_{\substack{l=1,\\ l\neq k}}^{K}\beta_l\epsilon_{u,l}E\{|\hat{\mathbf{h}}_k^H\mathbf{R}^{-1}_{yy|\hat{\mathbf{G}}_{rb},\hat{\mathbf{H}}}\hat{\mathbf{h}}_l|^2\}\right) \tag{A.7}$$

$$|\hat{\mathbf{h}}_k^H\mathbf{R}^{-1}_{yy|\hat{\mathbf{G}}_{rb},\hat{\mathbf{H}}}\hat{\mathbf{h}}_l|^2 = \frac{|\hat{\mathbf{h}}_k^H\mathbf{R}^{-1}_{yy|\hat{\mathbf{G}}_{rb},\hat{\mathbf{H}}_k}\hat{\mathbf{h}}_l|^2}{|1+\hat{\mathbf{h}}_k^H\mathbf{R}^{-1}_{yy|\hat{\mathbf{G}}_{rb},\hat{\mathbf{H}}_k}\hat{\mathbf{h}}_k|^2}, \tag{A.8}$$

and,

$$|\hat{\mathbf{h}}_k^H\mathbf{R}^{-1}_{yy|\hat{\mathbf{G}}_{rb},\hat{\mathbf{H}}_k}\hat{\mathbf{h}}_l|^2 = \left|\hat{\mathbf{h}}_k^H\mathbf{R}^{-1}_{yy|\hat{\mathbf{G}}_{rb},\hat{\mathbf{H}}_{k,l}}\hat{\mathbf{h}}_l - \frac{\hat{\mathbf{h}}_k^H\mathbf{R}^{-1}_{yy|\hat{\mathbf{G}}_{rb},\hat{\mathbf{H}}_{k,l}}\hat{\mathbf{h}}_l\hat{\mathbf{h}}_l^H\mathbf{R}^{-1}_{yy|\hat{\mathbf{G}}_{rb},\hat{\mathbf{H}}_{k,l}}\hat{\mathbf{h}}_k}{1+\hat{\mathbf{h}}_l^H\mathbf{R}^{-1}_{yy|\hat{\mathbf{G}}_{rb},\hat{\mathbf{H}}_{k,l}}\hat{\mathbf{h}}_l}\right|^2, \tag{A.9}$$

where $\hat{\mathbf{H}}_{k,l} \in C^{M\times(K-2)}$ contains all columns of $\hat{\mathbf{H}}$ except $\hat{\mathbf{h}}_k$ and $\hat{\mathbf{h}}_l$. But,

$$\mathbf{R}_{yy|\hat{\mathbf{G}}_{rb},\hat{\mathbf{H}}_{k,l}} = \hat{\mathbf{H}}_{k,l}\mathbf{D}_{k,l,\beta\epsilon_{u,s}}\hat{\mathbf{H}}_{k,l}^H + \sigma_r^2\hat{\mathbf{G}}_{rb}\hat{\mathbf{G}}_{rb}^H + \mathbf{S} + \rho\mathbf{I}_{M_a}, \tag{A.10}$$

where $\mathbf{D}_{k,l,\beta\epsilon_{u,m}}$ is a diagonal matrix of order $(K-2)$ having the mth diagonal entry as $\beta_m\epsilon_{u,m}$, $m \neq \{k, l\}$. Since, $\hat{\mathbf{h}}_k^H$, $\mathbf{R}^{-1}_{yy|\hat{\mathbf{G}}_{rb},\hat{\mathbf{H}}_{k,l}}$ and $\hat{\mathbf{h}}_l$ are independent, we have

$$|\hat{\mathbf{h}}_k^H\mathbf{R}^{-1}_{yy|\hat{\mathbf{G}}_{rb},\hat{\mathbf{H}}_{k,l}}\hat{\mathbf{h}}_l|^2 \xrightarrow[M\to\infty]{a.s.} \mathrm{Tr}\{\mathbf{R}^{-1}_{yy|\hat{\mathbf{G}}_{rb},\hat{\mathbf{H}}_{k,l}}\mathbf{B}_k\mathbf{R}^{-1}_{yy|\hat{\mathbf{G}}_{rb},\hat{\mathbf{H}}_{k,l}}\mathbf{B}_l\}. \tag{A.11}$$

Now,

$$\mathrm{Tr}\{\mathbf{R}^{-1}_{yy|\hat{\mathbf{G}}_{rb},\hat{\mathbf{H}}_{k,l}}\mathbf{B}_k\mathbf{R}^{-1}_{yy|\hat{\mathbf{G}}_{rb},\hat{\mathbf{H}}_{k,l}}\mathbf{B}_l\} \xrightarrow[M\to\infty]{a.s.} \mathrm{Tr}\{\mathbf{B}_l\mathbf{T}'_{k,l}(\rho)\}, \tag{A.12}$$

$$\hat{\mathbf{h}}_l^H\mathbf{R}^{-1}_{yy|\hat{\mathbf{G}}_{rb},\hat{\mathbf{H}}_{k,l}}\hat{\mathbf{h}}_l \xrightarrow[M\to\infty]{a.s.} \mathrm{Tr}\{\mathbf{R}^{-1}_{yy|\hat{\mathbf{G}}_{rb},\hat{\mathbf{H}}_{k,l}}\mathbf{B}_l\}, \tag{A.13}$$

$$\mathrm{Tr}\{\mathbf{R}^{-1}_{yy|\hat{\mathbf{G}}_{rb},\hat{\mathbf{H}}_{k,l}}\mathbf{B}_l\} \xrightarrow[M\to\infty]{a.s.} \mathrm{Tr}\{\mathbf{T}_{k,l}(\rho)\mathbf{B}_l\}. \tag{A.14}$$

Hence,

$$\hat{\mathbf{h}}_l^H \mathbf{R}^{-1}_{yy|\hat{\mathbf{G}}_{rb},\hat{\mathbf{H}}_{k,l}} \hat{\mathbf{h}}_l \xrightarrow[M\to\infty]{a.s.} \mu_{k,l}, \tag{A.15}$$

we can hence write,

$$|\hat{\mathbf{h}}_k^H \mathbf{R}^{-1}_{yy|\hat{\mathbf{G}}_{rb},\hat{\mathbf{H}}} \hat{\mathbf{h}}_l|^2 = \frac{1}{|1+\mu_k|^2}\left(\mu_{k,l}^{'} + \frac{(\mu_{k,l}^{'})^2}{|1+\mu_{k,l}|^2} - 2\Re\left\{\frac{(\mu_{k,l}^{'})^{3/2}}{1+\mu_{k,l}}\right\}\right), \tag{A.16}$$

back substituting the expressions in (A.7) to obtain (2.24).

$$\zeta_{E,k} = \sum_{l=1}^{K} \beta_l \epsilon_{u,l} E\{|\hat{\mathbf{h}}_k^H \mathbf{R}^{-1}_{yy|\hat{\mathbf{G}}_{rb},\hat{\mathbf{H}}} \tilde{\mathbf{h}}_l x_l[n]|^2\}, \tag{A.17}$$

where,

$$|\hat{\mathbf{h}}_k^H \mathbf{R}^{-1}_{yy|\hat{\mathbf{G}}_{rb},\hat{\mathbf{H}}} \tilde{\mathbf{h}}_l|^2 = \left|\frac{\hat{\mathbf{h}}_k^H \mathbf{R}^{-1}_{yy|\hat{\mathbf{G}}_{rb},\hat{\mathbf{H}}_k} \tilde{\mathbf{h}}_l}{1+\hat{\mathbf{h}}_k^H \mathbf{R}^{-1}_{yy|\hat{\mathbf{G}}_{rb},\hat{\mathbf{H}}_k} \hat{\mathbf{h}}_k}\right|^2, \tag{A.18}$$

$$|\hat{\mathbf{h}}_k^H \mathbf{R}^{-1}_{yy|\hat{\mathbf{G}}_{rb},\hat{\mathbf{H}}_k} \tilde{\mathbf{h}}_l|^2 \xrightarrow[M\to\infty]{a.s.} \mathrm{Tr}\{\mathbf{R}^{-1}_{yy|\hat{\mathbf{G}}_{rb},\hat{\mathbf{H}},k} \mathbf{B}_k \mathbf{R}^{-1}_{yy|\hat{\mathbf{G}}_{rb},\hat{\mathbf{H}},k} \bar{\mathbf{B}}_l^2\}, \tag{A.19}$$

$$\mathrm{Tr}\{\mathbf{R}^{-1}_{yy|\hat{\mathbf{G}}_{rb},\hat{\mathbf{H}},k} \mathbf{B}_k \mathbf{R}^{-1}_{yy|\hat{\mathbf{G}}_{rb},\hat{\mathbf{H}},k} \bar{\mathbf{B}}_l^2\} \xrightarrow[M\to\infty]{a.s.} \mathrm{Tr}\{\mathbf{T}_k^{'}(\rho)\bar{\mathbf{B}}_l^2\}, \tag{A.20}$$

we can use these values to obtain (2.28).

$$\zeta_{RC,k} = \sum_{i=1}^{M_t} \sigma_r^2 |\hat{\mathbf{h}}_k^H \mathbf{R}^{-1}_{yy|\hat{\mathbf{G}}_{rb},\hat{\mathbf{H}}} \hat{\mathbf{g}}_{rb,i}|^2, \tag{A.21}$$

where

$$\hat{\mathbf{h}}_k^H \mathbf{R}^{-1}_{yy|\hat{\mathbf{G}}_{rb},\hat{\mathbf{H}}} \hat{\mathbf{g}}_{rb,i} = \frac{\hat{\mathbf{h}}_k^H \mathbf{R}^{-1}_{yy|\hat{\mathbf{G}}_{rb},\hat{\mathbf{H}}_k} \hat{\mathbf{g}}_{rb,i}}{1+\hat{\mathbf{h}}_k^H \mathbf{R}^{-1}_{yy|\hat{\mathbf{G}}_{rb},\hat{\mathbf{H}}_k} \hat{\mathbf{h}}_k}, \tag{A.22}$$

and,

$$|\hat{\mathbf{h}}_k^H \mathbf{R}^{-1}_{yy|\hat{\mathbf{G}}_{rb},\hat{\mathbf{H}}_k} \hat{\mathbf{g}}_{rb,i}|^2 = \left|\hat{\mathbf{h}}_k^H \mathbf{R}^{-1}_{yy|\hat{\mathbf{G}}_{rb,i},\hat{\mathbf{H}}_k} \hat{\mathbf{g}}_{rb,i} - \frac{\hat{\mathbf{h}}_k^H \mathbf{R}^{-1}_{yy|\hat{\mathbf{G}}_{rb,i},\hat{\mathbf{H}}_k} \hat{\mathbf{g}}_{rb,i} \hat{\mathbf{g}}_{rb,i}^H \mathbf{R}^{-1}_{yy|\hat{\mathbf{G}}_{rb,i},\hat{\mathbf{H}}_k} \hat{\mathbf{h}}_k}{1+\hat{\mathbf{g}}_{rb,i}^H \mathbf{R}^{-1}_{yy|\hat{\mathbf{G}}_{rb,i},\hat{\mathbf{H}}_k} \hat{\mathbf{g}}_{rb,i}}\right|^2, \tag{A.23}$$

$$\mathbf{R}_{yy|\hat{\mathbf{G}}_{rb,i},\hat{\mathbf{H}}_k} = \hat{\mathbf{H}}_k \mathbf{D}_{k,\beta\epsilon_{u,m}} \hat{\mathbf{H}}_k^H + \sigma_r^2 \hat{\mathbf{G}}_{rb,i} \hat{\mathbf{G}}_{rb,i}^H + \mathbf{S} + \rho \mathbf{I}_{M_a}, \tag{A.24}$$

where $\hat{\mathbf{G}}_{rb,i}$ contains all the columns of $\hat{\mathbf{G}}_{rb}$ except $\hat{\mathbf{g}}_i$. Since, $\hat{\mathbf{h}}_k^H$, $\mathbf{R}^{-1}_{yy|\hat{\mathbf{G}}_{rb,i}\hat{\mathbf{H}}_k}$ and $\hat{\mathbf{g}}_{rb,i}$ are independent, we have

$$|\hat{\mathbf{h}}_k^H \mathbf{R}^{-1}_{yy|\hat{\mathbf{G}}_{rb,i}\hat{\mathbf{H}}_k} \hat{\mathbf{g}}_{rb,i}|^2 \xrightarrow[M\to\infty]{a.s.} \mathrm{Tr}\{\mathbf{R}^{-1}_{yy|\hat{\mathbf{G}}_{rb,i}\hat{\mathbf{H}}_k} \mathbf{B}_k \times \mathbf{R}^{-1}_{yy|\hat{\mathbf{G}}_{rb,i}\hat{\mathbf{H}}_k} (\eta_I - \eta_e)\mathbf{I}_{M_a}\}, \tag{A.25}$$

$$\mathrm{Tr}\{\mathbf{R}^{-1}_{yy|\hat{\mathbf{G}}_{rb,i}\hat{\mathbf{H}}_k}\mathbf{B}_k\mathbf{R}^{-1}_{yy|\hat{\mathbf{G}}_{rb,i}\hat{\mathbf{H}}_k}(\eta_I-\eta_e)\mathbf{I}_{M_a}\}\xrightarrow[M\to\infty]{a.s.}\mathrm{Tr}\{\mathbf{T}'_{k,i}(\rho)(\eta_I-\eta_e)\mathbf{I}_{M_a}\},\tag{A.26}$$

$$\hat{\mathbf{g}}^H_{rb,i}\mathbf{R}^{-1}_{yy|\hat{\mathbf{G}}_{rb,i},\hat{\mathbf{H}}_k}\hat{\mathbf{g}}_{rb,i}\xrightarrow[M\to\infty]{a.s.}\mathrm{Tr}\{\mathbf{R}^{-1}_{yy|\hat{\mathbf{G}}_{rb,i},\hat{\mathbf{H}}_k}(\eta_I-\eta_e)\mathbf{I}_{M_a}\},\tag{A.27}$$

$$\mathrm{Tr}\{\mathbf{R}^{-1}_{yy|\hat{\mathbf{G}}_{rb,i},\hat{\mathbf{H}}_k}(\eta_I-\eta_e)\mathbf{I}_{M_a}\}\xrightarrow[M\to\infty]{a.s.}\mathrm{Tr}\{\mathbf{T}_{k,i}(\rho)(\eta_I-\eta_e)\mathbf{I}_{M_a}\},\tag{A.28}$$

$$|\hat{\mathbf{h}}^H_k\mathbf{R}^{-1}_{yy|\hat{\mathbf{G}}_{rb},\hat{\mathbf{H}}_k}\hat{\mathbf{g}}_{rb,i}|^2=\mu'_{k,i}+\frac{(b_k^2\mu'_{k,i})^2}{|1+\mu_{k,i}|^2}-2\Re\left\{\frac{(b_k^2\mu'_{k,i})^{3/2}}{1+\mu_{k,i}}\right\},\tag{A.29}$$

we can use these values to obtain (2.30). Finally,

$$\zeta_{RE,k}=\sum_{i=1}^{M_t}E\left[|\hat{\mathbf{h}}^H_k\mathbf{R}^{-1}_{yy|\hat{\mathbf{G}}_{rb},\hat{\mathbf{H}}}\tilde{\mathbf{g}}_{rb,i}s_i[n]|^2\right],\tag{A.30}$$

and

$$\zeta_{w,k}=N_0E\left\{|\hat{\mathbf{h}}^H_k\mathbf{R}^{-1}_{yy|\hat{\mathbf{G}}_{rb},\hat{\mathbf{H}}}\mathbf{w}_b|^2\right\},\tag{A.31}$$

can be simplified using techniques similar to the ones used for $\zeta_{E,k}$.

A.2 Proof of Theorem 2

Let $\mathbf{Z}=[\mathbf{z}[1],\mathbf{z}[2],\ldots,\mathbf{z}[N]]$ such that $\mathbf{Z}$ consists of iid columns with $\mathbf{z}[n]\sim\mathcal{CN}(h_{rr}\mathbf{A}(\theta)\mathbf{s}[n],\sigma^2_{wr}\mathbf{I}_{M_r})$ where $\sigma^2_{wr}=\sum_{k=1}^{K}\epsilon_{u,p,k}\eta_{rk}+N_0$. Now, the log-likelihood function of $\mathbf{Z}$ is as given

$$\ln(f_{\mathbf{Z}}(\mathbf{z}))=-M_rN\ln(\pi\sigma^2_{wr})-\frac{1}{\sigma^2_{wr}}\sum_{n=1}^{N}\|\mathbf{z}_n\|^2+\frac{2}{\sigma^2_{wr}}\sum_{n=1}^{N}\Re\{h^*_{rr}\mathbf{s}^H[n]\mathbf{A}^H(\theta)\mathbf{z}_n\}-\frac{1}{\sigma^2_{wr}}\sum_{n=1}^{N}\|h_{rr}\mathbf{A}(\theta)\mathbf{s}[n]\|^2\tag{A.32}$$

where $\mathbf{A}_{:n_t}(\theta)$ denotes the n_tth column of $\mathbf{A}(\theta)$ and $\mathbf{\Omega}_{n_t}$ is the n_tth sufficient statistic defined as $\mathbf{\Omega}_{n_t}=\sum_{n=1}^{N}\mathbf{z}[n]s^*_{n_t}[n], n_t=1,2,\ldots,M_t$; that is obtained by multiplying the observed data with the n_tth transmitted signal. The sufficient statistic matrix $\mathbf{\Omega}$ can now be expressed as

$$\mathbf{\Omega}=\mathrm{vec}[\mathbf{\Omega}_1,\mathbf{\Omega}_2,\ldots,\mathbf{\Omega}_{M_t}]=h_{rr}\mathbf{d}(\theta)+\mathbf{v}_u,\tag{A.33}$$

where $\mathbf{d}(\theta)=\mathrm{vec}(\mathbf{A}(\theta))$, and $\mathbf{v}_u=\mathrm{vec}(\sum_{n=1}^{N}\sum_{k=1}^{K}\sqrt{\epsilon_{u,p,k}}\mathbf{g}_{kr}\psi_k[n]\mathbf{s}^H[n]+\sum_{n=1}^{N}\sqrt{N_0}\mathbf{w}_r[n]\mathbf{s}^H[n])$, such that $\mathbf{v}_u\sim\mathcal{CN}(\mathbf{0},(N_0\sigma^2_r+\sum_{k=1}^{K}\epsilon_{u,p,k}\eta_rk\sigma^2_r)\mathbf{I}_{M_rM_t})$. Now, the Fisher information [69] for

estimating θ is given as

$$J_{\theta\theta} = \frac{2\sigma_r^2|h_{rr}|^2}{N_0 + \sum_{k=1}^{K} \epsilon_{u,p,k}\eta_r k} \Re\{\mathrm{Tr}\{\dot{\mathbf{A}}(\theta)\dot{\mathbf{A}}^H(\theta)\}\}, \tag{A.34}$$

and hence the CRB for θ takes the form $\mathrm{CRB}(\theta) = \frac{1}{J_{\theta\theta}}$.

A.3 Proof of Theorem 3

We can write

$$\zeta_{r,k} = \beta_k \epsilon_{d,s,k} E[|\hat{\mathbf{h}}_k^T(\bar{\mathbf{H}}\bar{\mathbf{H}}^H + \alpha \mathbf{I}_{M_a})^{-1}\hat{\mathbf{h}}_k^*|^2] \tag{A.35}$$

Following steps similar to the proof of Theorem 1, we get (2.43). Similarly,

$$\zeta_{r,I,k} = \sum_{\substack{m=1,\\ m\neq k}}^{K} \beta_k \epsilon_{d,s,m} E\{|\hat{\mathbf{h}}_k^T(\bar{\mathbf{H}}\bar{\mathbf{H}}^H + \alpha \mathbf{I}_{M_a})^{-1}\hat{\mathbf{h}}_m^*|^2\}. \tag{A.36}$$

can be shown to reduce to (2.47), and

$$\zeta_{r,E,k} = \sum_{l=1}^{K} \beta_k \epsilon_{d,s,l} E\{|\tilde{\mathbf{h}}_k^T(\bar{\mathbf{H}}\bar{\mathbf{H}}^H + \alpha \mathbf{I}_{M_a})^{-1}\hat{\mathbf{h}}_l^*|^2\}, \tag{A.37}$$

can be shown to reduce to (2.58).

A.4 Proof of Theorem 4

Using results from [41]we can show that,

$$E[(\tilde{\mathbf{G}}_{br}^H \mathbf{Q}\mathrm{diag}(\sqrt{\boldsymbol{\epsilon}_{d,s}})\bar{\mathbf{p}}[n])(\tilde{\mathbf{G}}_{br}^H \mathbf{Q}\mathrm{diag}(\sqrt{\boldsymbol{\epsilon}_{d,s}})\bar{\mathbf{p}}[n])^H] \xrightarrow[M\to\infty]{a.s.} \mu_\alpha^{'}. \tag{A.38}$$

and

$$E[(\hat{\mathbf{g}}_{br,m}^H \mathbf{Q}_{\hat{\mathbf{g}}_{br,m}}\mathrm{diag}(\sqrt{\boldsymbol{\epsilon}_{d,s}}) \times \bar{\mathbf{p}}[n])(\hat{\mathbf{g}}_{br,m}^H \mathbf{Q}_{\hat{\mathbf{g}}_{br,m}}\mathrm{diag}(\sqrt{\boldsymbol{\epsilon}_{d,s}})\bar{\mathbf{p}}[n])^H] \xrightarrow[M\to\infty]{a.s.} \mu_{\hat{\mathbf{g}}_{br,m}}. \tag{A.39}$$

$$E[|(\hat{\mathbf{g}}_{br,m}^H \mathbf{Q}\mathrm{diag}(\sqrt{\boldsymbol{\epsilon}_{d,s}})\bar{\mathbf{p}}[n])|^2] = \frac{\mu_{i,\alpha}^{'}}{|1 + \mu_{\hat{\mathbf{g}}_{br,m}}|^H} \tag{A.40}$$

Letting $\tilde{\mathbf{z}}[n] = \hat{\mathbf{G}}_{br}\mathbf{Q}\mathrm{diag}(\sqrt{\boldsymbol{\epsilon}_{d,s}})\bar{\mathbf{p}}[n] + \tilde{\mathbf{G}}_{br}\mathbf{Q}\mathrm{diag}(\sqrt{\boldsymbol{\epsilon}_{d,s}})\bar{\mathbf{p}}[n] + \sqrt{N_0}\mathbf{w}_r[n]$, represent the noise and interference, it is easy to show that,

$$E[\mathbf{z}[n]\mathbf{z}^H[n]] \triangleq \sigma_{wr}^2 \mathbf{I}_{M_r} \tag{A.41}$$

Let $\mathbf{Z} = [\mathbf{z}[1], \mathbf{z}[2], \ldots, \mathbf{z}[N]]$ Therefore,

$$\ln(f_{\mathbf{Z}}(\mathbf{z})) = -M_r N \ln(\pi\sigma^2_{wr,d}) - \frac{1}{\sigma^2_{wr,d}} \sum_{n=1}^{N} \|\mathbf{z}_n\|^2 + \frac{2}{\sigma^2_{wr,d}} \Re\{h^*_{rr} \sum_{n_t=1}^{M_t} \mathbf{A}^H_{:n_t}(\theta)\mathbf{\Omega}_{n_t}\} - \frac{1}{\sigma^2_{wr,d}} \sum_{n=1}^{N} \|h_{rr}\mathbf{A}(\theta)\mathbf{s}[n]\|^2. \quad \text{(A.42)}$$

The sufficient statistic matrix $\mathbf{\Omega}_d$ can now be expressed as

$$\mathbf{\Omega}_d = \text{vec}[\mathbf{\Omega}_{1,d}, \mathbf{\Omega}_{2,d}, \ldots, \mathbf{\Omega}_{M_t,d}] = h_{rr}\mathbf{d}(\theta) + \mathbf{v}_d, \quad \text{(A.43)}$$

where

$$\mathbf{d}(\theta) = \text{vec}(\mathbf{A}(\theta)),$$

and

$$\mathbf{v}_d = \text{vec}\left(\sum_{n=1}^{N} (\hat{\mathbf{G}}^H_{br}\mathbf{Q}\text{diag}(\sqrt{\boldsymbol{\epsilon}_{d,s}})\bar{\mathbf{p}}[n] + \tilde{\mathbf{G}}^H_{br}\mathbf{Q}\text{diag}(\sqrt{\boldsymbol{\epsilon}_{d,s}})\bar{\mathbf{p}}[n]) \times \mathbf{s}^H[n] + \sum_{n=1}^{N} \sqrt{N_0}\mathbf{w}_r[n]\mathbf{s}^H[n]\right),$$

such that $\mathbf{v}_d \sim \mathcal{CN}(\mathbf{0}, \sigma^2_{wr,d}\sigma^2_r\mathbf{I}_{M_rM_t})$.

Therefore, the Fisher information [69] for estimating θ is given as

$$J_{\theta\theta} = \frac{2\sigma^2_r|h_{rr}|^2}{\sigma^2_{wr}} \Re\{\text{Tr}\{\dot{\mathbf{A}}(\theta)\dot{\mathbf{A}}^H(\theta)\}\}, \quad \text{(A.44)}$$

and hence the CRB for θ takes the form $\text{CRB}(\theta) = \frac{1}{J_{\theta\theta}}$.

B Appendix

B.1 Proof of Lemma 1

We note that the desired signal power in (4.18) can be calculated as

$$\xi_{s,k} = E\left[\left|\sum_{r_i \in \Phi_r} \hat{h}_{ki}^{*} \sqrt{\rho_{u,k}} x_k[n] \hat{h}_{ki}\right|^2\right] \tag{B.1}$$

that can be reduced to

$$\xi_{s,k} = \rho_{u,k} \sum_{r_i \in \Phi_r} E\left[|\hat{h}_{ki}|^4\right] + \sum_{r_n \in \Phi_r \setminus r_m} \sum_{r_m \in \Phi_r} E\left[|\hat{h}_{km}|^2\right] E\left[|\hat{h}_{kn}|^2\right] \tag{B.2}$$

and further reduced to (4.21).

The channel estimation error power, $\xi_{E,k}$ becomes

$$\xi_{E,k} = \rho_{u,k} \sum_{r_i \in \Phi_r} E\left[|\hat{h}_{ki}|^2 |\tilde{h}_{ki}|^2\right] \tag{B.3}$$

and is further reduced to (4.22). The inter user interference power, $\xi_{I,k}$ takes the form

$$\begin{aligned} \xi_{I,k} &= E\left[\left|\sum_{r_i \in \Phi_r} \sum_{u_l \in \Phi_u \setminus u_k} \hat{h}_{ki}^{*} \sqrt{\rho_{u,l}} x_l[n] h_{li}\right|^2\right] \\ &= \rho_{u,l} \sum_{r_i \in \Phi_r} \sum_{u_l \in \Phi_u \setminus u_k} E\left[|\hat{h}_{ki}|^2\right] E\left[|h_{li}|^2\right] \end{aligned} \tag{B.4}$$

and is further reduced to (4.23). The interference power due to radar sub-system, $\xi_{RC,k}$ can be calculated as

$$\xi_{RC,k} = E\left[\left|\sum_{r_i\in\Phi_r} \hat{h}^*_{ki}(\tilde{\mathbf{g}}^T_{ri}\boldsymbol{\zeta}[n])\right|^2\right] = E\left[\sum_{r_i\in\Phi_r} |\hat{h}_{ki}|^2|(\tilde{\mathbf{g}}^T_{ri}\boldsymbol{\zeta}[n])|^2\right] \tag{B.5}$$

and is further reduced to (4.24).

B.2 Proof of Theorem 5

We can express the coverage probability for a given threshold rate $R_{u,0}$ as $P_{\text{cov},u}(R_{u,0}) = \Pr\{\log_2(1+\gamma_{u,k}) > R_{u,0}\}$, and equivalently,

$$P_{\text{cov},u}(R_{u,0}) = \Pr\left\{\rho_{u,k}\left(\sum_{r_i\in\Phi_r}\sigma^4_{ki} + \sum_{r_n\in\Phi_r}\sum_{r_m\in\Phi_r}\sigma^2_{km}\sigma^2_{kn}\right) \geq \gamma_0\left(\rho_{u,k}\sum_{r_i\in\Phi_r}\sigma^2_{ki}\bar{\sigma}^2_{ki} + \sum_{r_i\in\Phi_r}\sum_{u_l\in\Phi_u\setminus u_k}\rho_{u,l}\beta_{li}\sigma^2_{ki} + \sum_{r_i\in\Phi_r}P_tN_t\eta_{ei}\sigma^2_{ki} + N_0\sum_{r_i\in\Phi_r}\sigma^2_{ki}\right)\right\} \tag{B.6}$$

Applying Campbell's theorem, we can replace the summations over the PPPs with their expected values as,

$$E\left[\sum_{r_i\in\Phi_{r'}}\sigma^4_{ki}\right] = (2\pi\lambda_r)^2\int_{d_{r1}}^{\infty}\int_{d_{k1}}^{\infty}\sigma^4(r,t)drdt, \tag{B.7}$$

$$E\left[\sum_{r_n\in\Phi_{r'}}\sum_{r_m\in\Phi_{r'}}(\sigma^2_{km})(\sigma^2_{kn})\right] = (2\pi\lambda_r)^4\int_{d_{r1}}^{\infty}\int_{d_{r1}}^{\infty}\int_{d_{k1}}^{\infty}\int_{d_{k1}}^{\infty}\sigma^2(r,t)\sigma^2(s,v)drdsdtdv. \tag{B.8}$$

Looking at the interference terms, we can write

$$E\left[\sum_{r_i\in\Phi_r}\sigma^2_{ki}\bar{\sigma}^2_{ki}\right] = (2\pi\lambda_r)^2\int_{d_{r1}}^{\infty}\bar{\sigma}^2(r,t)\sigma^2(r,t)drdt. \tag{B.9}$$

$$E\left[\sum_{r_i\in\Phi_r}\sum_{u_l\in\Phi_u\setminus u_k}\rho_{u,l}\beta_{li}\sigma^2_{ki}\right] = E\left[\sum_{r_i\in\Phi_r}\sum_{u_l\in\Phi_u}\rho_{u,l}\beta_{li}\sigma^2_{ki}\right] - E\left[\sum_{r_i\in\Phi_{r'}}\rho_{u,k}\beta_{ki}\sigma^2_{ki}\right], \tag{B.10}$$

where we can reduce the expected value of $\sum_{u_l\in\Phi_u\setminus u_k}\rho_{u,l}\beta_{li}$ as

$$E\left[\sum_{u_l\in\Phi_u}\rho_u\beta_{li}\right] = 2\pi\lambda_u\left(\int_z^{\infty}\rho_u\beta(u)udu\right) = I_1(z), \tag{B.11}$$

and

$$E\left[\sum_{r_i\in\Phi_r}\sum_{u_l\in\Phi_u}\rho_u\beta_{li}\sigma_{ki}^2\right]=(2\pi\lambda_r)^2 2\pi\lambda_u\int_{d_{r1}}^{\infty}\int_{d_{k1}}^{\infty}\int_{z}^{\infty}\rho_u\beta(u)u\sigma^2(r,t)dudrdt, \tag{B.12}$$

$$E\left[\sum_{r_i\in\Phi_{r'}}\beta_{ki}\sigma_{ki}^2\right]=(2\pi\lambda_r)^2\int_{d_{k1}}^{\infty}\int_{d_{r1}}^{\infty}\sigma^2(r,t)dtdr, \tag{B.13}$$

$$E\left[\sum_{r_i\in\Phi_{r'}}\eta_{ei}\sigma_{ki}^2\right]=(2\pi\lambda_r)^2\eta_e\int_{d_{k1}}^{\infty}\int_{d_{r1}}^{\infty}\beta(t)\sigma^2(r,t)dtdr, \tag{B.14}$$

and

$$E\left[\sum_{r_i\in\Phi_{r'}}\sigma_{ki}^2\right]=(2\pi\lambda_r)^2\int_{d_{r1}}^{\infty}\int_{d_{k1}}^{\infty}\sigma^2(r,t)drdt. \tag{B.15}$$

Now, the probability of coverage can be evaluated by substituting (B.7)-(B.14) into (B.6) and evaluating the corresponding integrals and expectations, for the first contact distributions given by (4.62a), (4.62b) and (4.62c). Consequently, (B.6) be simplified to (4.27).

B.3 Proof of Lemma 2

The Cramer-Rao lower bounds $\sigma_{R,l}^2[n], \sigma_{\theta,l}^2[n]$ and $\sigma_{v,l}^2[n]$ can be written as [61, 62, 67]

$$\sigma_{R,l}^2[n]=\frac{\sum_{k=1}^{K}\epsilon_{x,k}\beta(d_{kl})+\sigma_{r,l}^2}{h_{r,l}^2P_t}B^{-2}c_R, \tag{B.16a}$$

$$\sigma_{\theta,l}^2[n]=\frac{\sum_{k=1}^{K}\epsilon_{x,k}\beta(d_{kl})+\sigma_{r,l}^2}{h_{r,l}^2P_t}\theta_b^2c_\theta, \tag{B.16b}$$

$$\sigma_{v,l}^2[n]=\frac{\sum_{k=1}^{K}\epsilon_{x,k}\beta(d_{kl})+\sigma_{r,l}^2}{h_{r,l}^2P_t}B^2c_v \tag{B.16c}$$

Now, using Campbell's theorem we can replace $\sum_{k=1}^{K}\epsilon_{x,k}\eta_{kl}$ by $2\pi\lambda_k\int_0^{\infty}\int_u^{\infty}\beta(r)rdrp_{d_{l0}}(u)du$ and the expressions of $\sigma_{R,l}^2[n], \sigma_{\theta,l}^2[n]$ and $\sigma_{v,l}^2[n]$ can be reduced to (4.33a),(4.33b) and (4.33c) respectively.

B.4 Proof of Lemma 3

The desired signal power, $\xi_{d,s,k}$ can be calculated as

$$\xi_{d,s,k} = E\left[\left|\sum_{r_l\in\Phi_r} \hat{h}_{kl}\frac{\hat{h}^*_{kl}}{\sqrt{E|\hat{h}_{kl}|^2}}\sqrt{\rho_d}q_k\right|^2\right], \tag{B.17}$$

and is reduced to (4.57). The channel estimation error power $\xi_{d,E,k}$ can be calculated as

$$\xi_{d,E,k} = E\left[\left|\sum_{r_l\in\Phi_r} \tilde{h}_{kl}\frac{\hat{h}^*_{kl}}{\sqrt{E|\hat{h}_{kl}|^2}}\sqrt{\rho_d}q_k\right|^2\right] = \rho_d\left[\sum_{r_l\in\Phi_r} E[|\tilde{h}_{kl}|^2]\right], \tag{B.18}$$

and is reduced to (4.58). The inter user interference power $\xi_{d,I,k}$ can be calculated as

$$\begin{aligned}\xi_{d,I,k} &= E\left[\left|\sum_{r_l\in\Phi_r}\sum_{u_i\in\Phi_u\setminus u_k} h_{kl}\frac{\hat{h}^*_{il}}{\sqrt{E|\hat{h}_{il}|^2}}\sqrt{\rho_d}q_i\right|^2\right] \\ &= \rho_d\left[\sum_{r_l\in\Phi_r} E[|h_{kl}|^2]\right]\end{aligned} \tag{B.19}$$

and is reduced to (4.59). The radar generated interference power $\xi_{d,RC,k}$ can be calculated as

$$\xi_{d,RC,k} = E\left[\left|\mathbf{g}^T_{rk}\boldsymbol{\zeta}[n]\right|^2\right] \tag{B.20}$$

and is reduced to (4.60).

B.5 Proof of Theorem 10

The coverage probability for a given threshold $R_{d,1}$ can be expressed as

$$P_{\text{cov,d}}(R_{d,1}) = \Pr[\log_2(1+\gamma_{d,k}) > R_{d,1}], \tag{B.21}$$

and can be written as

$$\begin{aligned}P_{\text{cov},d}(R_{d,1}) = \Pr\Bigg\{\rho_d\sum_{r_m\in\Phi_r}\sum_{r_n\in\Phi_r}\sigma_{km}\sigma_{kn} + \left(\sum_{r_l\in\Phi_r}\sigma^2_{kl}\right) \geq \gamma_1\Bigg(\rho_d\sum_{r_l\in\Phi_r}(\bar{\sigma}^2_{kl}) + \rho_d\sum_{r_l\in\Phi_r}\sum_{u_i\in\Phi_u\setminus u_k}\beta_{kl} \\ + P_t\eta_e\beta_{kr} + N_0)\Bigg\}.\end{aligned} \tag{B.22}$$

Now, similar to the uplink case, using Campbell's theorem to replace the summations by their expected values, we get

$$E\left[\sum_{r_l\in\Phi_{r'}}\sigma_{kl}^2\right]=(2\pi\lambda_r)^2\int_{d_{r1}}^{\infty}\int_{d_{k1}}^{\infty}\sigma^2(r,t)drdt, \tag{B.23}$$

$$E\left[\sum_{r_n\in\Phi_{r'}}\sum_{r_m\in\Phi_{r'}}\sigma_{km}\sigma_{kn}\right]=(2\pi\lambda_r)^4\int_{d_{rN}}^{\infty}\int_{d_{rN}}^{\infty}\int_{d_{kN}}^{\infty}\int_{d_{kN}}^{\infty}\sigma(r,t)\sigma(s,v)drdsdtdv, \tag{B.24}$$

$$E\left[\sum_{r_l\in\Phi_{r'}}\sum_{u_i\in\Phi_u\setminus u_k}\beta_{kl}\right]=4\pi^2\lambda_r\lambda_u\int_{d_{u1}}^{\infty}\int_{d_{k1}}^{\infty}\beta(r)rtdrdt, \tag{B.25}$$

$$P_t\eta_e E\left[\beta_{kr}\right]=P_t\eta_e\beta(z), \tag{B.26}$$

with z being the first contact between the radar and the UE. Again we can compute the probability of coverage by substituting (B.23)-(B.26) into (B.22) and averaging over the first contact distributions given by (4.62a), (4.62b) and (4.62c).

Bibliography

[1] Government of India, "Road accidents in india 2019," https://morth.nic.in/sites/default/files/RA_Uploading.pdf, 2019, [Online; accessed 19-October-2021].

[2] N. H. T. S. Administration, "Vehicle-to-vehicle (V2V) communication," https://www.nhtsa.gov/technology-innovation/vehicle-vehicle-communication, May 2021.

[3] Wikipedia contributors, "Intelligent transportation system — Wikipedia, the free encyclopedia," https://en.wikipedia.org/w/index.php?title=Intelligent_transportation_system&oldid=1034993715, 2021, [Online; accessed 28-August-2021].

[4] H. Griffiths, L. Cohen, S. Watts, E. Mokole, C. Baker, M. Wicks, and S. Blunt, "Radar spectrum engineering and management: Technical and regulatory issues," *Proceedings of the IEEE*, vol. 103, no. 1, pp. 85–102, 2014.

[5] F. Liu, C. Masouros, A. P. Petropulu, H. Griffiths, and L. Hanzo, "Joint radar and communication design: Applications, state-of-the-art, and the road ahead," *IEEE Transactions on Communications*, vol. 68, no. 6, pp. 3834–3862, 2020.

[6] G. M. Jacyna, B. Fell, and D. McLemore, "A high-level overview of fundamental limits studies for the darpa ssparc program," in *2016 IEEE Radar Conference (RadarConf)*. IEEE, 2016, pp. 1–6.

[7] A. R. Chiriyath, B. Paul, and D. W. Bliss, "Radar-communications convergence: Coexistence, cooperation, and co-design," *IEEE Transactions on Cognitive Communications and Networking*, vol. 3, no. 1, pp. 1–12, 2017.

[8] F. Liu, Y. Cui, C. Masouros, J. Xu, T. X. Han, Y. C. Eldar, and S. Buzzi, "Integrated sensing and communications: Towards dual-functional wireless networks for 6g and beyond," *arXiv preprint arXiv:2108.07165*, 2021.

[9] Y. Liu, G. Liao, Z. Yang, and J. Xu, "Design of integrated radar and communication system based on MIMO-OFDM waveform," *Journal of Systems Engineering and Electronics*, vol. 28, no. 4, pp. 669–680, 2017.

[10] C. Sturm and W. Wiesbeck, "Waveform design and signal processing aspects for fusion of wireless communications and radar sensing," *Proceedings of the IEEE*, vol. 99, no. 7, pp. 1236–1259, 2011.

[11] P. Kumari, S. A. Vorobyov, and R. W. Heath, "Adaptive virtual waveform design for millimeter-wave joint communication–radar," *IEEE Transactions on Signal Processing*, vol. 68, pp. 715–730, 2020.

[12] H. Nosrati, E. Aboutanios, and D. Smith, "Array partitioning for multi-task operation in dual function MIMO systems," *Digital Signal Processing*, vol. 82, pp. 106–117, 2018.

[13] C. D'Andrea, S. Buzzi, and M. Lops, "Communications and radar coexistence in the massive mimo regime: Uplink analysis," *IEEE Transactions on Wireless Communications*, vol. 19, no. 1, pp. 19–33, 2020.

[14] S. Haykin, "Cognitive radar: a way of the future," *IEEE Signal Processing Magazine*, vol. 23, no. 1, pp. 30–40, 2006.

[15] Y.-C. Liang, K.-C. Chen, G. Y. Li, and P. Mahonen, "Cognitive radio networking and communications: An overview," *IEEE transactions on vehicular technology*, vol. 60, no. 7, pp. 3386–3407, 2011.

[16] R. Saruthirathanaworakun, J. M. Peha, and L. M. Correia, "Opportunistic sharing between rotating radar and cellular," *IEEE Journal on Selected Areas in Communications*, vol. 30, no. 10, pp. 1900–1910, 2012.

[17] H. Wang, J. T. Johnson, and C. J. Baker, "Spectrum sharing between communications and ATC radar systems," *IET Radar, Sonar & Navigation*, vol. 11, no. 6, pp. 994–1001, 2017.

[18] J. M. Peha, "Spectrum sharing in the gray space," *Telecommunications Policy*, vol. 37, no. 2-3, pp. 167–177, 2013.

[19] J. H. Reed, A. W. Clegg, A. V. Padaki, T. Yang, R. Nealy, C. Dietrich, C. R. Anderson, and D. M. Mearns, "On the co-existence of TD-LTE and radar over 3.5 GHz band: An experimental study," *IEEE Wireless Communications Letters*, vol. 5, no. 4, pp. 368–371, 2016.

[20] S. Sodagari, A. Khawar, T. C. Clancy, and R. McGwier, "A projection based approach for radar and telecommunication systems coexistence," in *2012 IEEE Global Communications Conference (GLOBECOM)*, 2012, pp. 5010–5014.

[21] A. Babaei, W. H. Tranter, and T. Bose, "A nullspace-based precoder with subspace expansion for radar/communications coexistence," in *2013 IEEE Global Communications Conference (GLOBECOM)*, 2013, pp. 3487–3492.

[22] A. Khawar, A. Abdel-Hadi, and T. C. Clancy, "Spectrum sharing between s-band radar and lte cellular system: A spatial approach," in *2014 IEEE International Symposium on Dynamic Spectrum Access Networks (DYSPAN)*. IEEE, 2014, pp. 7–14.

[23] A. Khawar, A. Abdelhadi, and T. C. Clancy, "On the impact of time-varying interference-channel on the spatial approach of spectrum sharing between s-band radar and communication system," in *2014 IEEE Military Communications Conference*. IEEE, 2014, pp. 807–812.

[24] L. Zheng, M. Lops, X. Wang, and E. Grossi, "Joint design of overlaid communication systems and pulsed radars," *IEEE Transactions on Signal Processing*, vol. 66, no. 1, pp. 139–154, 2017.

[25] B. Li and A. Petropulu, "Mimo radar and communication spectrum sharing with clutter mitigation," in *2016 IEEE Radar Conference (RadarConf)*. IEEE, 2016, pp. 1–6.

[26] B. Li, A. P. Petropulu, and W. Trappe, "Optimum co-design for spectrum sharing between matrix completion based mimo radars and a mimo communication system," *IEEE Transactions on Signal Processing*, vol. 64, no. 17, pp. 4562–4575, 2016.

[27] E. H. Yousif, M. C. Filippou, F. Khan, T. Ratnarajah, and M. Sellathurai, "A new lsa-based approach for spectral coexistence of mimo radar and wireless communications systems," in *2016 IEEE International Conference on Communications (ICC)*. IEEE, 2016, pp. 1–6.

[28] F. Liu, C. Masouros, A. Li, and T. Ratnarajah, "Robust MIMO beamforming for cellular and radar coexistence," *IEEE Wireless Communications Letters*, vol. 6, no. 3, pp. 374–377, 2017.

[29] A. R. Chiriyath, B. Paul, G. M. Jacyna, and D. W. Bliss, "Inner bounds on performance of radar and communications co-existence," *IEEE Transactions on Signal Processing*, vol. 64, no. 2, pp. 464–474, 2015.

[30] J. Guerci, R. Guerci, A. Lackpour, and D. Moskowitz, "Joint design and operation of shared spectrum access for radar and communications," in *2015 IEEE Radar Conference (RadarCon)*. IEEE, 2015, pp. 0761–0766.

[31] T. L. Marzetta, *Fundamentals of massive MIMO*. Cambridge University Press, 2016.

[32] Z. Behdad, O. T. Demir, K. W. Sung, E. Bjornson, and C. Cavdar, "Power allocation for joint communication and sensing in cell-free massive mimo," 2022. [Online]. Available: https://arxiv.org/abs/2209.01864

[33] Q. Wu, S. Zhang, B. Zheng, C. You, and R. Zhang, "Intelligent reflecting surface-aided wireless communications: A tutorial," *IEEE Transactions on Communications*, vol. 69, no. 5, pp. 3313–3351, 2021.

[34] L. Lu, G. Y. Li, A. L. Swindlehurst, A. Ashikhmin, and R. Zhang, "An overview of massive MIMO: Benefits and challenges," vol. 8, no. 5, pp. 742–758, Oct. 2014.

[35] E. Björnson, E. G. Larsson, and T. L. Marzetta, "Massive MIMO: Ten myths and one critical question," vol. 54, no. 2, pp. 114–123, Feb. 2016.

[36] T. L. Marzetta, *Fundamentals of massive MIMO*. Cambridge University Press, 2016.

[37] S. Fortunati, L. Sanguinetti, F. Gini, M. S. Greco, and B. Himed, "Massive MIMO radar for target detection," *IEEE Transactions on Signal Processing*, vol. 68, pp. 859–871, 2020.

[38] J. A. Mahal, A. Khawar, A. Abdelhadi, and T. C. Clancy, "Spectral coexistence of MIMO radar and MIMO cellular system," *IEEE Transactions on Aerospace and Electronic Systems*, vol. 53, no. 2, pp. 655–668, 2017.

[39] S. Buzzi, C. D'Andrea, and M. Lops, "Using massive mimo arrays for joint communication and sensing," in *2019 53rd Asilomar Conference on Signals, Systems, and Computers*, 2019, pp. 5–9.

[40] S. Buzzi, C. D'Andrea, and M. Lops, "Transmit power allocation for joint communication and sensing through massive mimo arrays," in *WSA 2020; 24th International ITG Workshop on Smart Antennas*, Feb 2020, pp. 1–6.

[41] A. K. Papazafeiropoulos, "Impact of general channel aging conditions on the downlink performance of massive MIMO," *IEEE Transactions on Vehicular Technology*, vol. 66, no. 2, pp. 1428–1444, Feb. 2016.

[42] J. Li and P. Stoica, "Mimo radar with colocated antennas," *IEEE Signal Processing Magazine*, vol. 24, no. 5, pp. 106–114, 2007.

[43] S. Sun, W. U. Bajwa, and A. P. Petropulu, "Mimo-mc radar: A mimo radar approach based on matrix completion," *IEEE Transactions on Aerospace and Electronic Systems*, vol. 51, no. 3, pp. 1839–1852, 2015.

[44] R. Chopra, C. R. Murthy, H. A. Suraweera, and E. G. Larsson, "Performance analysis of fdd massive mimo systems under channel aging," *IEEE Transactions on Wireless Communications*, vol. 17, no. 2, pp. 1094–1108, 2018.

[45] ——, "Blind channel estimation for downlink massive mimo systems with imperfect channel reciprocity," *IEEE Transactions on Signal Processing*, vol. 68, pp. 3132–3145, 2020.

[46] A. K. Papazafeiropoulos, "Impact of general channel aging conditions on the downlink performance of massive mimo," *IEEE Transactions on Vehicular Technology*, vol. 66, no. 2, pp. 1428–1442, 2017.

[47] O. A. Oumar, M. F. Siyau, and T. P. Sattar, "Comparison between music and esprit direction of arrival estimation algorithms for wireless communication systems," in *The First International Conference on Future Generation Communication Technologies*, 2012, pp. 99–103.

[48] A. K. Papazafeiropoulos and T. Ratnarajah, "Deterministic equivalent performance analysis of time-varying massive mimo systems," *IEEE Transactions on Wireless Communications*, vol. 14, no. 10, pp. 5795–5809, 2015.

[49] S. Zarei, W. H. Gerstacker, J. Aulin, and R. Schober, "I/q imbalance aware widely-linear receiver for uplink multi-cell massive mimo systems: Design and sum rate analysis," *IEEE Transactions on Wireless Communications*, vol. 15, no. 5, pp. 3393–3408, 2016.

[50] W. C. Jakes and D. C. Cox, Eds., *Microwave Mobile Communications*, 2nd ed. IEEE Press, New York: IEEE Press, 1994.

[51] H. Q. Ngo, A. Ashikhmin, H. Yang, E. G. Larsson, and T. L. Marzetta, "Cell-free massive mimo versus small cells," *IEEE Transactions on Wireless Communications*, vol. 16, no. 3, pp. 1834–1850, 2017.

[52] S. Mukherjee and R. Chopra, "Performance analysis of cell-free massive mimo systems in los/ nlos channels," *IEEE Transactions on Vehicular Technology*, vol. 71, no. 6, pp. 6410–6423, 2022.

[53] H. Q. Ngo, A. Ashikhmin, H. Yang, E. G. Larsson, and T. L. Marzetta, "Cell-free massive mimo versus small cells," *IEEE Transactions on Wireless Communications*, vol. 16, no. 3, pp. 1834–1850, 2017.

[54] E. Nayebi, A. Ashikhmin, T. L. Marzetta, H. Yang, and B. D. Rao, "Precoding and power optimization in cell-free massive mimo systems," *IEEE Transactions on Wireless Communications*, vol. 16, no. 7, pp. 4445–4459, 2017.

[55] E. Nayebi, A. Ashikhmin, T. L. Marzetta, and H. Yang, "Cell-free massive mimo systems," in *2015 49th Asilomar Conference on Signals, Systems and Computers*. IEEE, 2015, pp. 695–699.

[56] E. Björnson and L. Sanguinetti, "Making cell-free massive mimo competitive with mmse processing and centralized implementation," *IEEE Transactions on Wireless Communications*, vol. 19, no. 1, pp. 77–90, 2019.

[57] H. Q. Ngo, L.-N. Tran, T. Q. Duong, M. Matthaiou, and E. G. Larsson, "On the total energy efficiency of cell-free massive mimo," *IEEE Transactions on Green Communications and Networking*, vol. 2, no. 1, pp. 25–39, 2017.

[58] A. Sakhnini, M. Guenach, A. Bourdoux, H. Sahli, and S. Pollin, "A target detection analysis in cell-free massive mimo joint communication and radar systems," in *ICC 2022 - IEEE International Conference on Communications*, 2022, pp. 2567–2572.

[59] X. Wang, D. Musicki, R. Ellem, and F. Fletcher, "Efficient and enhanced multi-target tracking with doppler measurements," *IEEE Transactions on Aerospace and Electronic Systems*, vol. 45, no. 4, pp. 1400–1417, 2009.

[60] L. Wu, K. V. Mishra, M. R. B. Shankar, and B. Ottersten, "Resource allocation in heterogeneously-distributed joint radar-communications under asynchronous bayesian tracking framework," *IEEE Journal on Selected Areas in Communications*, vol. 40, no. 7, pp. 2026–2042, 2022.

[61] M. I. Skolnik, "Theoretical accuracy of radar measurements," *IRE Transactions on Aeronautical and Navigational Electronics*, vol. ANE-7, no. 4, pp. 123–129, 1960.

[62] P. Z. Peebles, *Radar principles*. John Wiley & Sons, 2007.

[63] E. Björnson, J. Hoydis, L. Sanguinetti *et al.*, "Massive mimo networks: Spectral, energy, and hardware efficiency," *Foundations and Trends® in Signal Processing*, vol. 11, no. 3-4, pp. 154–655, 2017.

[64] W. Lu and M. Di Renzo, "Stochastic geometry modeling of cellular networks: Analysis, simulation and experimental validation," in *Proceedings of the 18th ACM International Conference on Modeling, Analysis and Simulation of Wireless and Mobile Systems*, 2015, pp. 179–188.

[65] Z. Chen and E. Björnson, "Channel hardening and favorable propagation in cell-free massive mimo with stochastic geometry," *IEEE Transactions on Communications*, vol. 66, no. 11, pp. 5205–5219, 2018.

[66] P. Parida and H. S. Dhillon, "Cell-free massive mimo with finite fronthaul capacity: A stochastic geometry perspective," *IEEE Transactions on Wireless Communications*, vol. 22, no. 3, pp. 1555–1572, 2022.

[67] A. Mishra, R. Chopra, and B. S. MR, "On the coexistence of multi-static tracking radars with cell free massive mimo," in *2024 National Conference on Communications (NCC)*. IEEE, 2024, pp. 1–6.

[68] P. Parida and H. S. Dhillon, "Cell-free massive mimo with finite fronthaul capacity: A stochastic geometry perspective," *IEEE Transactions on Wireless Communications*, vol. 22, no. 3, pp. 1555–1572, 2023.

[69] S. M. Kay, *Fundamentals of statistical signal processing: estimation theory*. Prentice-Hall, Inc., 1993.

[70] E. Basar, M. Di Renzo, J. De Rosny, M. Debbah, M.-S. Alouini, and R. Zhang, "Wireless communications through reconfigurable intelligent surfaces," *IEEE Access*, vol. 7, pp. 116 753–116 773, 2019.

[71] C. Pan, H. Ren, K. Wang, W. Xu, M. Elkashlan, A. Nallanathan, and L. Hanzo, "Multicell mimo communications relying on intelligent reflecting surfaces," *IEEE Transactions on Wireless Communications*, vol. 19, no. 8, pp. 5218–5233, 2020.

[72] Q.-U.-A. Nadeem, H. Alwazani, A. Kammoun, A. Chaaban, M. Debbah, and M.-S. Alouini, "Intelligent reflecting surface-assisted multi-user miso communication: Channel estimation and beamforming design," *IEEE Open Journal of the Communications Society*, vol. 1, pp. 661–680, 2020.

[73] M. Levy-Israel, I. Bilik, and J. Tabrikian, "Mcrb on doa estimation for automotive mimo radar in the presence of multipath," *IEEE Transactions on Aerospace and Electronic Systems*, vol. 59, no. 5, pp. 4831–4843, 2023.

[74] E. Grossi, M. Lops, and L. Venturino, "Detection rate optimization for swerling 0, i, and iii target models," in *2017 IEEE Radar Conference (RadarConf)*, 2017, pp. 0606–0609.

[75] T. Van Le and K. Lee, "Adaptive perturbation-aided opportunistic hybrid beamforming for mmwave systems," *IEEE Transactions on Vehicular Technology*, vol. 69, no. 6, pp. 6554–6562, 2020.

[76] B. Hassibi and B. M. Hochwald, "How much training is needed in multiple-antenna wireless links?" vol. 49, no. 4, pp. 951–963, Apr. 2003.

[77] K. Zhi, C. Pan, H. Ren, and K. Wang, "Uplink achievable rate of intelligent reflecting surface-aided millimeter-wave communications with low-resolution adc and phase noise," *IEEE Wireless Communications Letters*, vol. 10, no. 3, pp. 654–658, March 2021.

[78] A. Mishra and R. Chopra, "MIMO radars and massive MIMO communication systems can coexist," *CoRR*, vol. abs/2304.00890, 2023. [Online]. Available: https://doi.org/10.48550/arXiv.2304.00890

[79] S. Fortunati, L. Sanguinetti, F. Gini, M. S. Greco, and B. Himed, "Massive MIMO radar for target detection," *IEEE Transactions on Signal Processing*, vol. 68, pp. 859–871, 2020.

[80] B. Hassibi and B. Hochwald, "How much training is needed in multiple-antenna wireless links?" *IEEE Transactions on Information Theory*, vol. 49, no. 4, pp. 951–963, 2003.